[redacted]

CONFIDENTIAL

NASA TECHNICAL MEMORANDUM

NASA TM X-2977

NASA TM X-2977

AERODYNAMIC CHARAC
OF TWO 10-PERCENT-TH
SUPERCRITICAL AIRFOIL
DIFFERENT UPPER SURF
CURVATURE DISTRIBUT

by Charles D. Harris

Langley Research Center
Hampton, Va. 23665

NATIONAL AERONAUTICS AND SPACE AD

~~CONFIDENTIAL~~

1. Report No.	2. Government Accession No.	3. Recipient's Catalog No.
NASA TM X-2977		

4. Title and Subtitle	5. Report Date
AERODYNAMIC CHARACTERISTICS OF TWO 10-PERCENT-THICK NASA SUPERCRITICAL AIRFOILS WITH DIFFERENT UPPER SURFACE CURVATURE DISTRIBUTIONS (U)	February 1974
	6. Performing Organization Code
7. Author(s)	8. Performing Organization Report No.
Charles D. Harris	L-8522
9. Performing Organization Name and Address	10. Work Unit No.
NASA Langley Research Center Hampton, Va. 23665	501-06-05-02
	11. Contract or Grant No.
12. Sponsoring Agency Name and Address	13. Type of Report and Period Covered
National Aeronautics and Space Administration Washington, D.C. 20546	Technical Memorandum
	14. Sponsoring Agency Code

15. Supplementary Notes

16. Abstract

In order to assess the degree to which the characteristic region of low curvature of the supercritical airfoil can be practically extended on the upper surface, wind-tunnel measurements of the aerodynamic characteristics of two supercritical airfoils with different upper surface curvature distributions have been made at Mach numbers from 0.60 to 0.81. Integrated section force and moment data, surface pressure distributions, and typical wake survey profiles are presented.

17. Key Words (Suggested by Author(s))

Supercritical airfoils
Transonic aerodynamics

19. Security Classif. (of this report)	20. S
~~Confidential~~	

~~CONFIDENTIAL~~

[redacted]

AERODYNAMIC CHARACTERISTICS OF TWO 10-PERCENT-THICK NASA SUPERCRITICAL AIRFOILS WITH DIFFERENT UPPER SURFACE CURVATURE DISTRIBUTIONS*

By Charles D. Harris
Langley Research Center

SUMMARY

An experimental investigation has been conducted to evaluate the chordwise extent of the characteristic region of low curvature over the upper surface of the supercritical airfoil. The results indicated that although extending this region of low curvature further than on earlier supercritical airfoils provided a modest improvement in drag divergence Mach number, it would have an adverse effect on drag at lower Mach numbers.

INTRODUCTION

An airfoil which operates efficiently in the mixed conditions of supercritical flow has been developed by the National Aeronautics and Space Administration. (See refs. 1 to 7.) This distinctive airfoil shape, based on the concept of local supersonic flow with isentropic recompression and referred to as the supercritical airfoil, is characterized by a large leading-edge radius, a flattened upper surface, and a substantially cambered trailing edge. The broad region of relatively low, nearly uniform, upper surface curvature extends from slightly rearward of the leading edge to about the 70- or 75-percent chord station. It was speculated that extending this region of low curvature nearer the trailing edge than on previously reported (refs. 2 to 4) supercritical airfoils would permit a more rearward location of the upper surface shock wave without rapid increases in wave losses and associated separation; thus, the drag divergence Mach number at a particular normal-force coefficient would be delayed or the drag break for a particular Mach number would be delayed to a higher normal-force coefficient.

As part of the development program for the supercritical airfoil, wind-tunnel measurements of the aerodynamic characteristics of two early supercritical airfoils with different upper surface curvature distributions have been made in the Langley 8-foot transonic pressure tunnel at Mach numbers from 0.60 to 0.81. The primary difference between the two airfoils was the relative chordwise extent to which the low curvature

*[redacted]

[redacted]

or flattened region was maintained over the upper surface (both fore and aft of the midchord).

The results of extending the region of low upper surface curvature on the supercritical airfoil are presented herein as integrated section force and moment coefficients, surface pressure distributions, and typical wake survey profiles.

SYMBOLS

Values are given in both SI and U.S. Customary Units. The measurements and calculations were made in U.S. Customary Units.

C_p pressure coefficient, $\frac{p_l - p_\infty}{q_\infty}$

$C_{p,sonic}$ pressure coefficient corresponding to local Mach number of 1.0

c chord of airfoil, 63.5 centimeters (25.0 in.)

c_d section drag coefficient, $\sum c_{d'} \frac{\Delta z}{c}$

$c_{d'}$ point drag coefficient (ref. 8)

c_m section pitching-moment coefficient about the quarter-chord point,

$$\sum_l C_p \left(0.25 - \frac{x}{c}\right)\frac{\Delta x}{c} - \sum_u C_p \left(0.25 - \frac{x}{c}\right)\frac{\Delta x}{c}$$

c_n section normal-force coefficient, $\sum_l C_p \frac{\Delta x}{c} - \sum_u C_p \frac{\Delta x}{c}$

K surface curvature, reciprocal of local radius of curvature

M Mach number

m surface slope, dy/dx

p static pressure, newtons per meter^2 (pounds per foot^2)

Δp_t total-pressure loss, newtons per meter^2 (pounds per foot^2)

q	dynamic pressure, newtons per meter^2 (pounds per foot^2)
R	Reynolds number based on airfoil chord
x	ordinate along airfoil reference line measured from airfoil leading edge, centimeters (inches)
y	ordinate normal to airfoil reference line, centimeters (inches)
z	vertical distance in wake profile measured from bottom of rake, centimeters (inches)
α	angle of attack of airfoil reference line, degrees

Subscripts:

l	local point on airfoil
∞	undisturbed stream

Abbreviations:

l	airfoil lower surface
u	airfoil upper surface

APPARATUS AND TECHNIQUES

The apparatus and testing techniques used during this investigation were the same as those described in references 1 to 5. These descriptions, where appropriate, are repeated herein for completeness.

Model

Supercritical airfoil design philosophy.- In brief, the essence of the design philosophy of the supercritical airfoil is that it be free from wave drag at supercritical design Mach numbers. Although it is not the intent of this report to review the overall supercritical airfoil design philosophy, restatement of some of the fundamental considerations involved

may prove helpful in understanding the results presented herein. References 2 to 6 also contain brief discussions of various aspects of the supercritical airfoil concept.

At supercritical Mach numbers, a local region of supersonic flow extends vertically from the airfoil as indicated in figure 1(a) by the pressure coefficients above the $C_{p,sonic}$ line and by the shaded areas of the flow field. On conventional airfoils, this pocket of supersonic flow is terminated by a more or less pronounced shock wave with attendant wave losses. In addition, the positive pressure gradient through the shock wave may, when superimposed on the subcritical pressure recovery, cause separation of the boundary layer with further increases in drag.

The forward upper surface of the airfoil may be contoured so that the expansion waves from the leading edge are reflected from the sonic line and, in turn, from the upper surface as a series of Mach number decreasing, compression waves in the vicinity of the shock. In figure 1(b) this effect is illustrated schematically for a single expansion wave originating near the leading edge. Isentropic recompression is thus encouraged and an extensive chordwise region of generally constant supersonic flow is maintained over the upper surface at design conditions with a weak shock wave near the three-quarter-chord station. (See fig. 1(a).)

Wave losses are approximately proportional to the local Mach number entering the shock and can be minimized by maintaining a region of low curvature and thereby reducing local velocities ahead of the shock. Extending this low curvature region too near the trailing edge, however, forces a region of relatively high curvature in the vicinity of the trailing edge with increased trailing-edge slope. This high curvature would be expected to produce a more adverse pressure gradient at the trailing edge where the boundary layer is most sensitive and would result in a greater tendency toward trailing-edge separation. The degree and chordwise extent of low curvature therefore strongly influences both the strength of the shock wave and onset of trailing-edge separation, the two principal causes of drag divergence.

Another design consideration is the shaping of the rear upper surface to produce a short region of near-sonic or slightly supersonic velocity immediately behind the shock wave at design conditions. Such a plateau has been found to be desirable to permit the flow to stabilize before going through its final recompression at the trailing edge and also to prevent disturbances from propagating forward and strengthening the shock wave. At intermediate off-design conditions (between the onset of supersonic flow and the design point), the surface curvature required to produce the near-sonic plateau generates a second supersonic velocity peak near the three-quarter-chord station. Extending the low-curvature region rearward would be expected to reduce the magnitude of this second velocity peak.

The lower surface of the airfoil is generally shaped to prevent supercritical velocities on the lower surface which would lead to shock-wave formation and boundary-layer separation and also to provide a highly cambered trailing edge to compensate for the reduced lifting capacity of the relatively lightly cambered forward and middle regions of the airfoil.

The original design of the supercritical airfoil (ref. 1) included a slot near the trailing edge to permit high-energy lower surface flow to stabilize the boundary layer on the upper surface between the shock wave and the subsonic pressure recovery. The slot was later eliminated without degradation of performance potential.

Wind-tunnel models.- Two airfoil models (fig. 2), each having a maximum thickness-chord ratio of approximately 0.10 and a thickness-chord ratio at the trailing edge of about 0.01, were used in this investigation. The airfoils in figure 2 have been assigned number designations (8 and 9a) for identification purposes and are referred to by these designations hereafter. Coordinates of the two airfoils are presented as table I and other pertinent model geometry (surface slopes and upper surface curvature) are given in figures 3 and 4. The aerodynamic characteristics of airfoil 9a have been reported in reference 2 in relation to effects of trailing-edge geometry and both airfoils include the trailing-edge cavity described in reference 2 and shown in figure 5(b). Extension of the region of low upper surface curvature forward resulted in airfoil 8 having a larger leading-edge radius to blend the circular leading edge into the upper surface profile and avoid discontinuities in surface slopes. There were minor differences in the lower surfaces of the two airfoils but their effects on the aerodynamic characteristics were considered to be secondary and overshadowed by the differences in the upper surface.

The models, mounted in an inverted position, spanned the width of the tunnel with a span-chord ratio of 3.4. Angle of attack was changed manually by rotating the model about pivots in the tunnel side walls. A photograph of one of the models and the profile drag rake mounted in the tunnel is shown as figure 5 and sketches of one of the airfoils and the profile drag rake are presented in figure 6.

Wind Tunnel

The investigation was conducted in the Langley 8-foot transonic pressure tunnel (ref. 9). This tunnel is a continous-flow variable-pressure wind tunnel with controls that permit the independent variation of Mach number, stagnation pressure and temperature, and dewpoint. It has a 2.16-meter-square (85.2-inch-square) test section with filleted corners so that the total cross-sectional area is equivalent to a 2.44-meter-diameter (8-foot-diameter) circle. The upper and lower test section walls are axially slotted to

permit testing through the transonic speed range. The total slot width at the position of the model averaged about 5 percent of the width of the upper and lower walls.

The solid side walls and slotted upper and lower walls make this tunnel well suited to the investigation of two-dimensional models since the side walls act as end plates and the slots permit development of the flow field in the vertical direction.

Boundary-Layer Transition

Based on the technique discussed in reference 10, boundary-layer transition was fixed along the 28-percent chord line on the upper and lower surfaces in an attempt to simulate full-scale Reynolds numbers by providing the same relative trailing-edge boundary-layer displacement thickness at model scale as would exist at full-scale flight conditions. The simulation technique, which requires that laminar flow be maintained ahead of the transition trip, is limited on the upper surface to those test conditions in which shock waves or other steep adverse pressure gradients occur behind the point of fixed transition so that the flow is not tripped prematurely. Full-scale simulation on the lower surface would be valid through the Mach number range of the investigation since laminar flow can be maintained ahead of the trip for all test conditions. The transition trips consisted of 0.25-cm-wide (0.10-in.) bands of number 90 carborundum grains.

Measurements

Surface pressure measurements.- Normal forces and pitching moments acting on the airfoils were determined from surface static-pressure measurements. The surface pressure measurements were obtained from chordwise rows of orifices located approximately 0.32c from the tunnel center line. Orifices were concentrated near the leading and trailing edges of the airfoils to define the severe pressure gradients in these regions. In addition, a rearward-facing orifice was included in the cavity at the trailing edge (identified at an upper surface x/c location of 1.00). The transducers used in the differential pressure scanning valves to measure the static pressure at the airfoil surface had a range of ± 68.9 kN/m^2 (10 lb/in^2).

Wake measurements.- Drag forces acting on the airfoils, as measured by the momentum deficiency within the wake, were derived from vertical variations of the total and static pressures measured across the wake with the profile drag rake shown in figure 6(b). The rake was positioned in the vertical-center-line plane of the tunnel, approximately 1 chord length rearward of the trailing edge of the airfoil. The total-pressure tubes were flattened horizontally and closely spaced vertically (0.36 percent of the airfoil chord) in the region of the wake associated with skin-friction boundary-layer losses. Outside this region, the tube vertical spacing progressively widened until in the region above the wing where only

shock losses were anticipated, the total-pressure tubes were spaced about 7.2 percent of the chord apart. Static-pressure tubes were distributed as shown in figure 6(b). The rake was attached to the conventional center-line sting mount of the tunnel which permitted it to be moved vertically to center the close concentration of tubes in the boundary-layer wake.

Total and static pressures across the wake were also measured with the use of differential-pressure scanning valves. The transducer in the valve connected to total-pressure tubes intended to measure boundary-layer losses had a range of ± 17.2 kN/m^2 (2.5 lb/in^2); and the transducer in the valve for measuring shock losses and static pressure had a range of ± 6.9 kN/m^2 (1 lb/in^2).

Reduction of Data and Corrections

Calculation of c_n and c_m.- Section normal-force and pitching-moment coefficients were obtained by numerical integration (based on the trapezoidal method) of the local surface-pressure coefficient measured at each orifice multiplied by an appropriate weighting factor (incremental area).

Calculation of c_d.- To obtain section drag coefficients from the total and static pressures behind the model, point drag coefficients for each of the total-pressure measurements were computed by using the procedure of reference 8. These point drag values were then summed by numerical integration across the wake, based on the trapezoidal method.

Corrections for wind-tunnel-wall effects.- The most significant effect of wall interference on the data was a lift-induced angle-of-attack shift which must be subtracted from the measured geometric angle of attack. According to theory (ref. 11), the mean value of this angle-of-attack correction at the midchord, in degrees, is estimated to be approximately three times the section normal-force coefficient. However, based on experience in other two-dimensional tests in the Langley 8-foot transonic pressure tunnel, such a correction is believed to be unrealistically large. Because of this uncertainty, the uncorrected geometric angles of attack are used herein.

The theory of reference 11 also indicates that tunnel blockage effects would be small; consequently, no corrections have been applied to the data for blockage effects.

TEST CONDITIONS

Tests were conducted at Mach numbers from 0.60 to 0.81 for a stagnation pressure of 0.1013 MN/m^2 (1 atm) with resultant wind-tunnel Reynolds numbers based on the airfoil chord as shown in figure 7. The stagnation temperature of the tunnel air was automatically controlled at approximately 322 K (120° F) and the air was dried until the dew-point in the test section was reduced sufficiently to avoid condensation effects.

PRESENTATION OF RESULTS

Section force and moment coefficients of airfoils 9a and 8 are presented over an extensive angle-of-attack range in figures 8 and 9, respectively. In several instances, drag data are not presented for the higher angles of attack because momentum losses in the wake exceeded the measuring capability of the profile drag rake. Comparison of the aerodynamic characteristics of the two airfoils over an abbreviated angle-of-attack range near the design normal-force coefficient of 0.7 is presented in figure 10. The drag rise characteristics of the two airfoils at the design normal-force coefficient of 0.7 are summarized in figure 11. Chordwise pressure profiles of the two airfoils are compared in figure 12 and typical wake profiles are compared in figure 13. The profiles presented in figure 13 are representative of the momentum losses in the wake as indicated by stagnation-pressure deficits across the wake. The middle part of these profiles reflects viscous and separation losses in the boundary layer, whereas the "wings" of the profiles reflect direct losses in stagnation pressure across the shock waves.

DISCUSSION

As noted in the model section, dissimilarities between the lower surfaces of the two airfoils investigated (figs. 2 and 3) were considered to have only secondary import and to be overshadowed by the differences in the upper surfaces. The effects of these lower surface dissimilarities on the aerodynamic characteristics will not be considered except to note that the small variations in the pressure distributions over the lower surface (fig. 12) appear to be consistent with the geometric dissimilarities.

It was believed that maintaining the region of low curvature over a greater chordwise extent of the upper surface than on earlier supercritical airfoils would result in a higher drag divergence Mach number and reduce the magnitude of the intermediate off-design second velocity peak. Figures 11 and 12 do indeed indicate a modest improvement in drag divergence Mach number and a reduction in the magnitude of the second velocity peak for airfoil 8. Also apparent in the pressure profiles of figure 12 are the larger and more rearwardly located leading-edge suction peaks for airfoil 8 which are associated with the larger leading-edge radius.

The small difference in drag divergence Mach numbers between the two airfoils may be related to the difference in the pressure profiles in figure 12 and, in turn, to the differences in curvatures (fig. 4). Figure 12(t) illustrates how the extended low curvature distribution of airfoil 8 allowed the upper surface shock wave to move to a more rearward location before rapid increases in shock losses and associated boundary-layer separation became apparent. Although the shock location of the two airfoils are approximately the

same in this figure, the more rapidly increasing curvature of airfoil 9a between approximately the 60- and 80-percent chord station allowed the flow to expand to higher induced velocities entering the shock wave that resulted in a stronger shock and incipient trailing-edge separation with higher drag than airfoil 8.

These relatively small improvements were achieved, however, at the expense of substantially higher drag levels of airfoil 8 at lower Mach numbers. (See fig. 11.) Comparisons of the surface-pressure distributions in figure 12 and the stagnation-pressure deficits across the wake (fig. 13(a)) indicate the higher drag level for airfoil 8 at $M = 0.60$ may be attributed to the steeper adverse pressure gradient of the trailing edge (with greater attendant boundary-layer losses) since there are no perceptible shock losses at these conditions. As Mach number is increased beyond 0.60 to 0.70, airfoil 8 exhibits a more rapid increase in drag than airfoil 9a (fig. 11) because of the higher leading-edge suction peaks and stronger shock waves near the leading edge (fig. 12). Figure 13(b) suggests, however, that the more rapid drag buildup was not due to losses through the shock wave itself but was due to the influence of the shock wave on boundary-layer development.

It would appear from the results of this investigation, therefore, that although simply extending the region of low curvature over very much more of the upper surface than on earlier supercritical airfoils provided a modest improvement in drag divergence Mach number, it would have an unacceptably adverse effect on drag at lower Mach numbers.

CONCLUDING REMARKS

An investigation has been conducted in the Langley 8-foot transonic pressure tunnel to evaluate the chordwise extent of the characteristic region of low curvature over the upper surface of the supercritical airfoil. Maintaining the region of low curvature over a greater chordwise extent than on earlier supercritical airfoils resulted in a modest improvement in drag divergence Mach number and significantly reduced second velocity peaks. These improvements were accompanied, however, by substantial drag penalties due to increased boundary-layer losses at lower Mach numbers. The data indicate, therefore, that extending the region of low curvature very much farther than on earlier supercritical airfoils would have an adverse effect on the aerodynamic characteristics of the supercritical airfoil.

Langley Research Center,
National Aeronautics and Space Administration,
Hampton, Va., November 26, 1973.

REFERENCES

1. Whitcomb, Richard T.; and Clark, Larry R.: An Airfoil Shape for Efficient Flight at Supercritical Mach Numbers. NASA TM X-1109, 1965.

2. Harris, Charles D.: Wind-Tunnel Investigation of Effects of Trailing-Edge Geometry on a NASA Supercritical Airfoil Section. NASA TM X-2336, 1971.

3. Harris, Charles D.; and Blackwell, James A., Jr.: Wind-Tunnel Investigation of Effects of Rear Upper Surface Modification on an NASA Supercritical Airfoil. NASA TM X-2454, 1972.

4. Harris, Charles D.: Aerodynamic Characteristics of Two NASA Supercritical Airfoils With Different Maximum Thicknesses. NASA TM X-2532, 1972.

5. Blackwell, James A., Jr.: Aerodynamic Characteristics of an 11-Percent-Thick Symmetrical Supercritical Airfoil at Mach Numbers Between 0.30 and 0.85. NASA TM X-1831, 1969.

6. McGhee, Robert J.; and Bingham, Gene J.: Low-Speed Aerodynamic Characteristics of a 17-Percent-Thick Supercritical Airfoil Section, Including a Comparison Between Wind-Tunnel and Flight Data. NASA TM X-2571, 1972.

7. Anon.: Supercritical Wing Technology – A Progress Report on Flight Evaluations. NASA SP-301, 1972.

8. Baals, Donald D.; and Mourhess, Mary J.: Numerical Evaluation of the Wake-Survey Equations for Subsonic Flow Including the Effect of Energy Addition. NACA WR L-5, 1945. (Formerly NACA ARR L5H27.)

9. Schaefer, William T., Jr.: Characteristics of Major Active Wind Tunnels at the Langley Research Center. NASA TM X-1130, 1965.

10. Blackwell, James A., Jr.: Preliminary Study of Effects of Reynolds Number and Boundary-Layer Transition Location on Shock-Induced Separation. NASA TN D-5003, 1969.

11. Davis, Don D., Jr.; and Moore, Dewey: Analytical Study of Blockage- and Lift-Interference Corrections for Slotted Tunnels Obtained by the Substitution of an Equivalent Homogeneous Boundary for the Discrete Slots. NACA RM L53E07b, 1953.

TABLE I.- EXPERIMENTAL SECTION COORDINATES

x/c	$(y/c)_u$	$(y/c)_l$	$(y/c)_u$	$(y/c)_l$
	Airfoil 9a		Airfoil 8	
0	0	0	0	0
.0075	.0160	-.0165	.0184	-.0164
.0125	.0196	-.0201	.0221	-.0205
.0250	.0250	-.0259	.0275	-.0265
.0375	.0286	-.0299	.0310	-.0303
.050	.0314	-.0329	.0337	-.0333
.075	.0358	-.0374	.0374	-.0378
.100	.0389	-.0407	.0402	-.0412
.125	.0415	-.0432	.0423	-.0435
.150	.0433	-.0451	.0442	-.0452
.175	.0448	-.0465	.0456	-.0465
.200	.0461	-.0476	.0469	-.0475
.250	.0479	-.0491	.0488	-.0489
.300	.0491	-.0498	.0499	-.0499
.350	.0498	-.0500	.0504	-.0503
.400	.0500	-.0494	.0505	-.0500
.450	.0499	-.0485	.0503	-.0491
.500	.0494	-.0468	.0497	-.0476
.550	.0485	-.0440	.0485	-.0449
.575	.0480	-.0420	.0479	-.0430
.600	.0474	-.0393	.0472	-.0403
.625	.0465	-.0357	.0461	-.0365
.650	.0456	-.0310	.0451	-.0321
.675	.0445	-.0250	.0439	-.0267
.700	.0433	-.0200	.0427	-.0213
.725	.0419	-.0152	.0413	-.0160
.750	.0401	-.0109	.0398	-.0112
.775	.0382	-.0072	.0380	-.0071
.800	.0359	-.0041	.0359	-.0036
.825	.0332	-.0014	.0335	-.0005
.850	.0300	+.0005	.0309	+.0018
.875	.0264	+.0016	.0278	+.0032
.900	.0220	+.0016	.0242	+.0036
.925	.0167	+.0004	.0196	+.0027
.950	.0103	-.0026	.0140	-.0001
.975	.0035	-.0073	.0056	-.0048
.990	-.0016	-.0120	-----	-.0094
1.000	------	-.0157	-----	-.0136
	Leading-edge radius, 0.0212c		Leading-edge radius, 0.0228c	

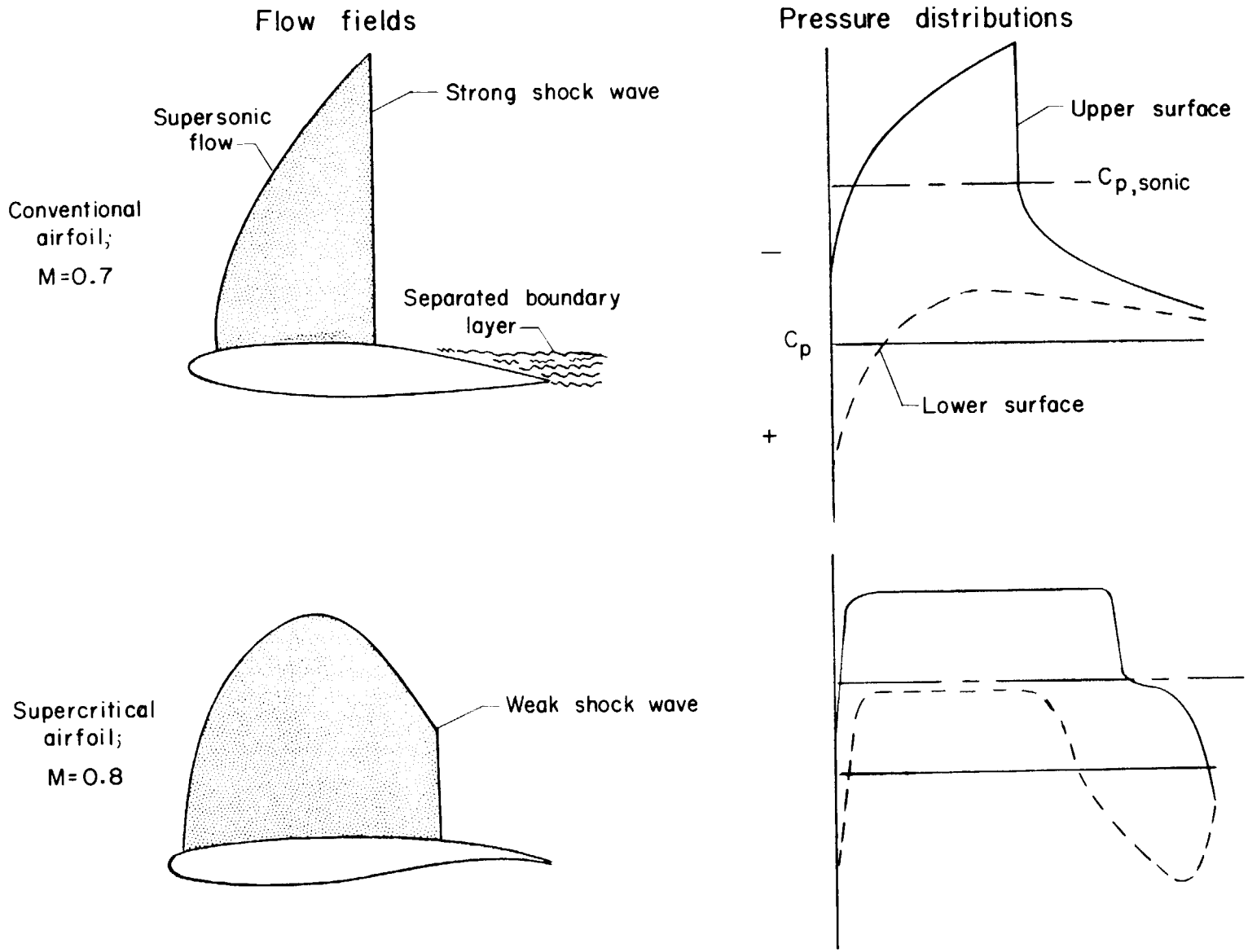

(a) Comparison of flow fields around supercritical and conventional airfoils.

Figure 1.- Schematic of supercritical phenomena.

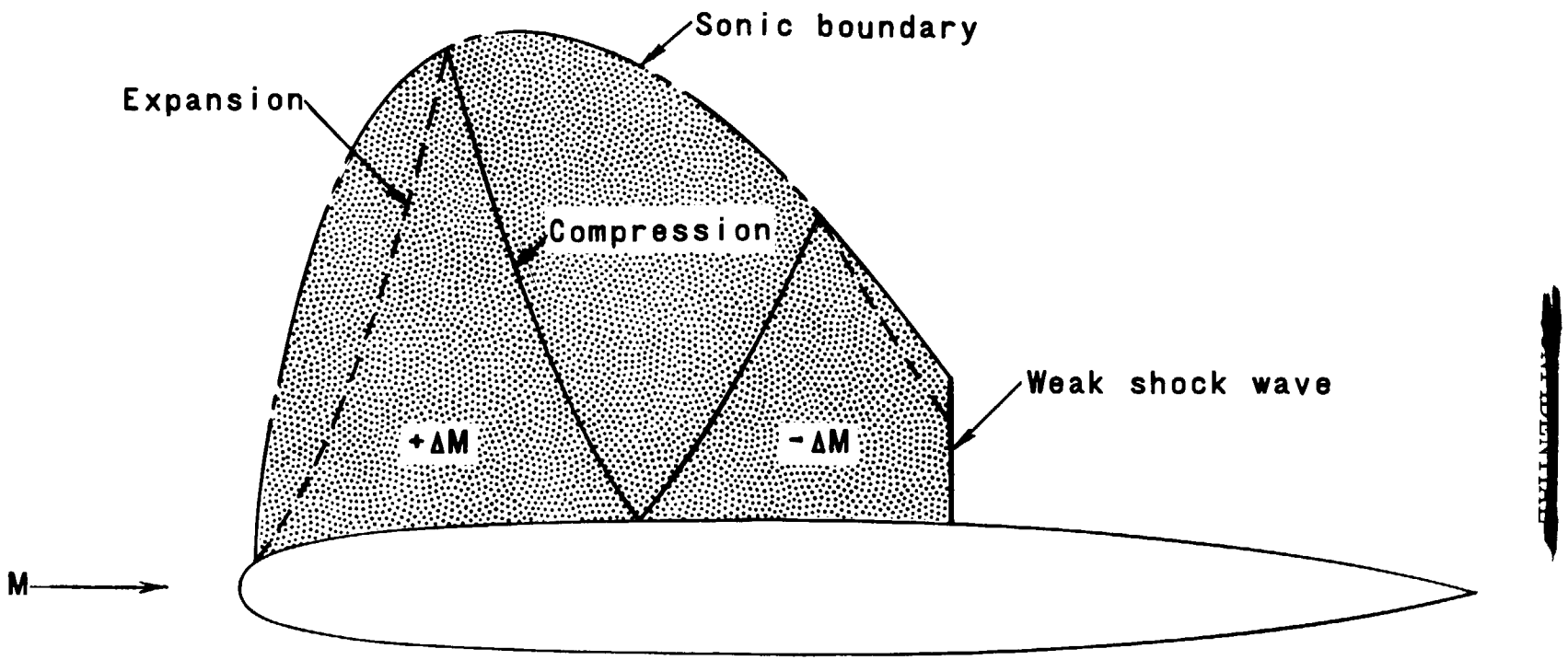

(b) Schematic flow field of supercritical airfoil.

Figure 1.- Concluded.

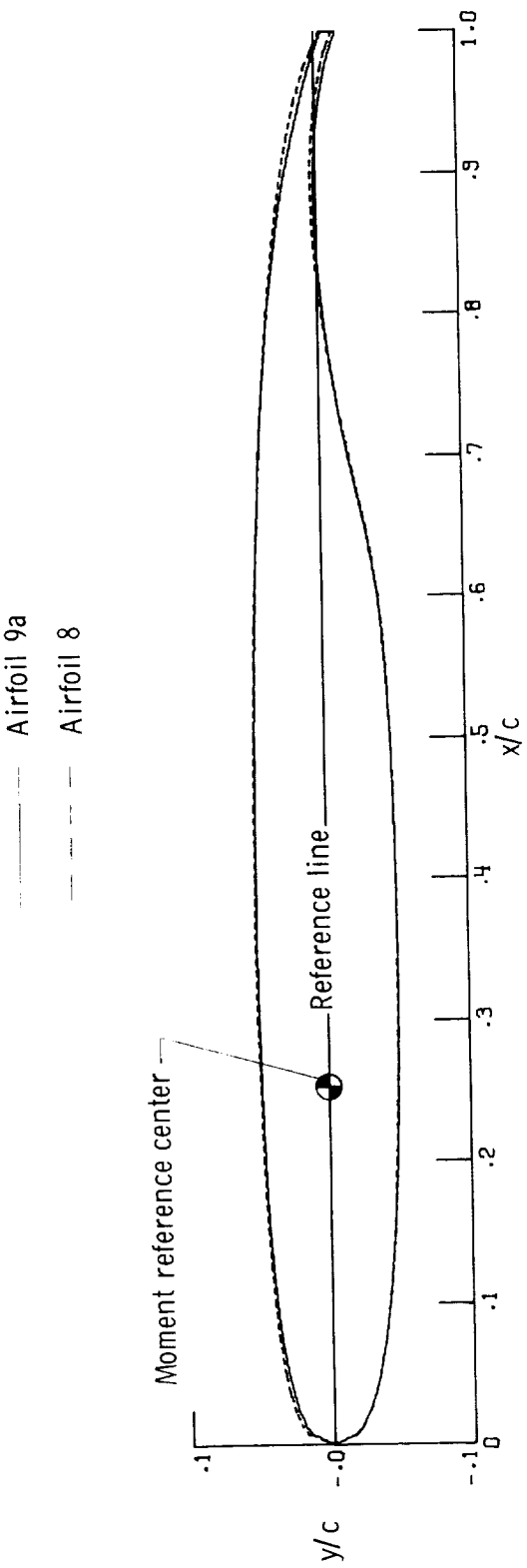

Figure 2.- Airfoil sketches.

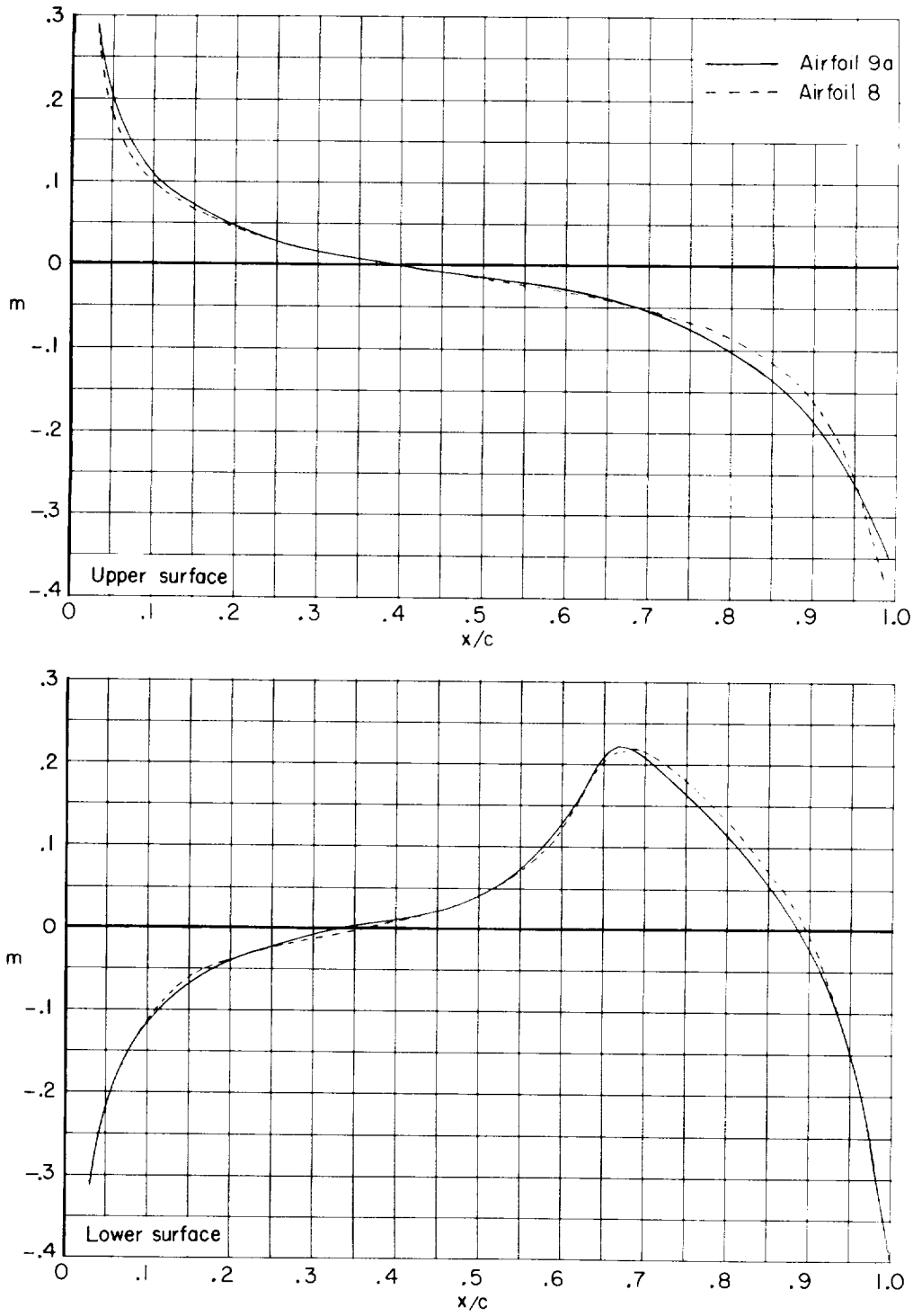

Figure 3.- Chordwise distribution of airfoil surface slopes.

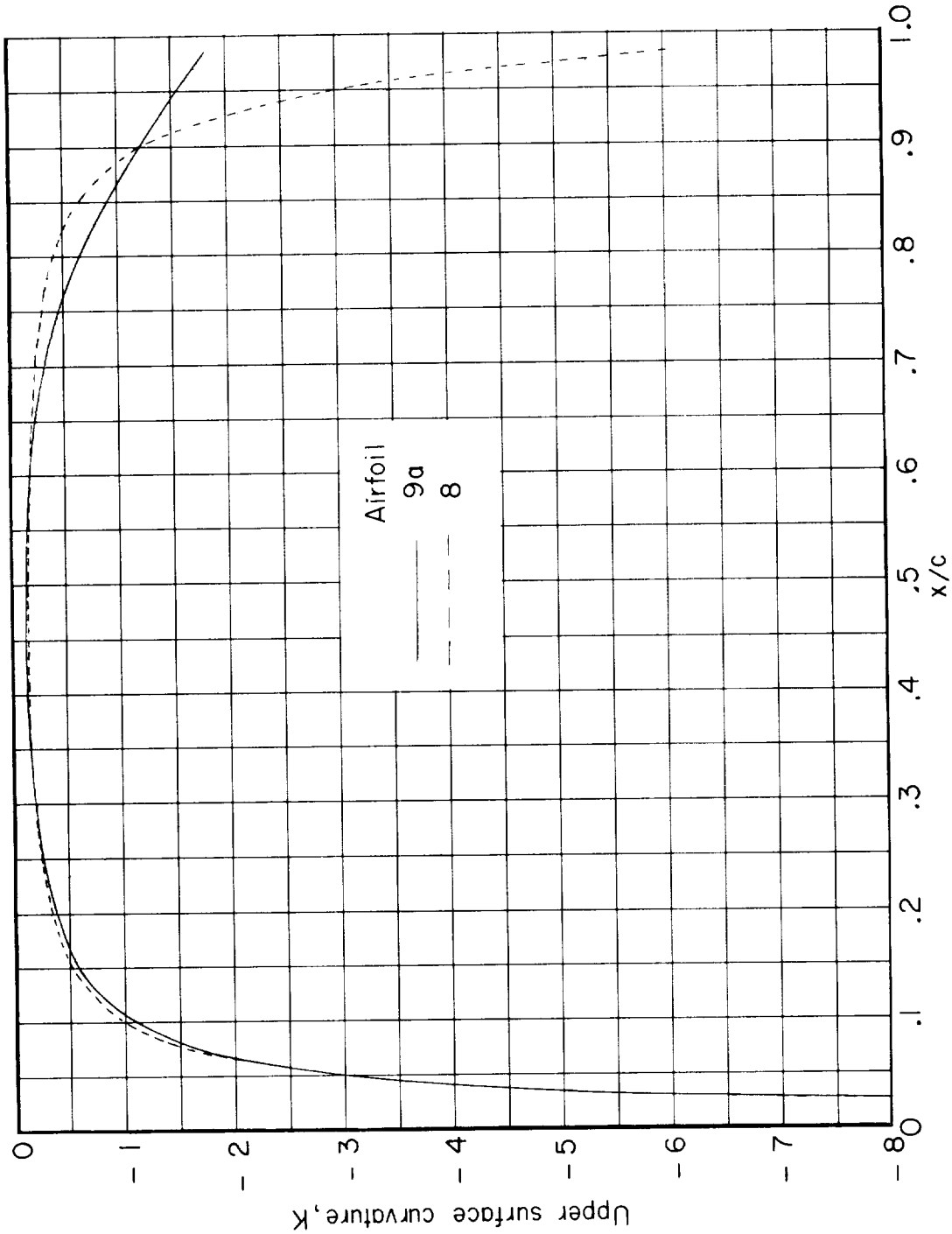

Figure 4.- Upper surface curvature distribution.

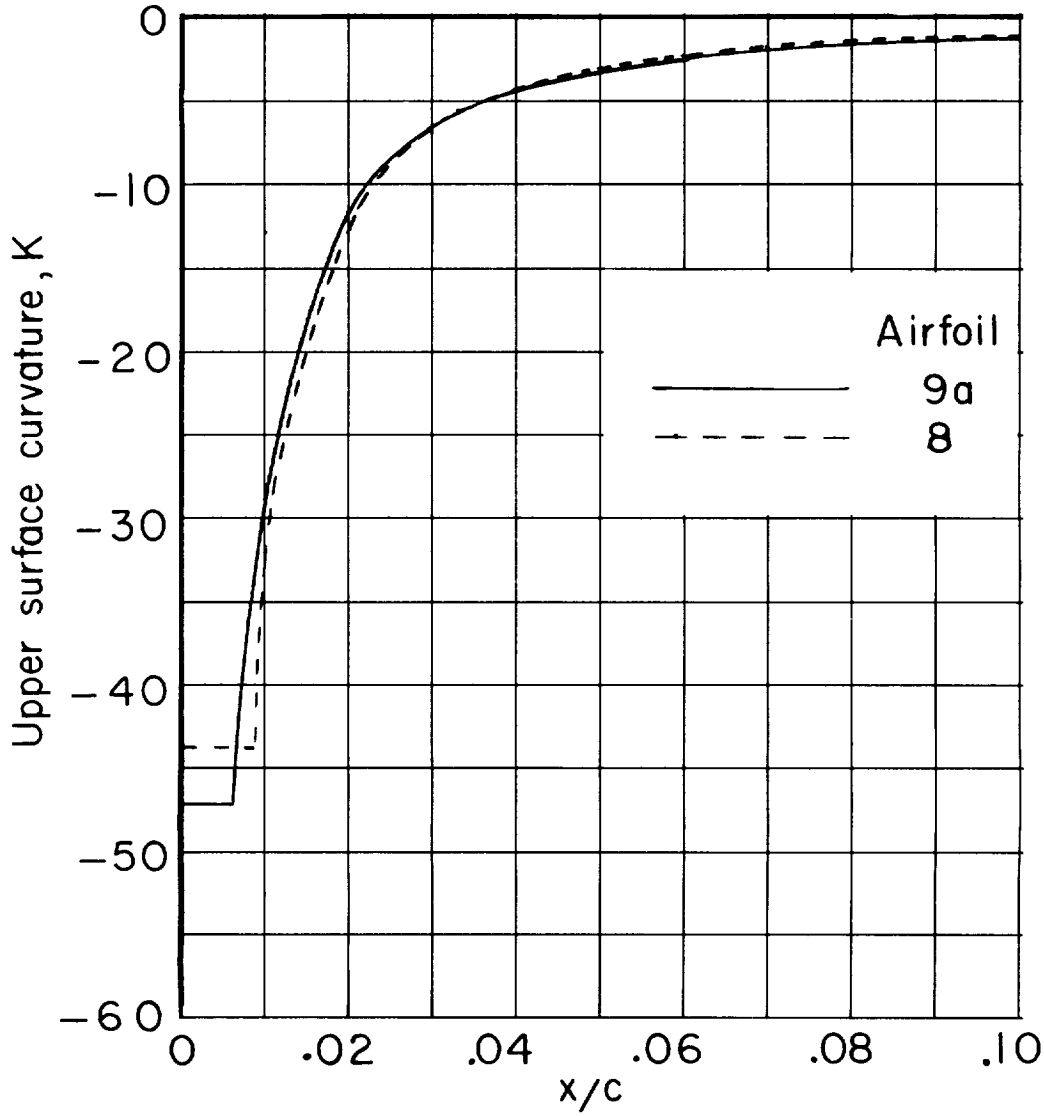

Figure 4.- Concluded.

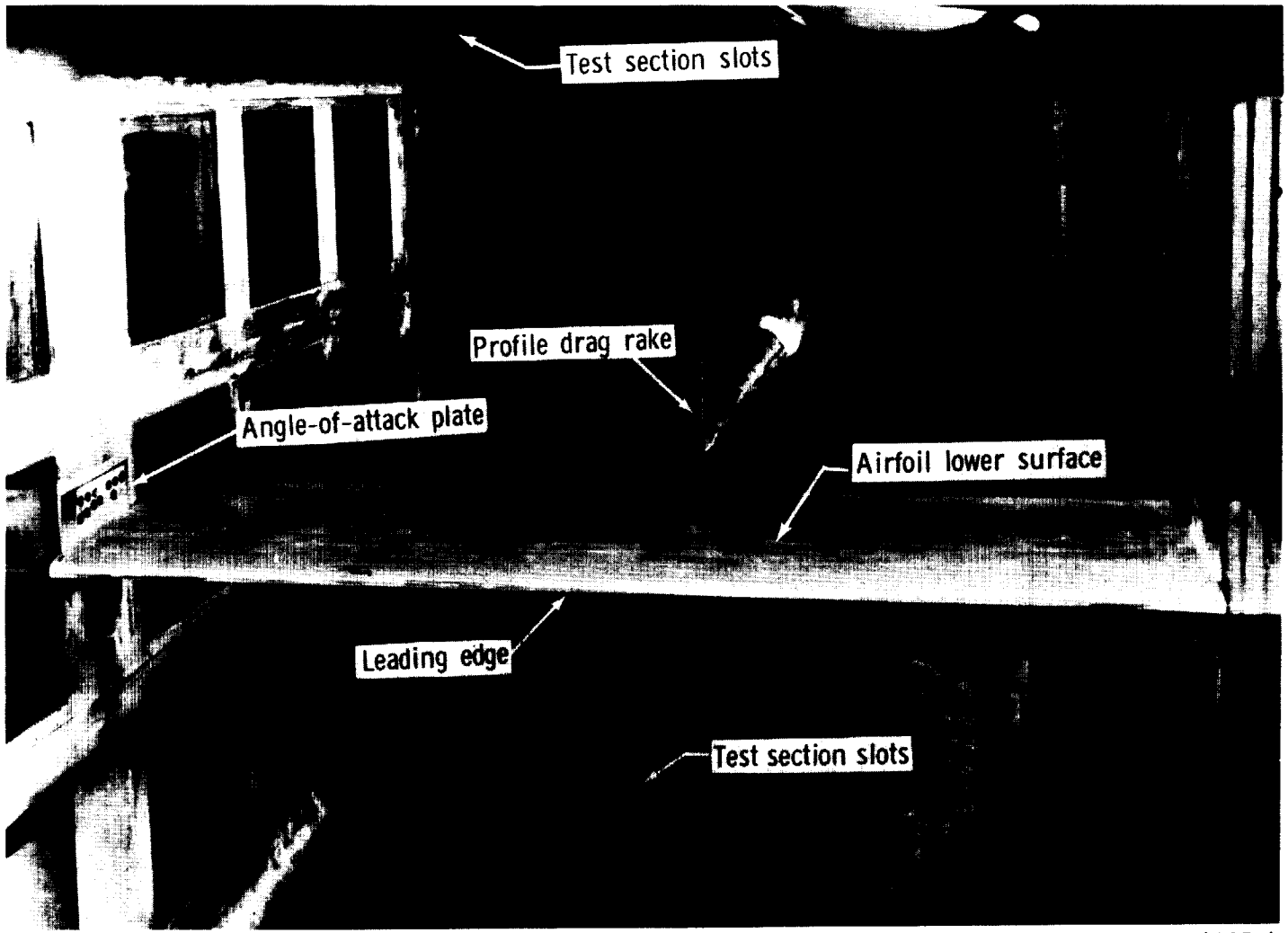

L-73-1225.1

(a) Supercritical airfoil and profile drag rake mounted in tunnel.

Figure 5.- Photographs of model in tunnel.

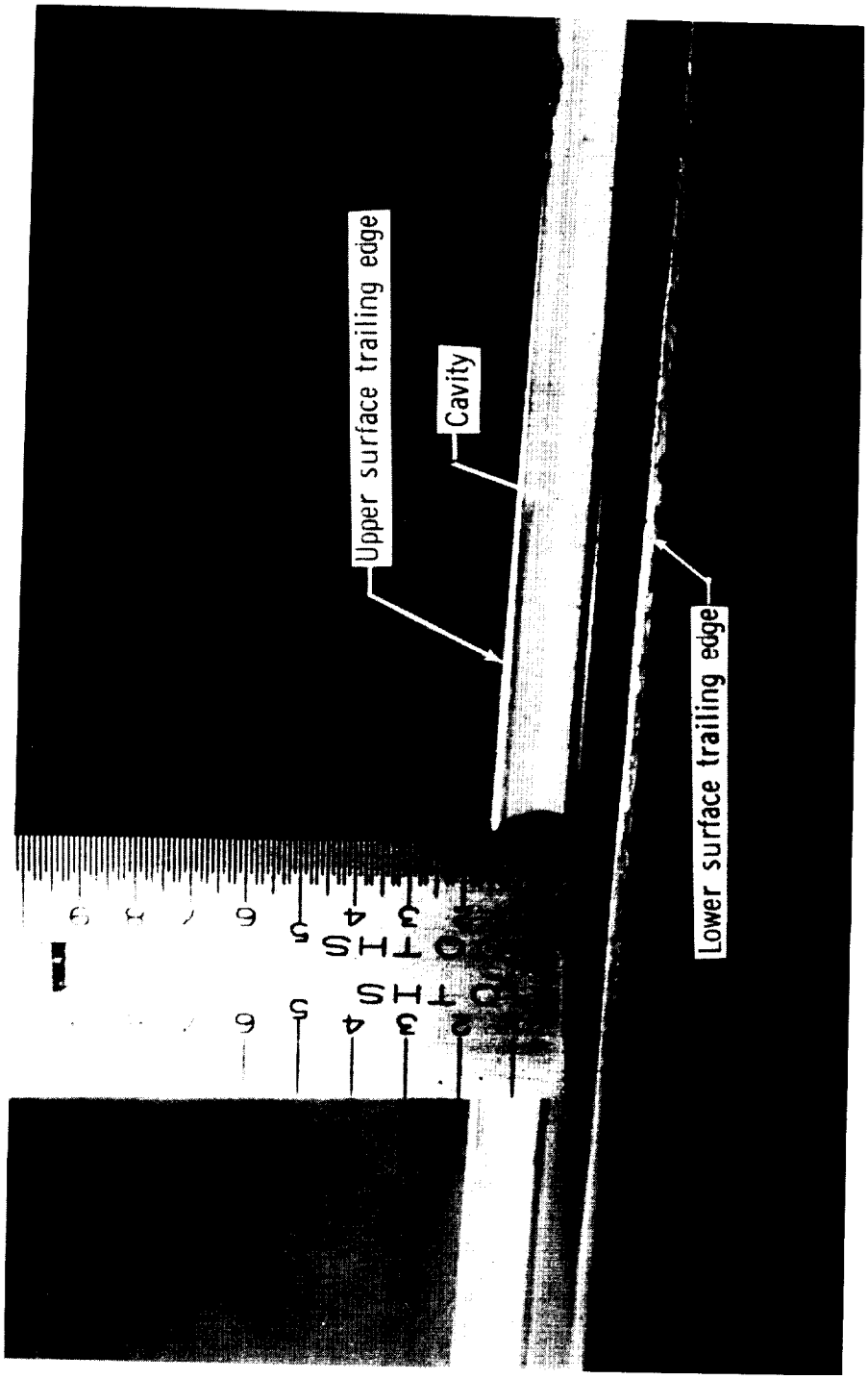

L-73-1227.1

(b) Trailing-edge cavity.

Figure 5.- Concluded.

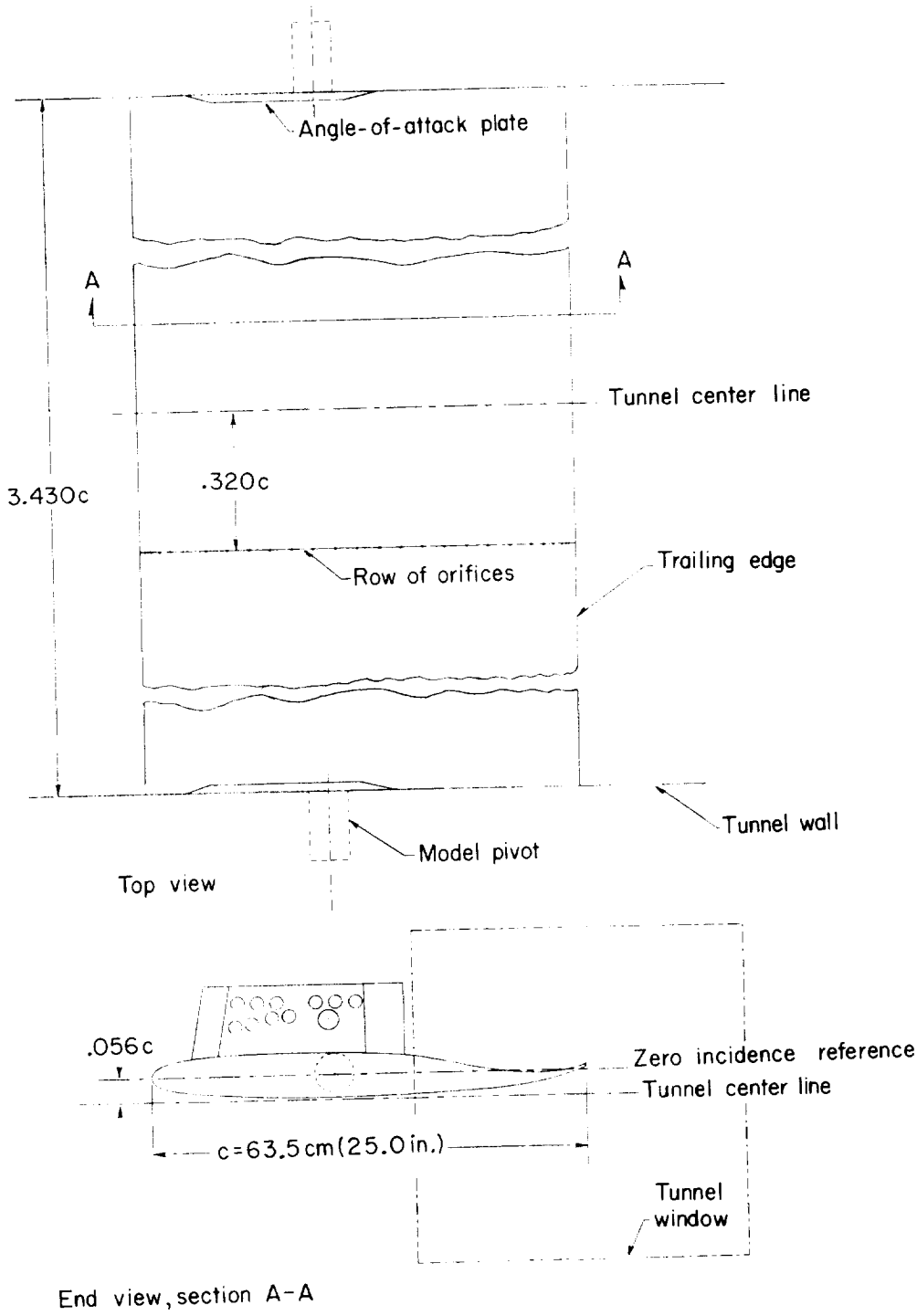

(a) Airfoil mounted in tunnel.

Figure 6.- Apparatus. Dimensions are in terms of chord (c = 63.5 cm (25 in.)).

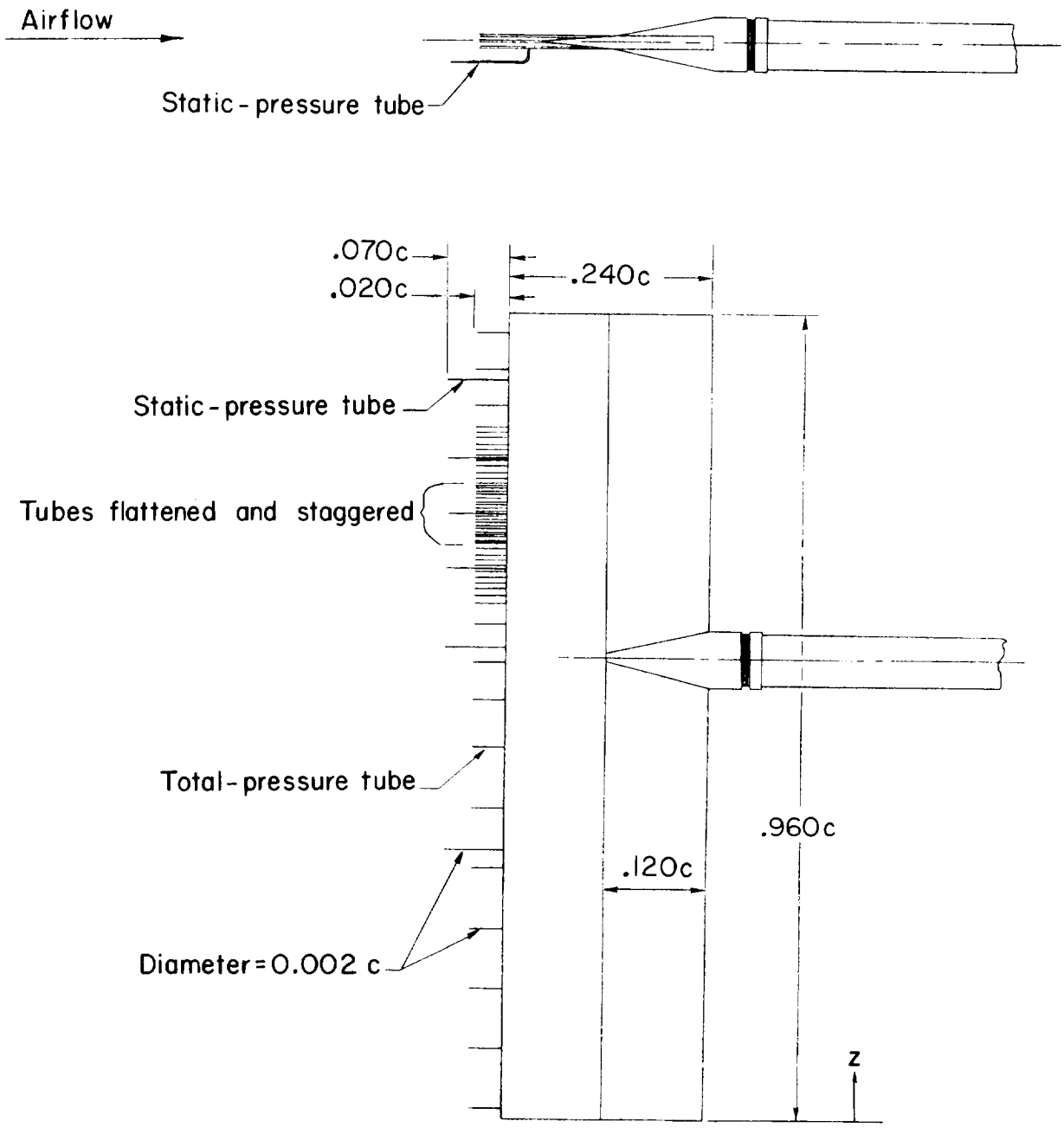

(b) Profile drag rake.

Figure 6.- Concluded.

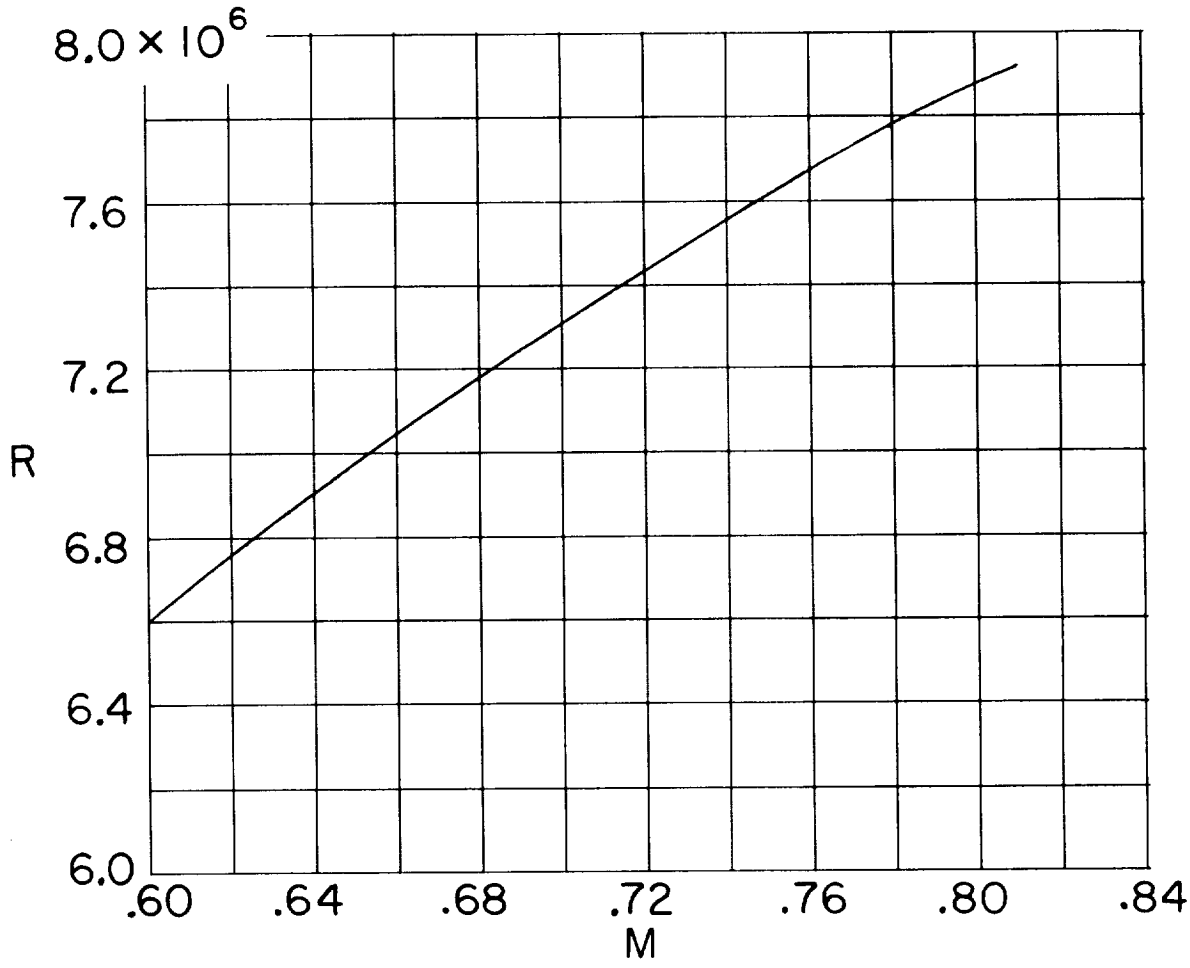

Figure 7.- Variation of test Reynolds number with Mach number.

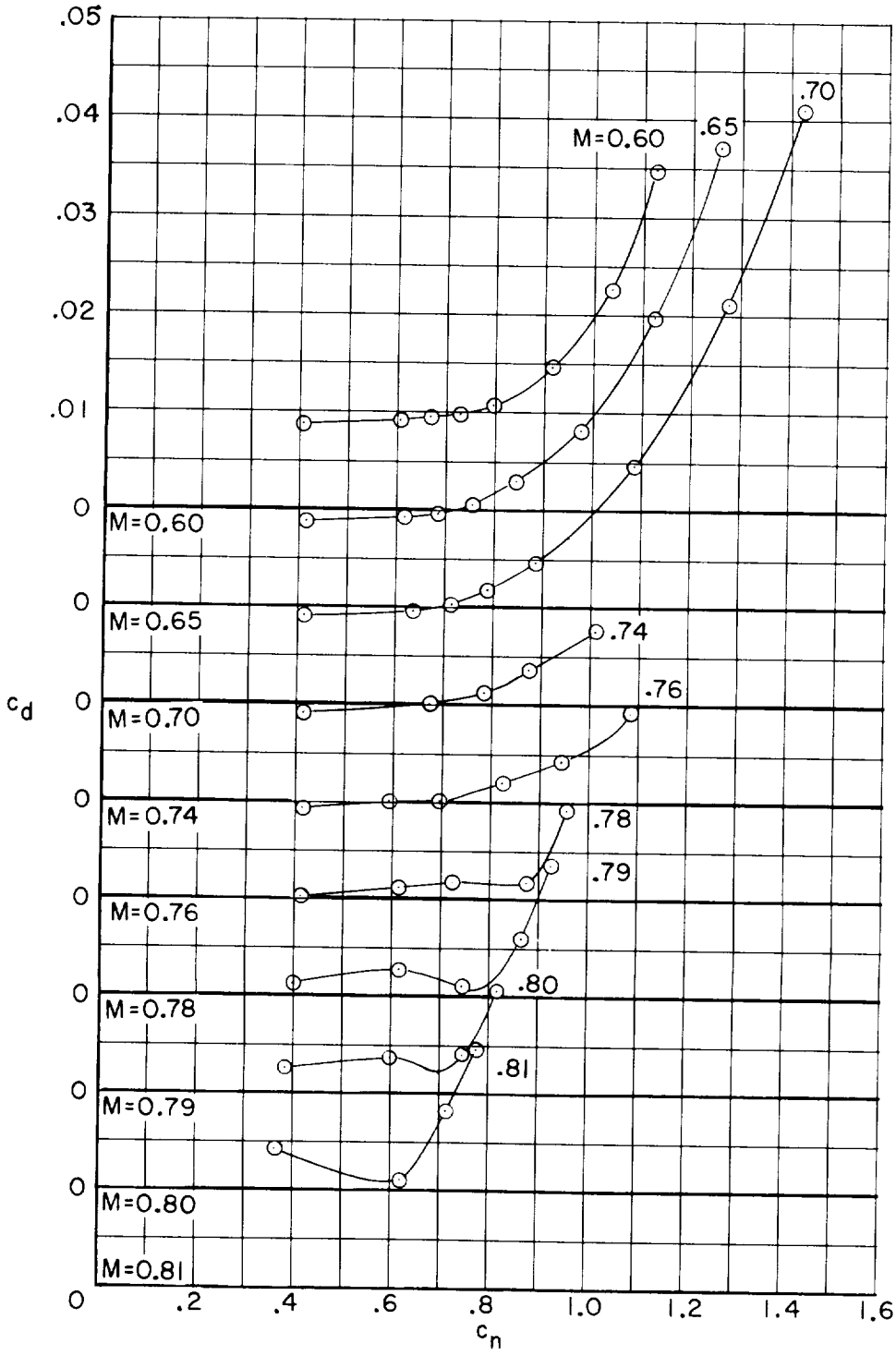

Figure 8.- Variation of section drag coefficient, angle of attack, and section pitching-moment coefficient at various Mach numbers for supercritical airfoil 9a.

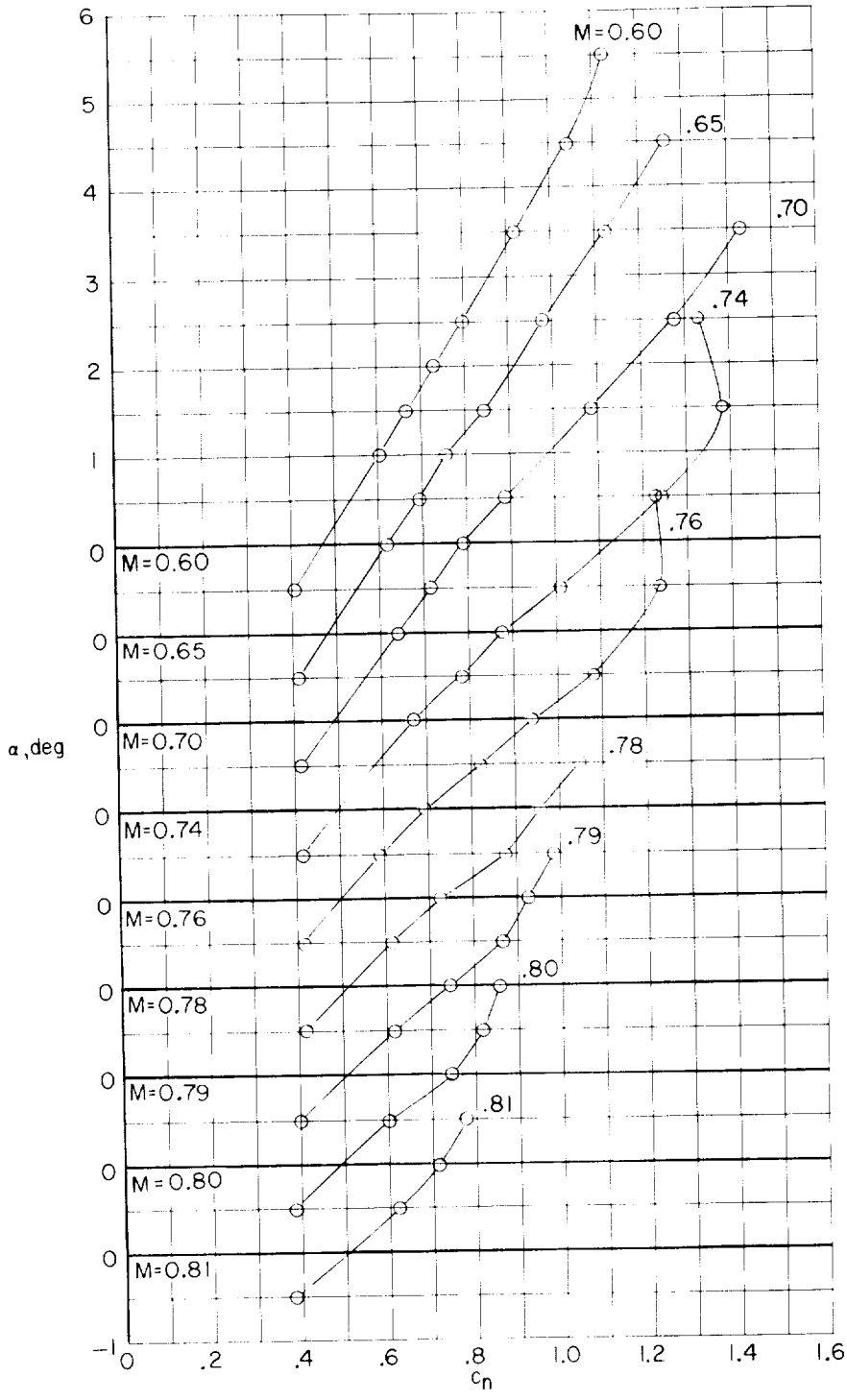

Figure 8.- Continued.

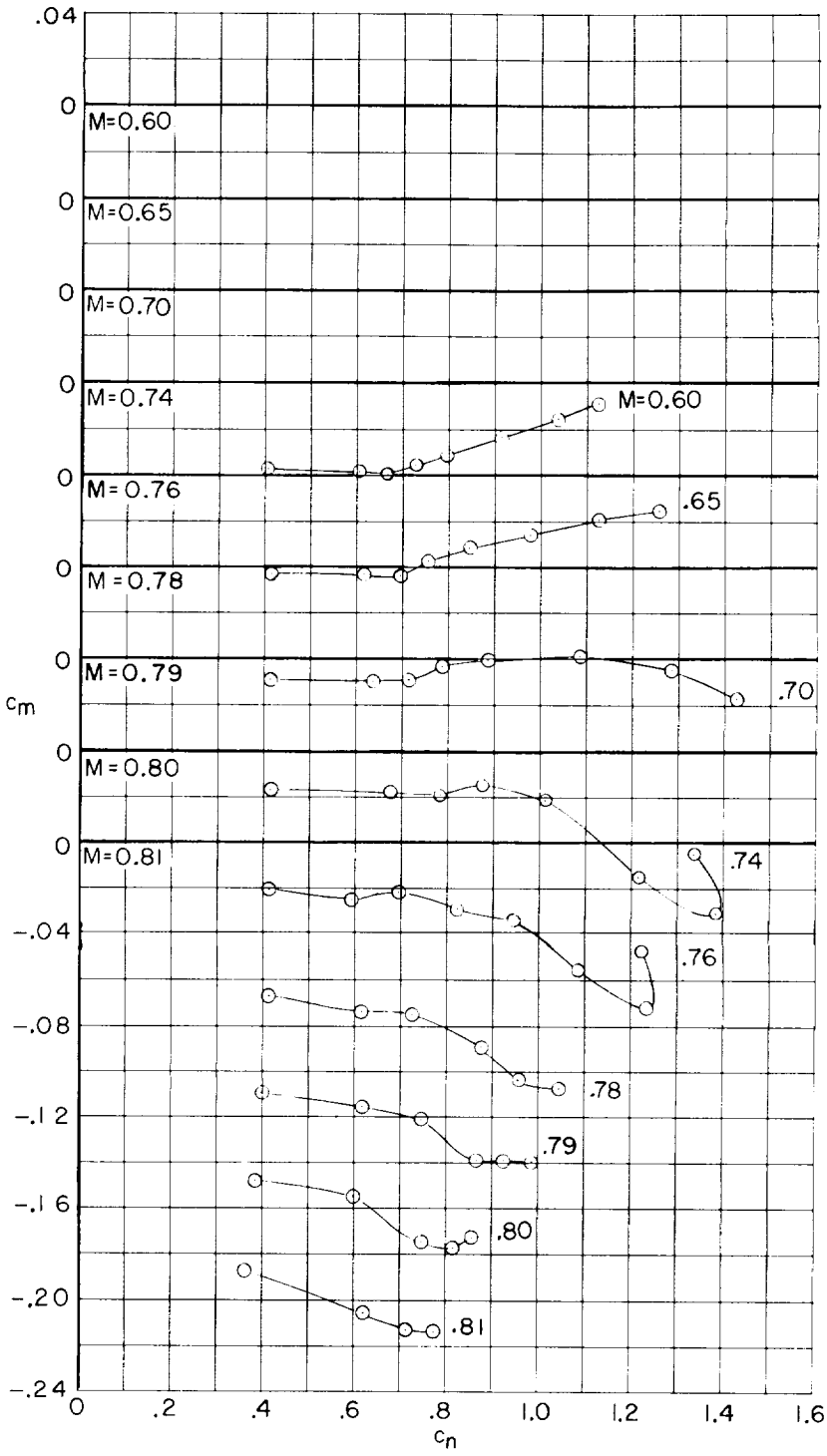

Figure 8.- Concluded.

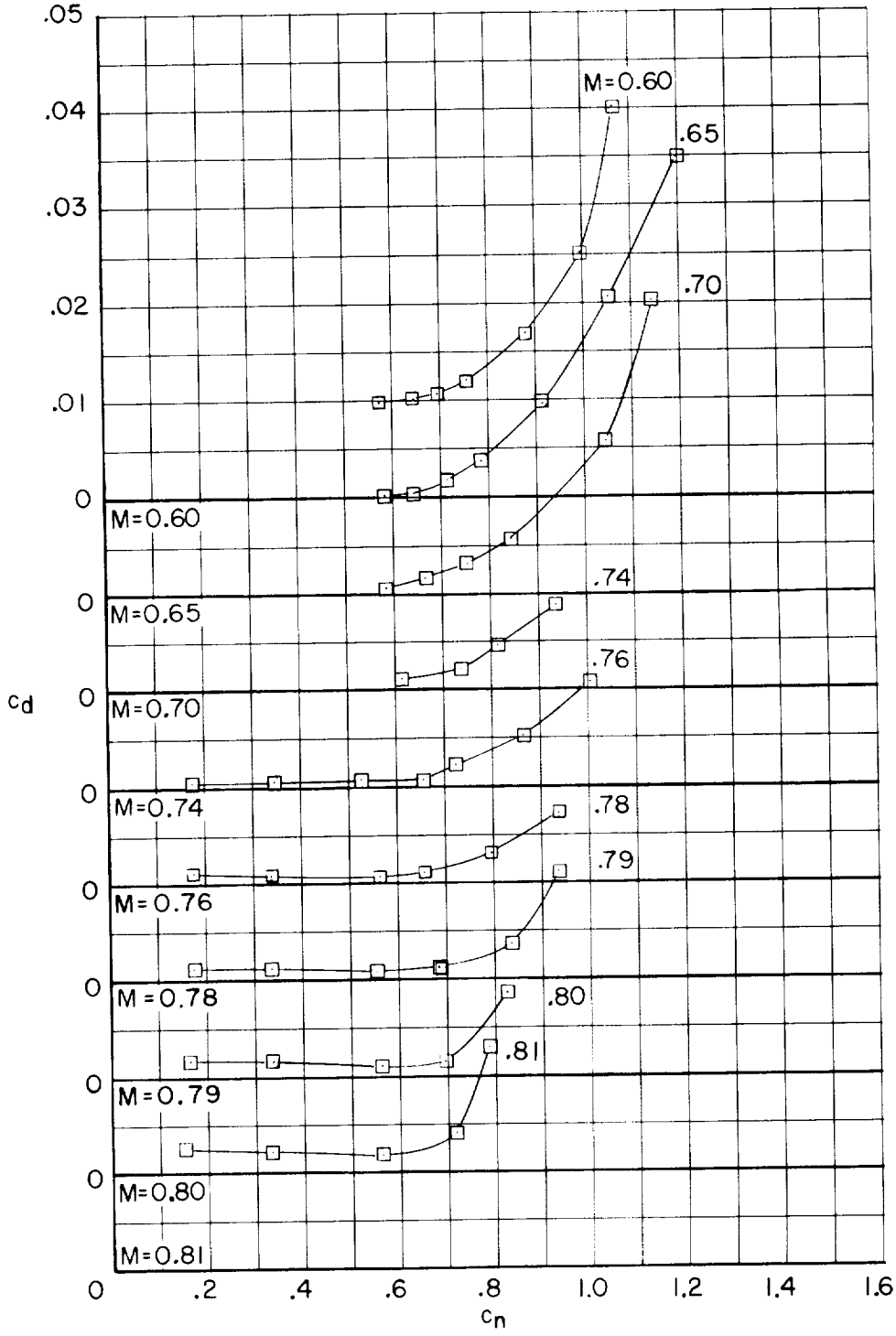

Figure 9.- Variation of section drag coefficient, angle of attack, and section pitching-moment coefficient at various Mach numbers for supercritical airfoil 8.

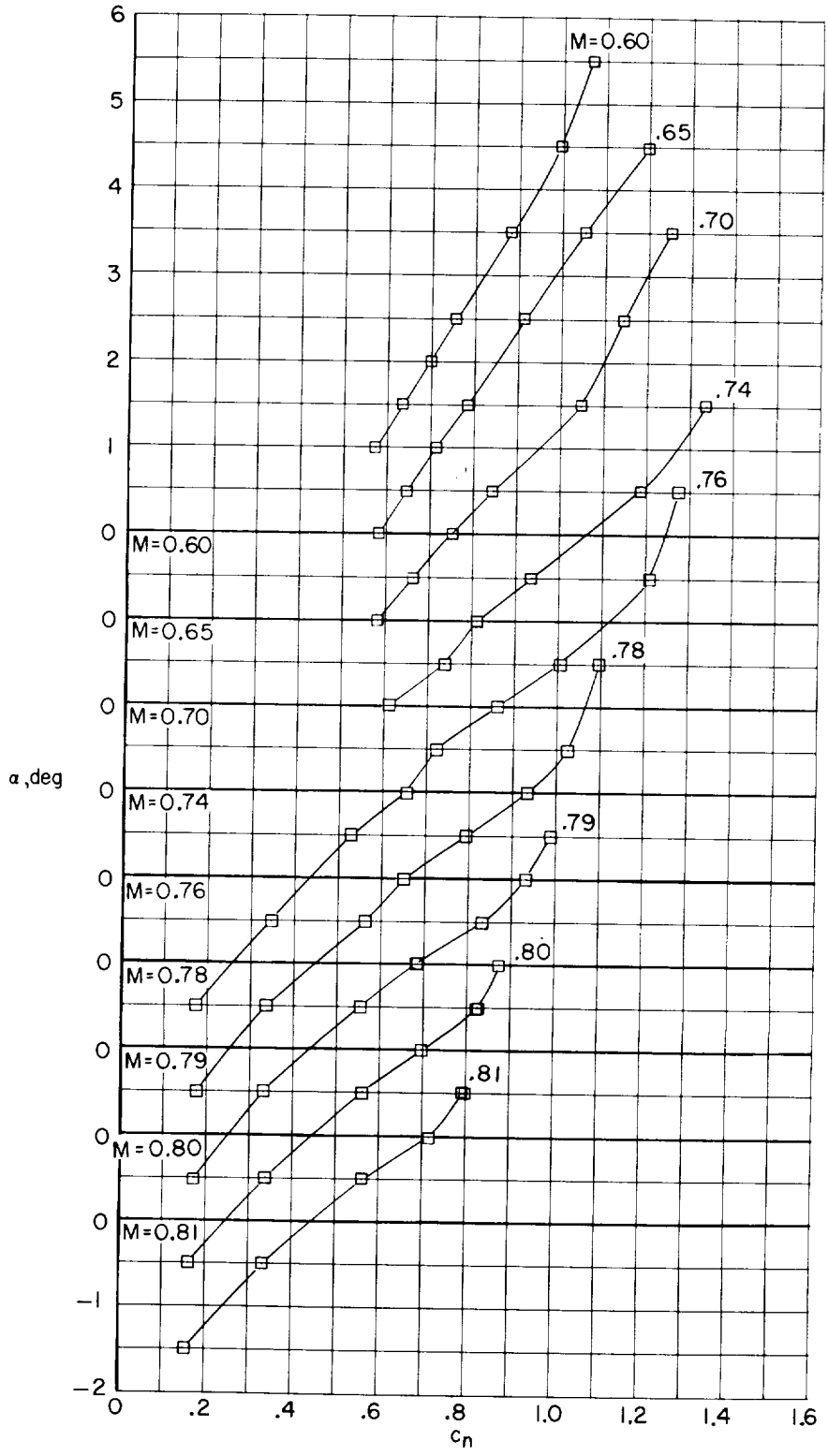

Figure 9.- Continued.

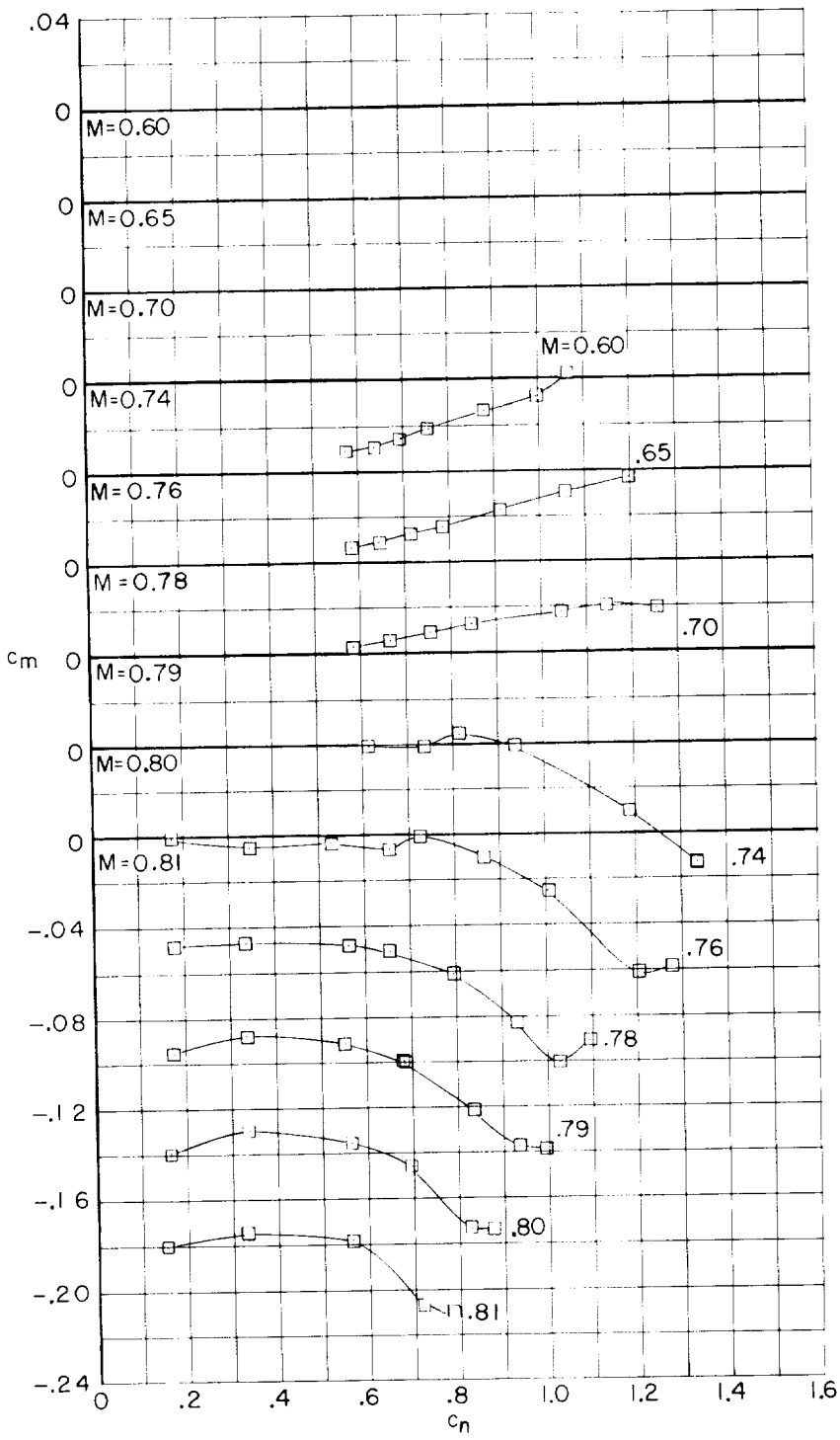

Figure 9.- Concluded.

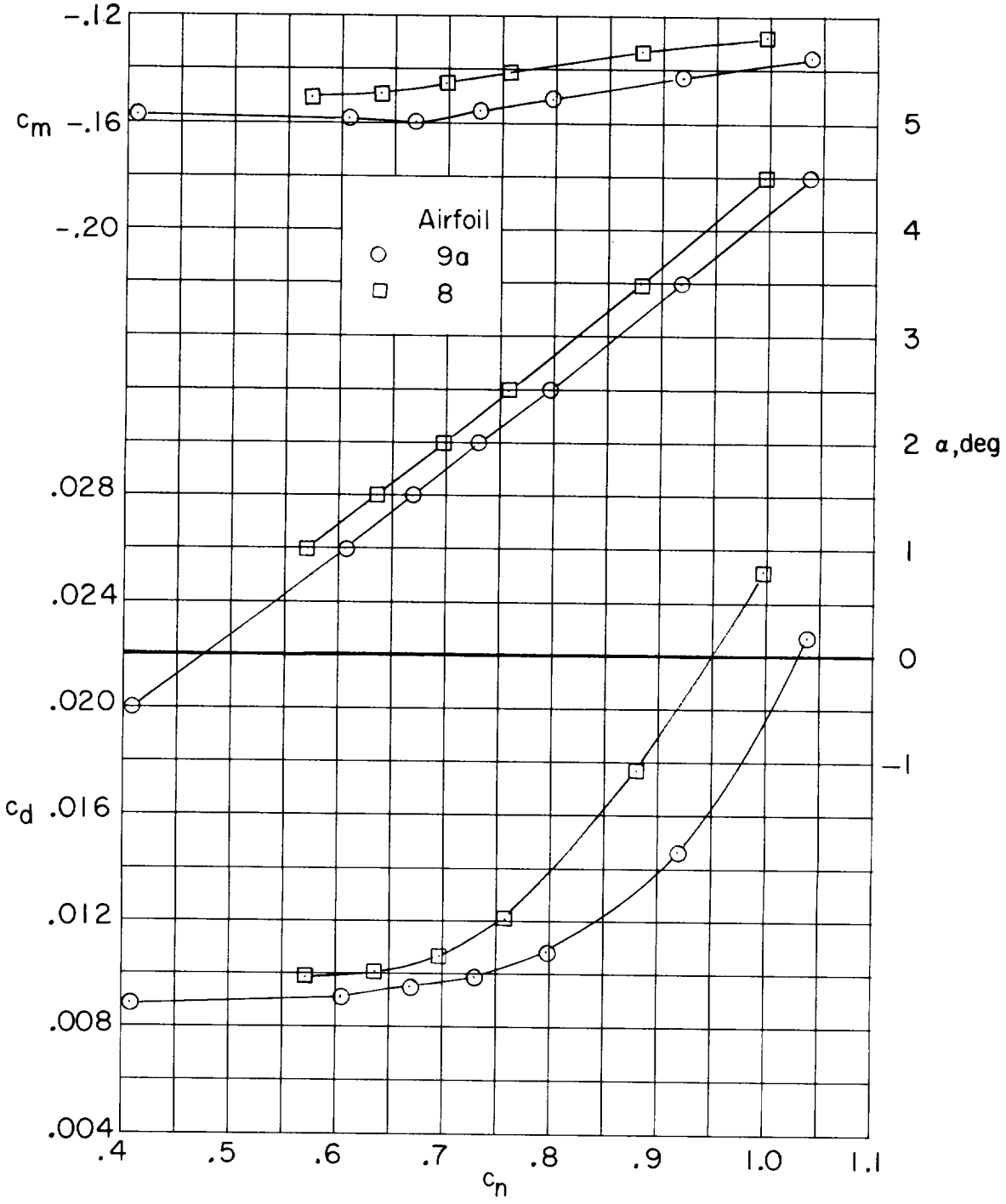

(a) M = 0.60.

Figure 10.- Comparison of aerodynamic characteristics of airfoils 9a and 8.

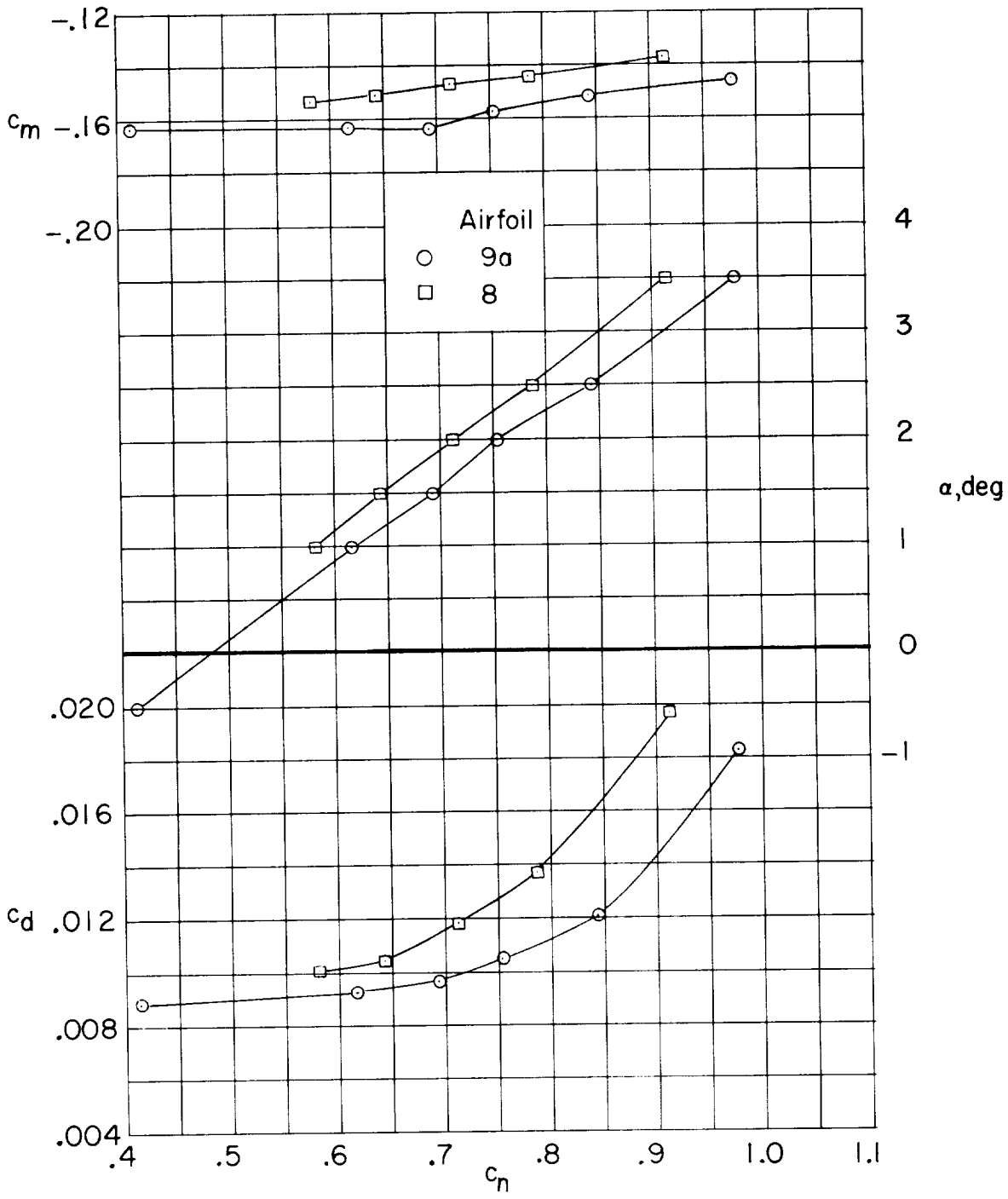

(b) M = 0.65.

Figure 10.- Continued.

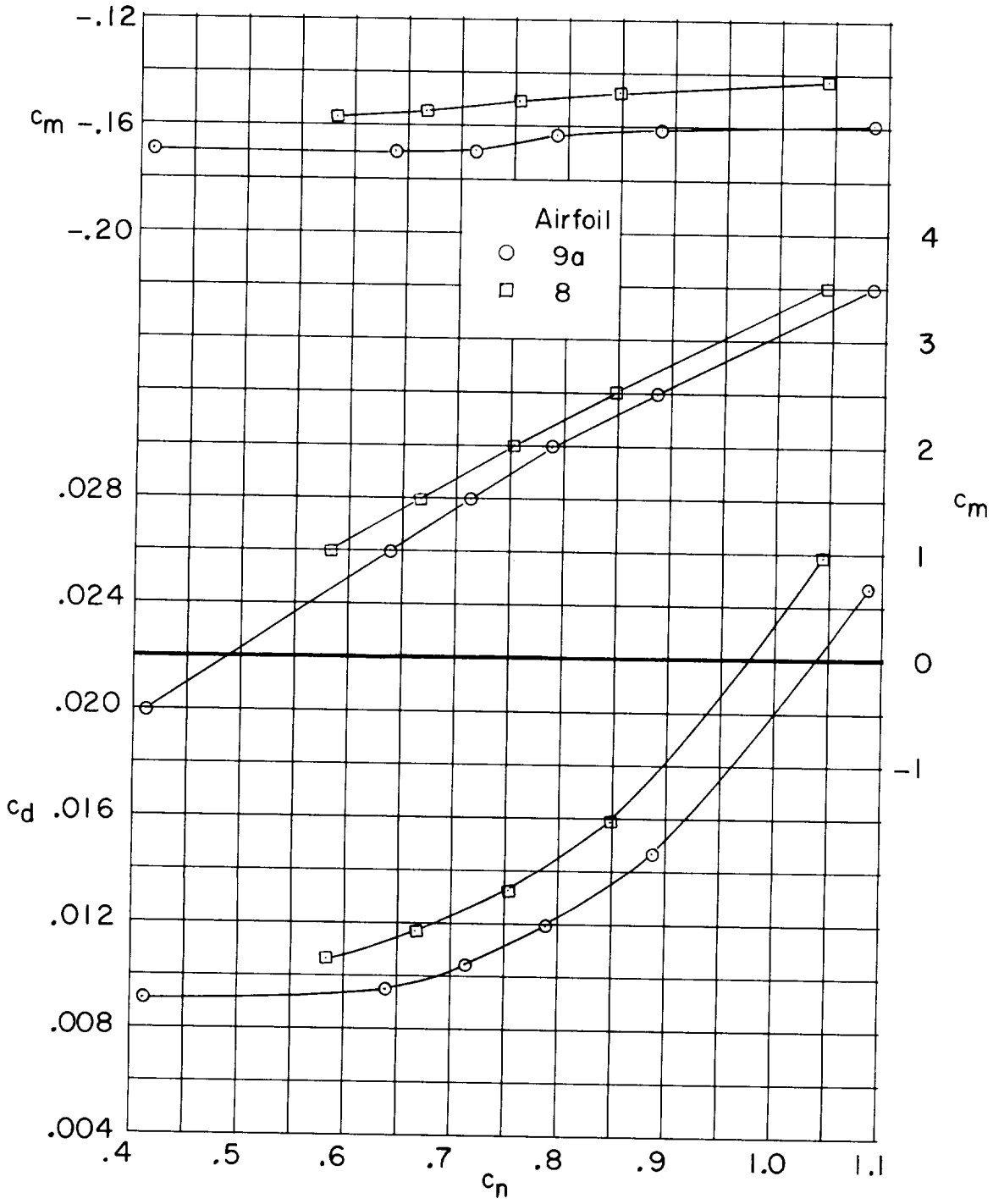

(c) M = 0.70.

Figure 10.- Continued.

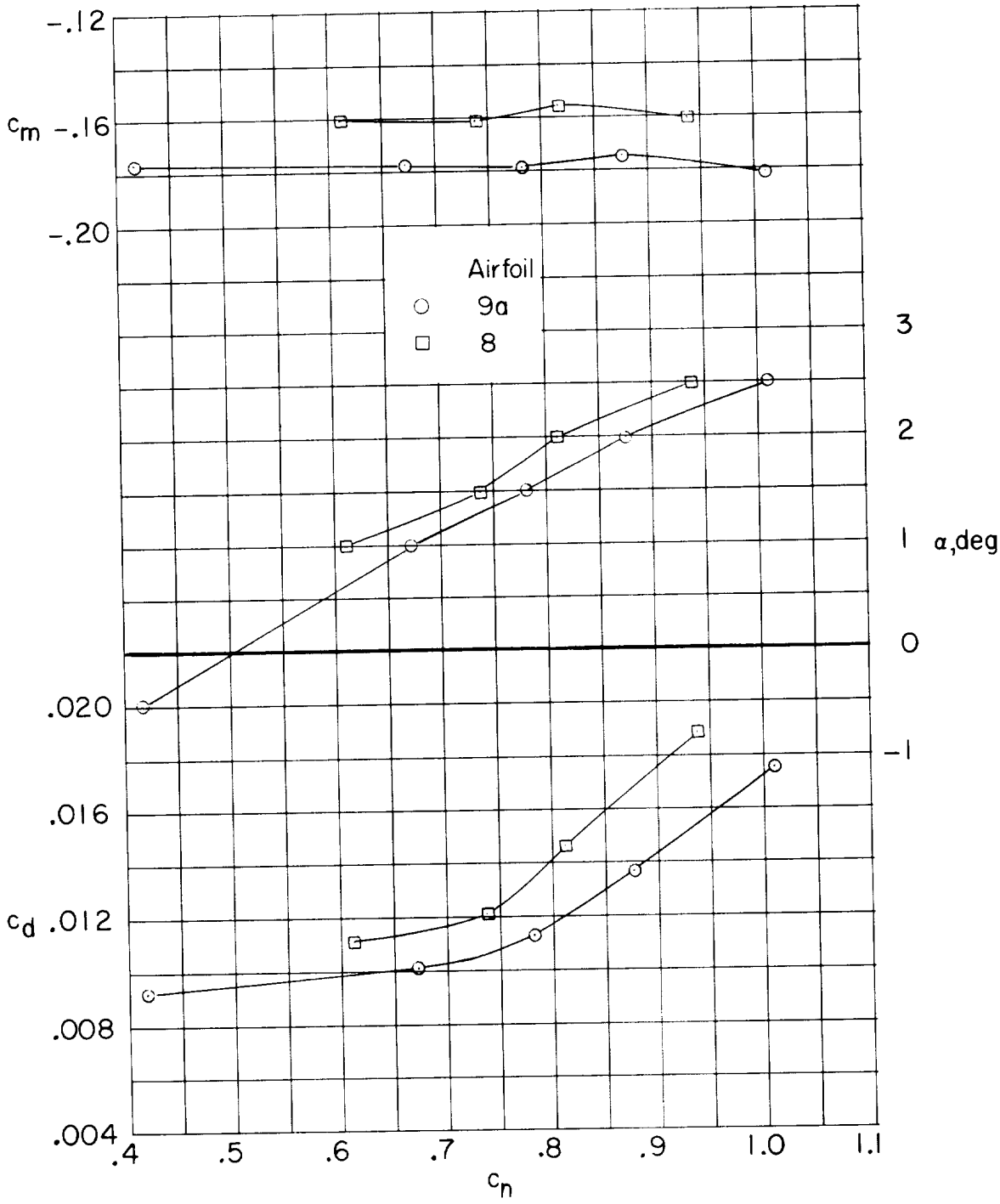

(d) M = 0.74.

Figure 10.- Continued.

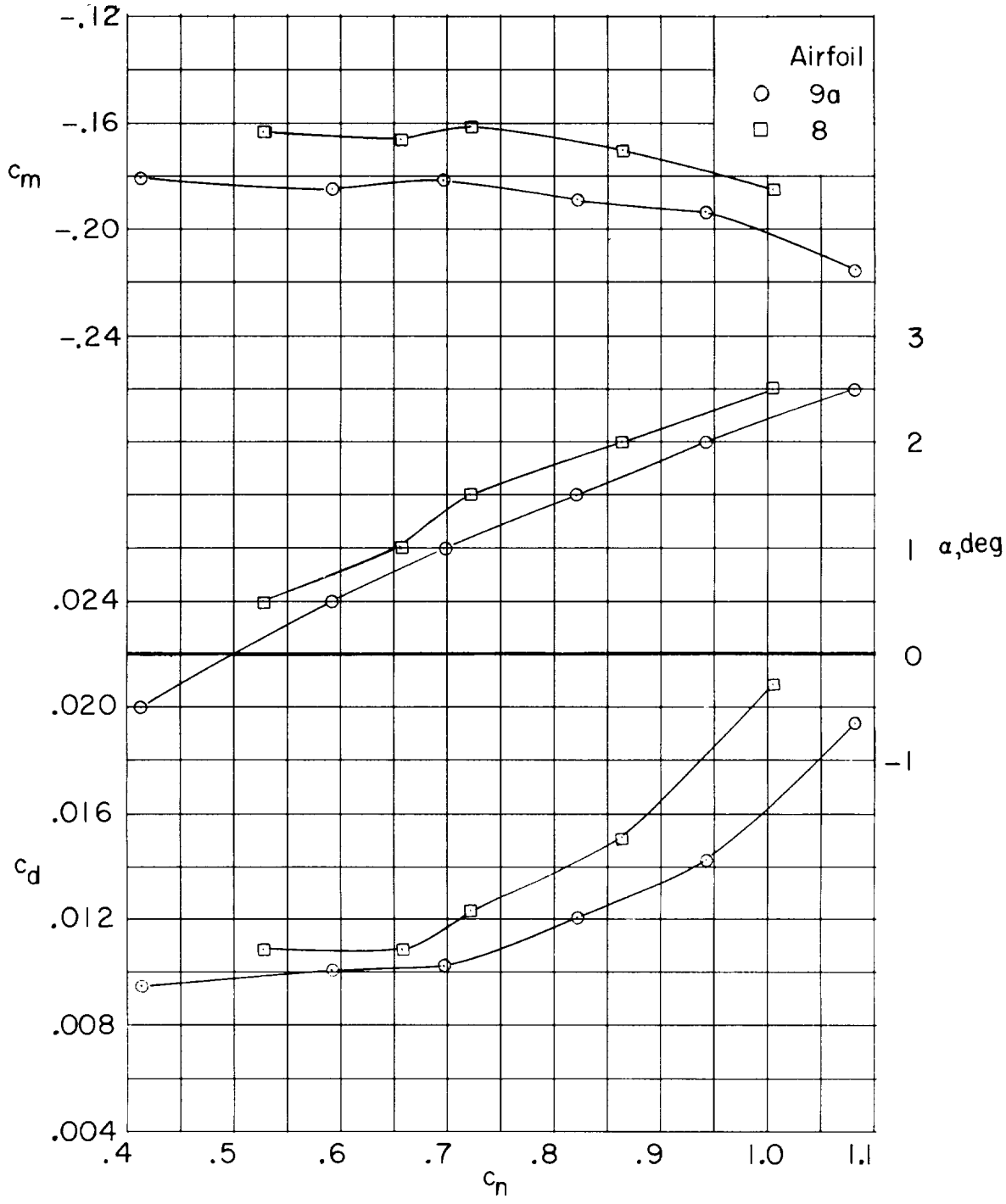

(e) M = 0.76.

Figure 10.- Continued.

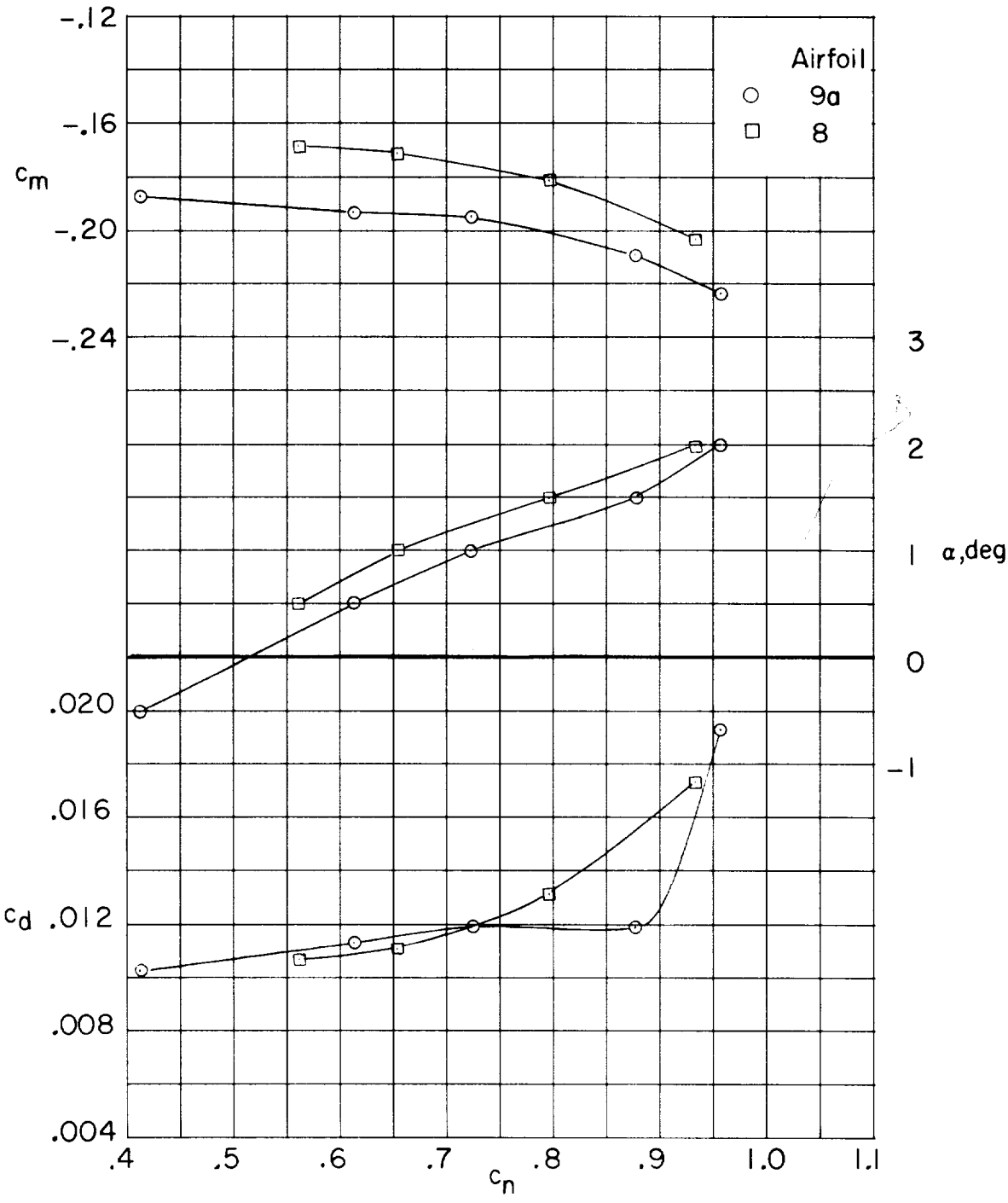

(f) M = 0.78.

Figure 10.- Continued.

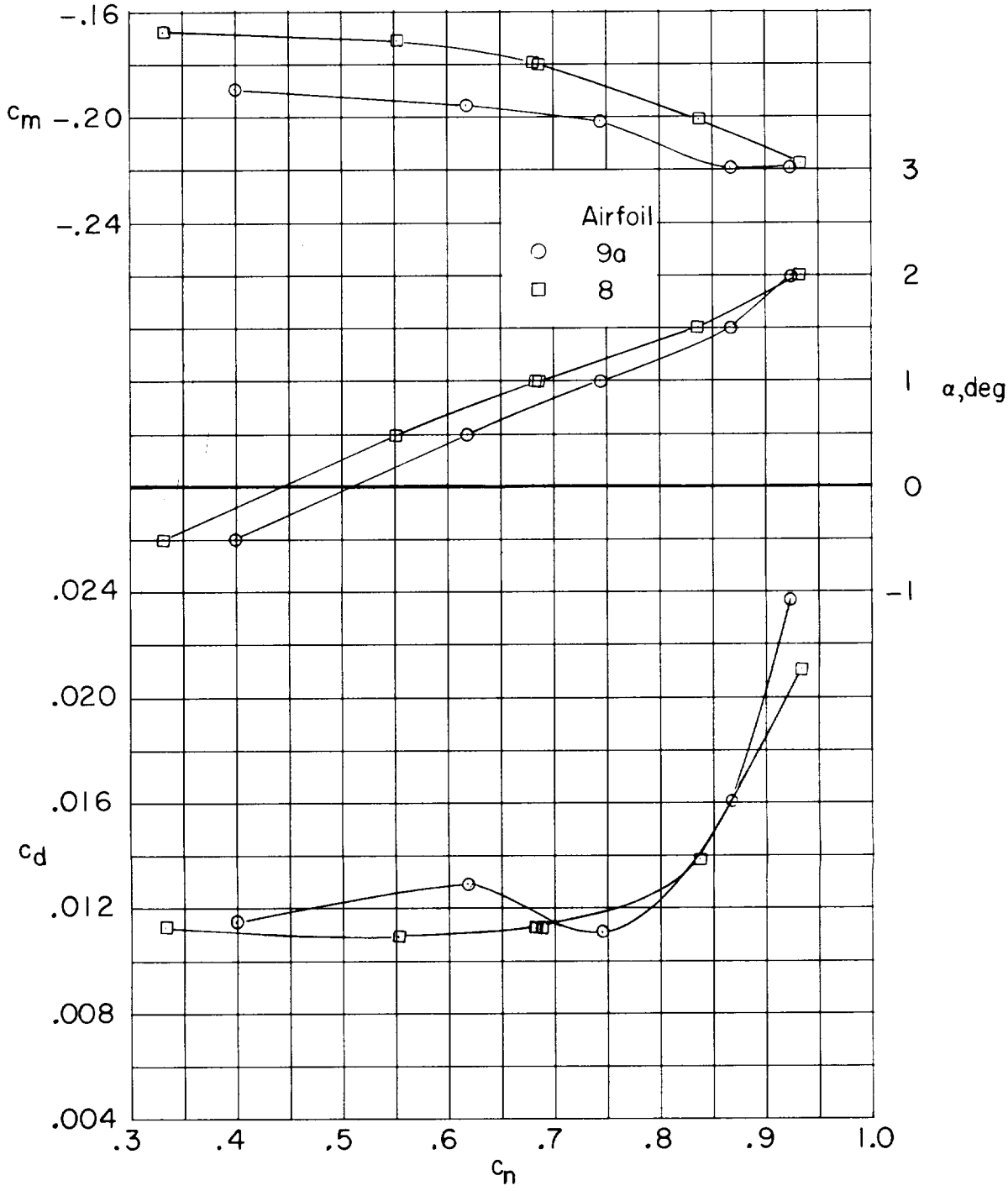

(g) M = 0.79.

Figure 10.- Continued.

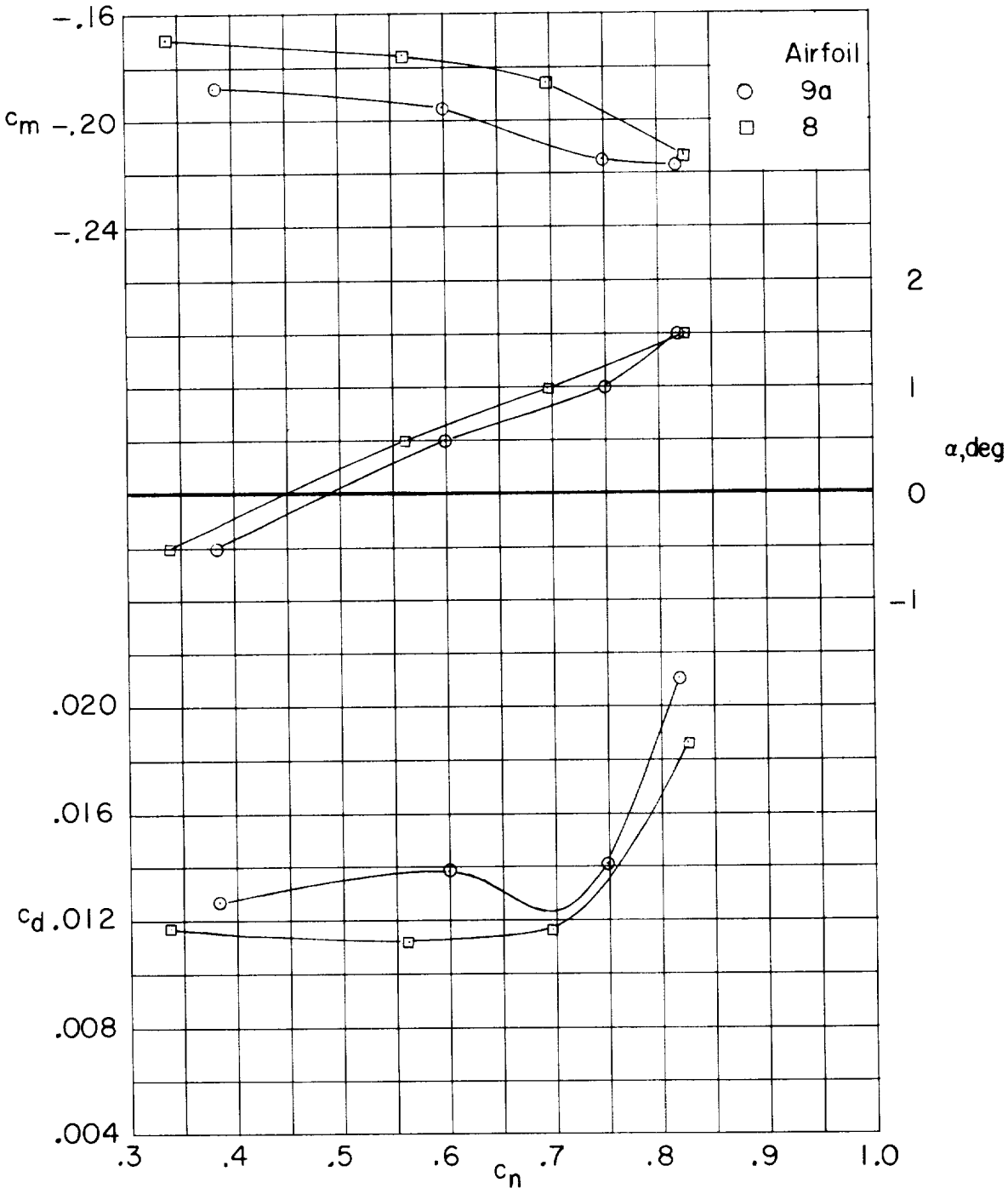

(h) M = 0.80.

Figure 10.- Continued.

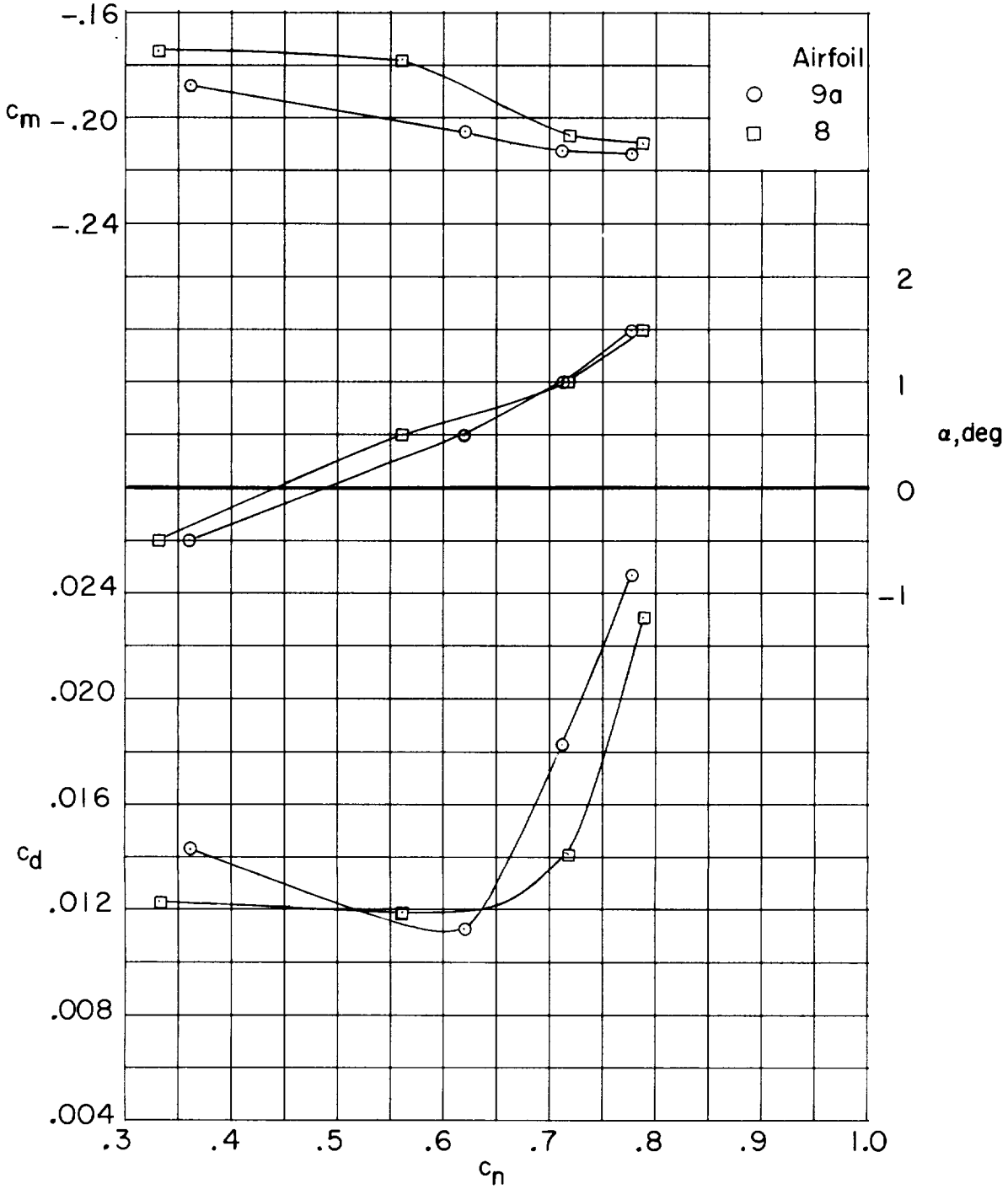

(i) M = 0.81.

Figure 10.- Concluded.

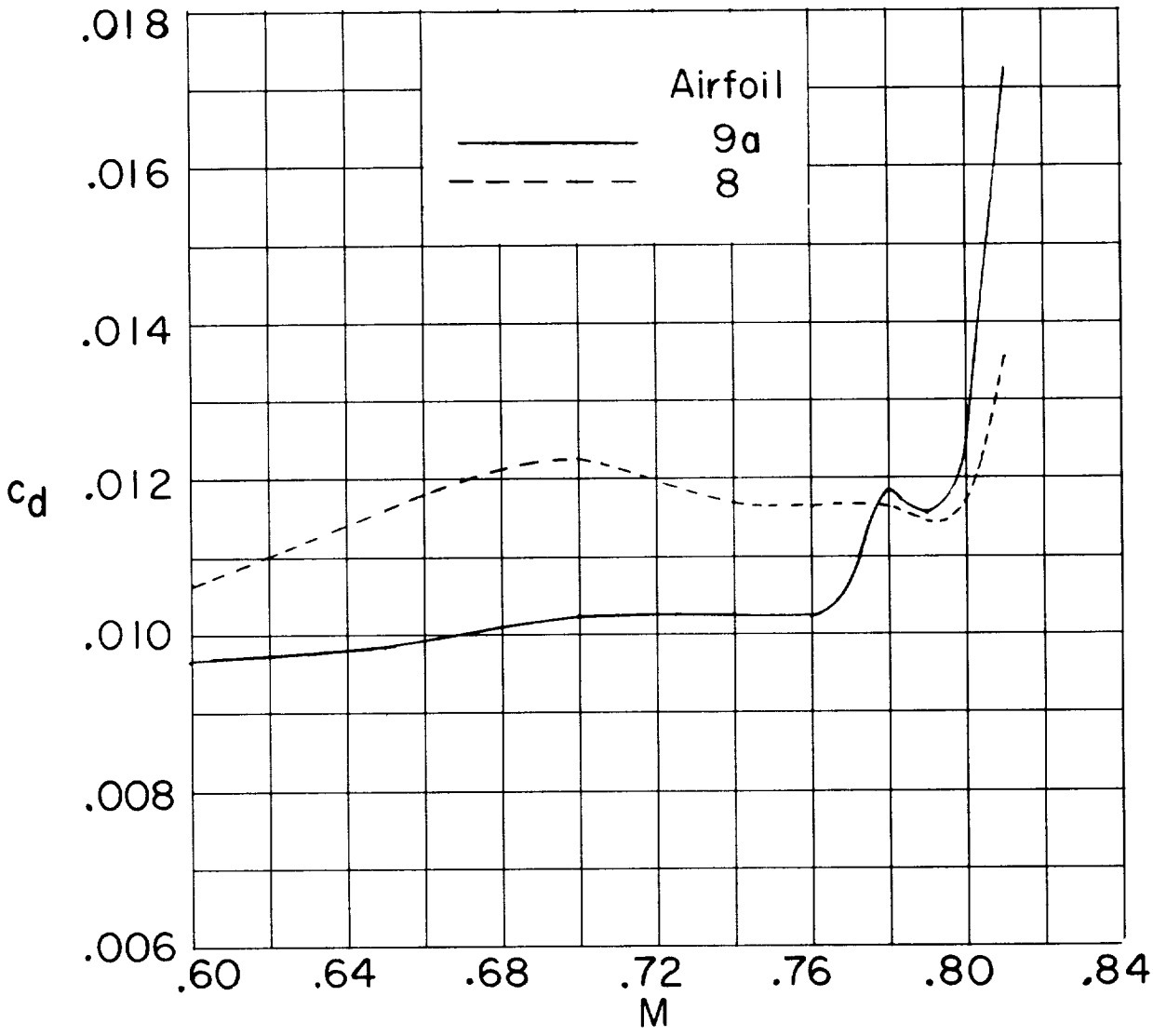

Figure 11.- Variation of section drag coefficient with Mach number at a normal-force coefficient of 0.70.

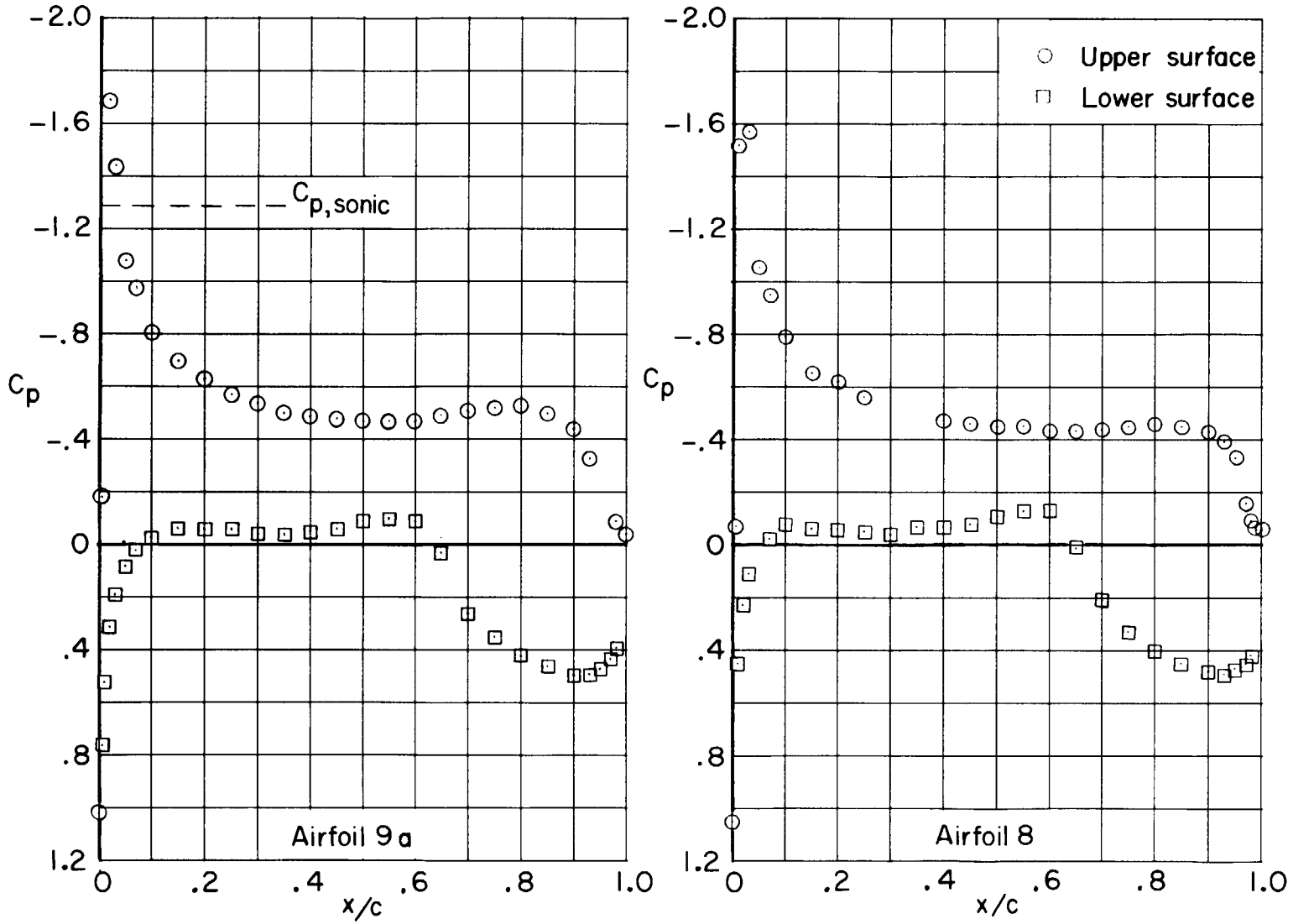

(a) M = 0.60; $\alpha = 1.5^{\circ}$.

Figure 12.- Chordwise pressure distribution for angles of attack near the design normal-force coefficient of 0.70.

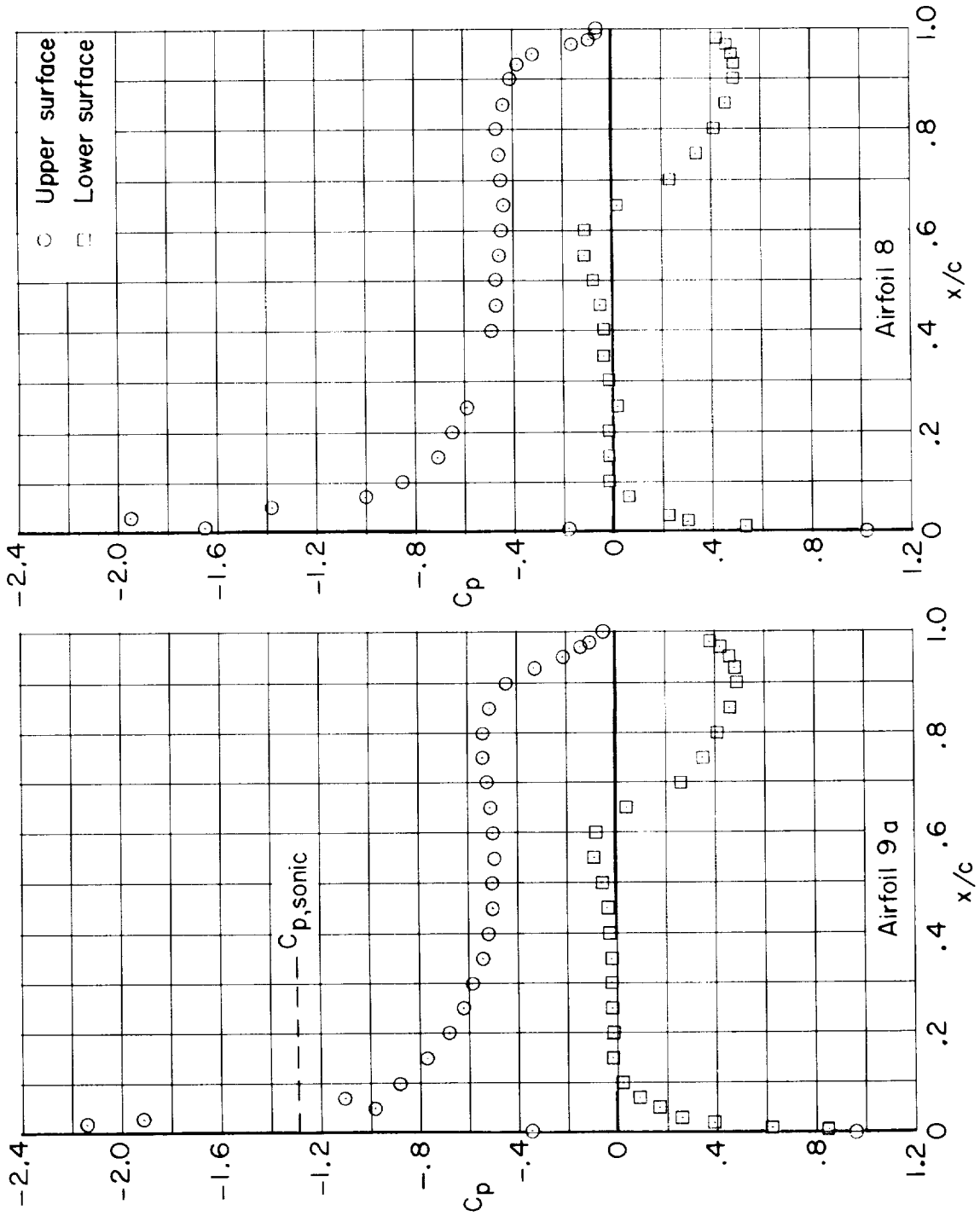

(b) M = 0.60; $\alpha = 2^0$.

Figure 12.- Continued.

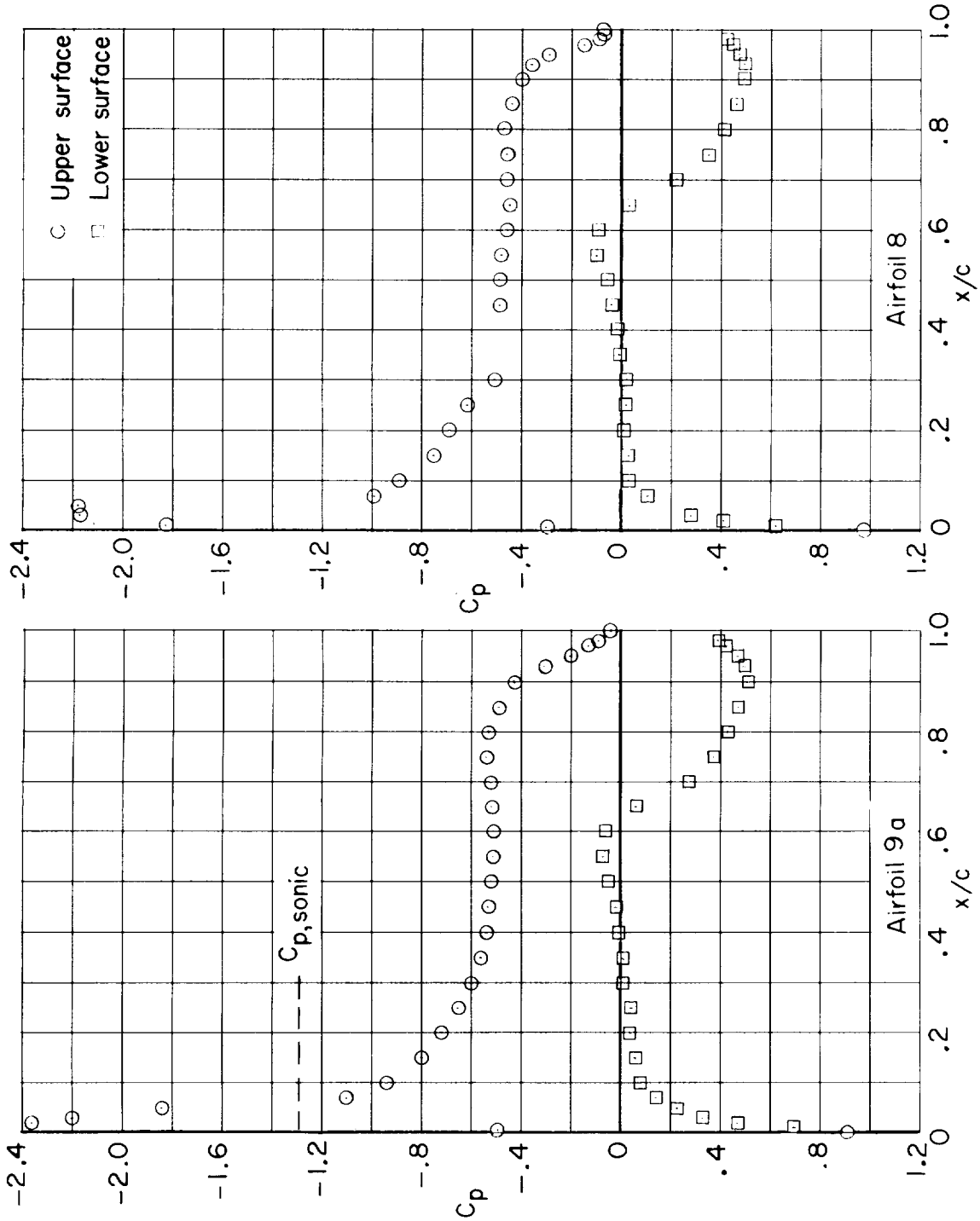

(c) M = 0.60; $\alpha = 2.5^{\circ}$.

Figure 12.- Continued.

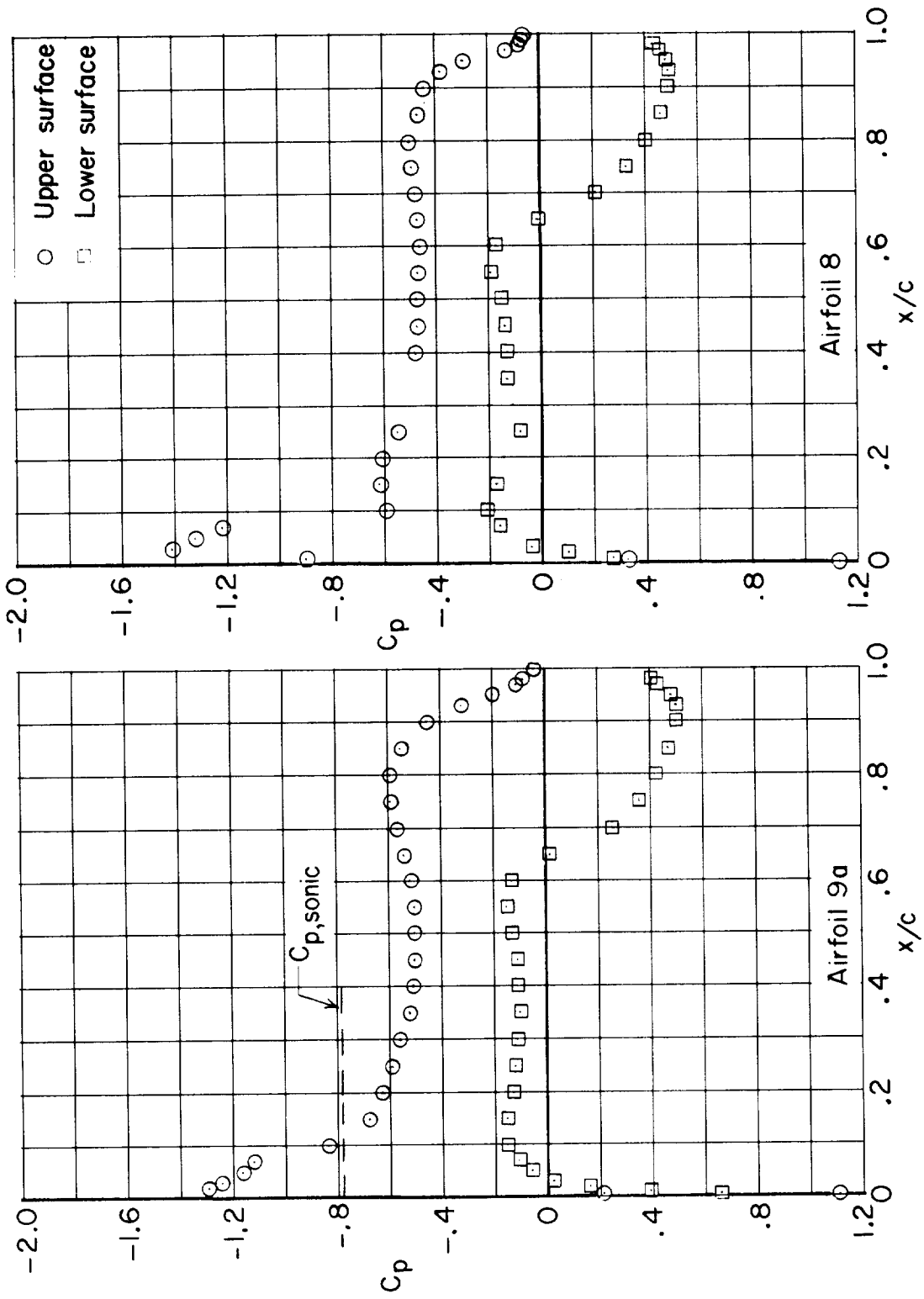

(d) $M = 0.70$; $\alpha = 1^\circ$.

Figure 12.- Continued.

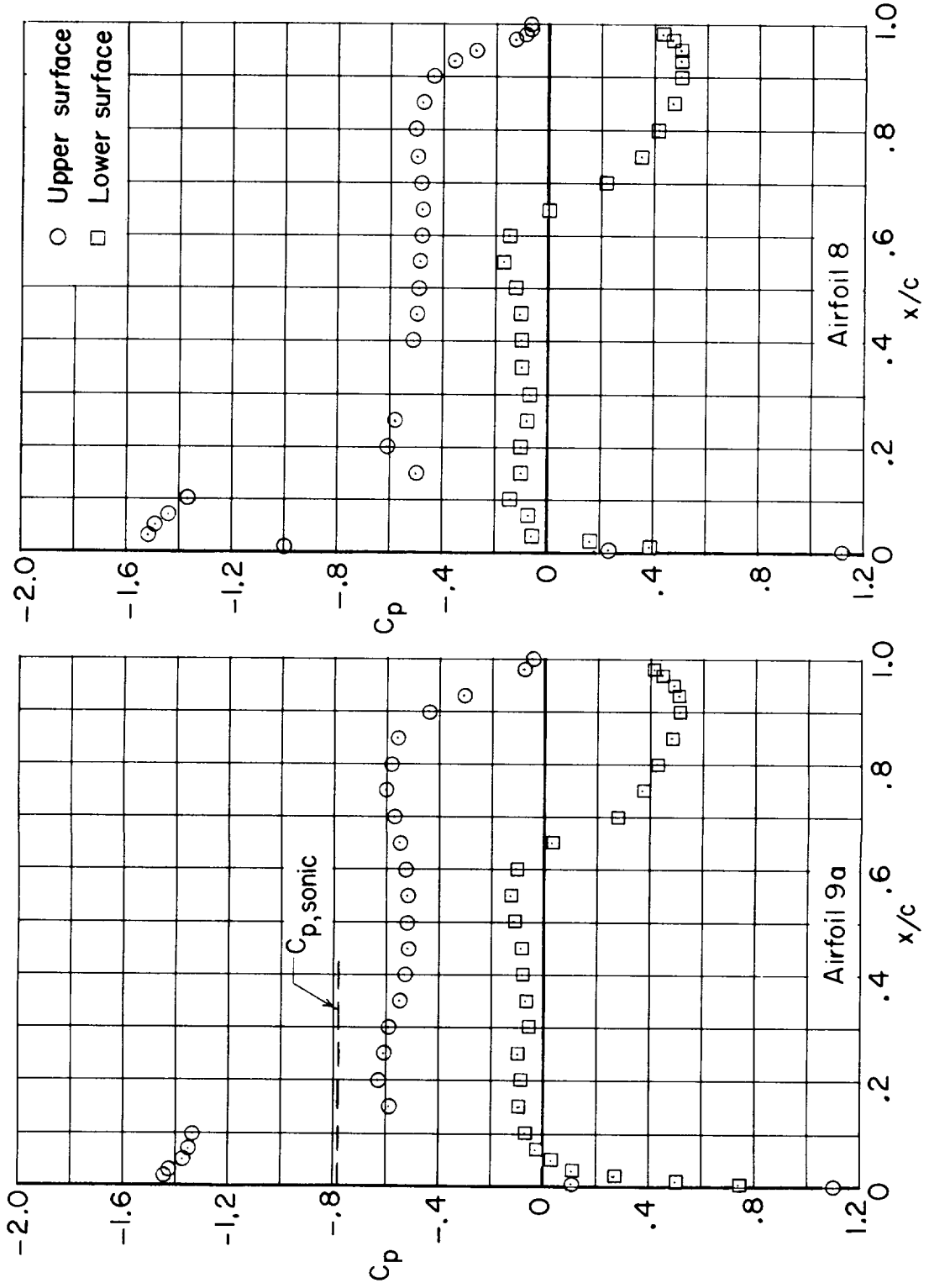

(e) M = 0.70; $\alpha = 1.5^{\circ}$.

Figure 12.- Continued.

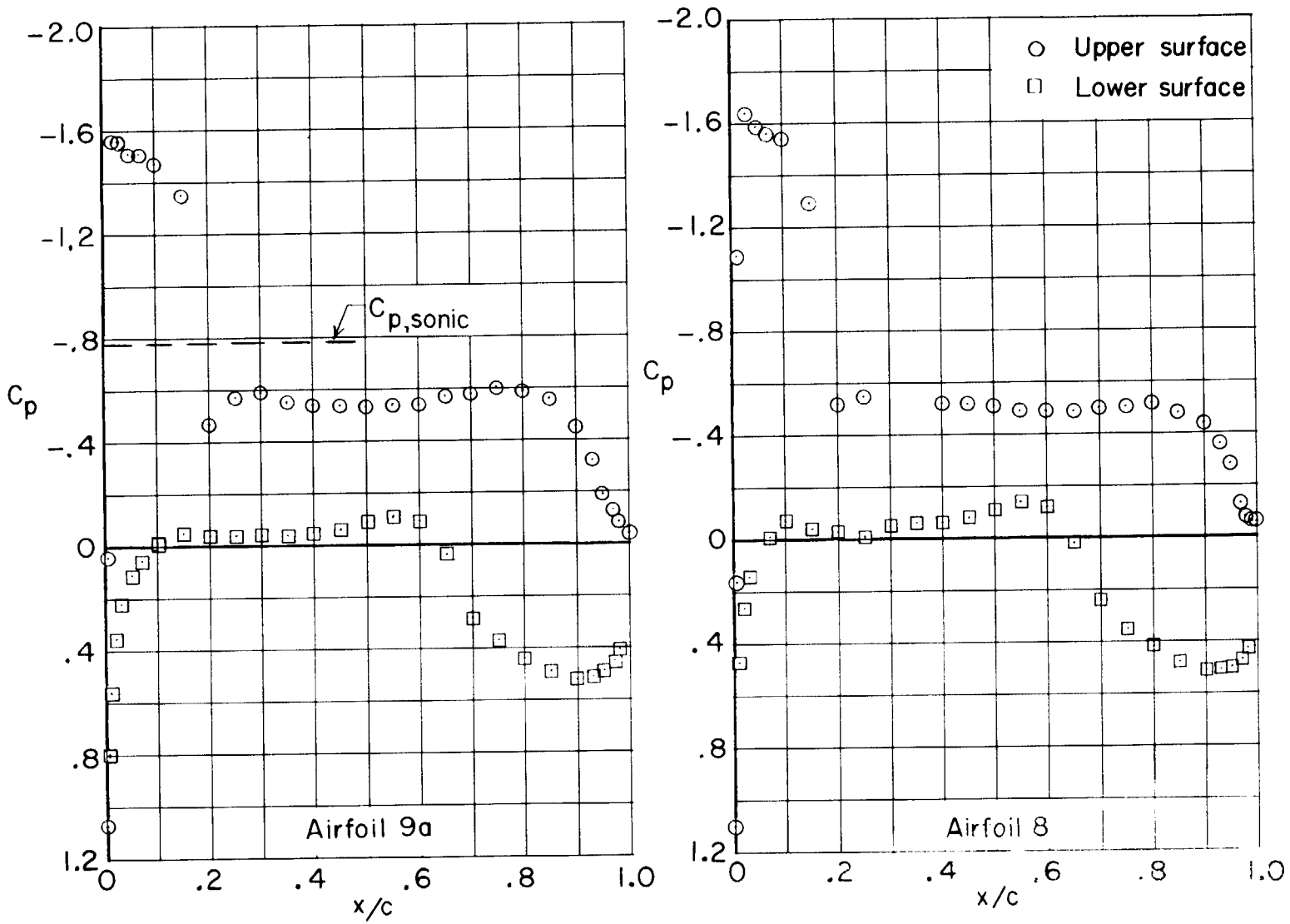

(f) M = 0.70; $\alpha = 2^{o}$.

Figure 12.- Continued.

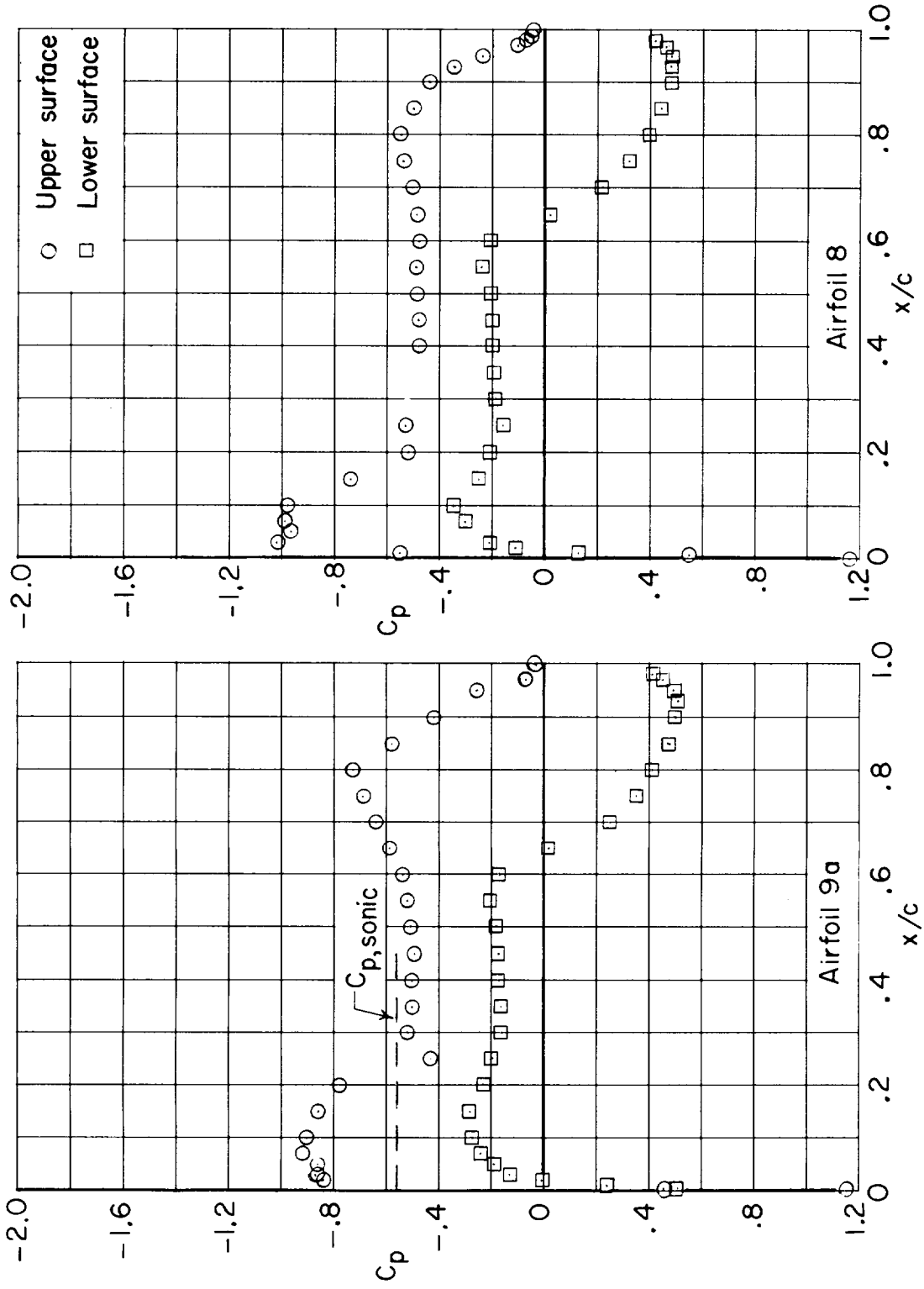

(g) M = 0.76; $\alpha = 0.5^{\circ}$.

Figure 12.- Continued.

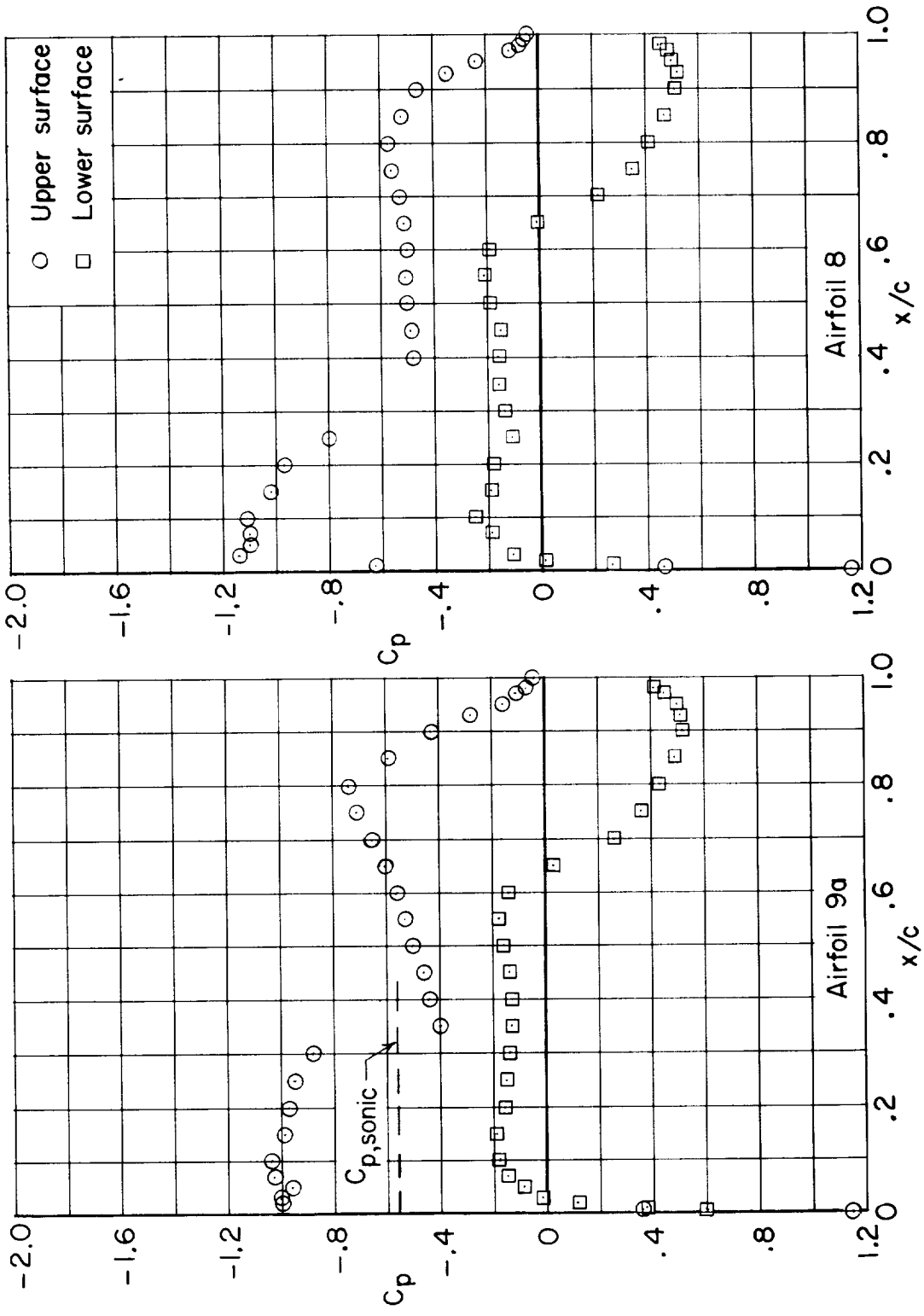

(h) M = 0.76; $\alpha = 1^{\circ}$.

Figure 12.- Continued.

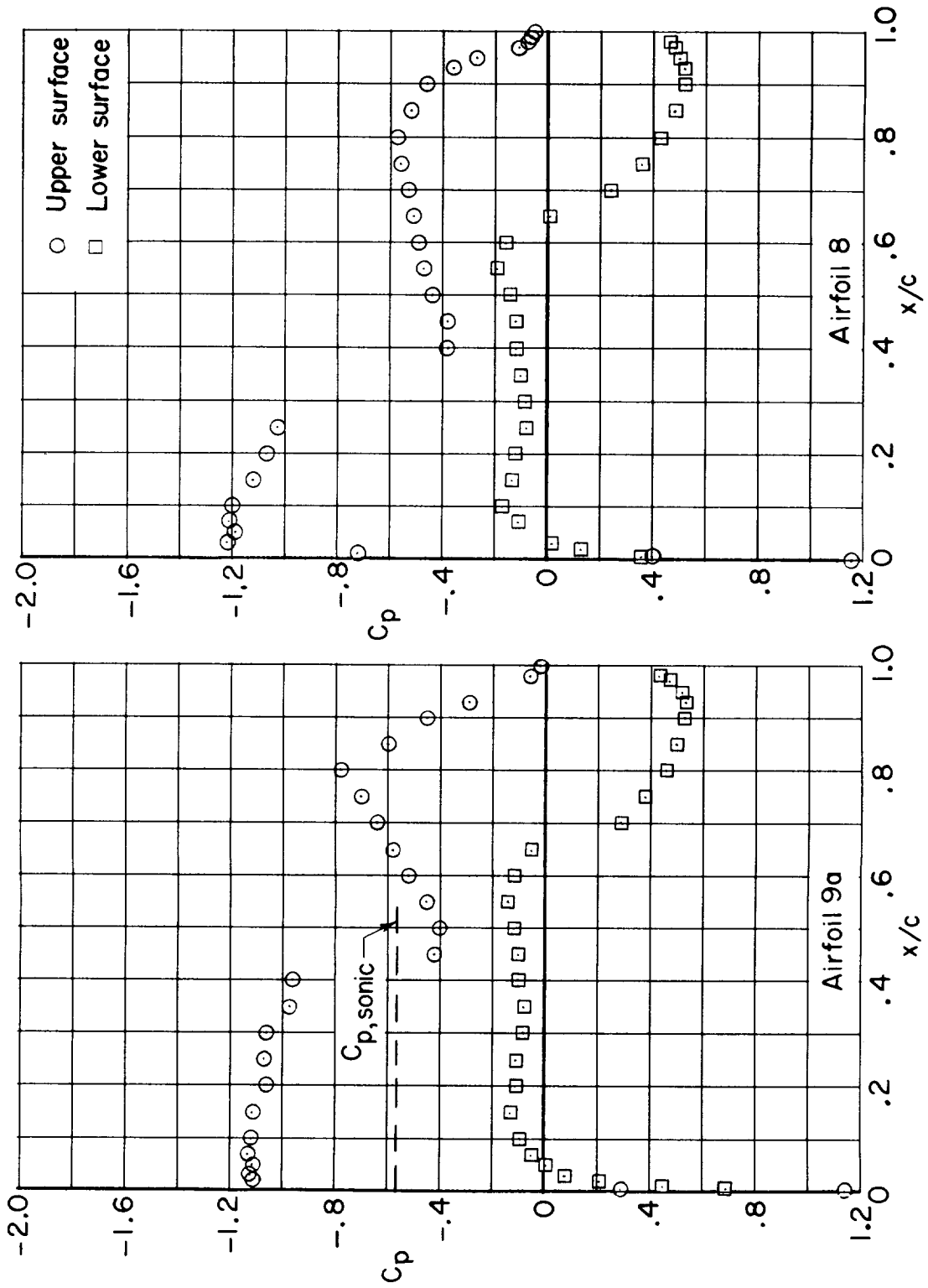

(i) M = 0.76; $\alpha = 1.5^{\circ}$.

Figure 12.- Continued.

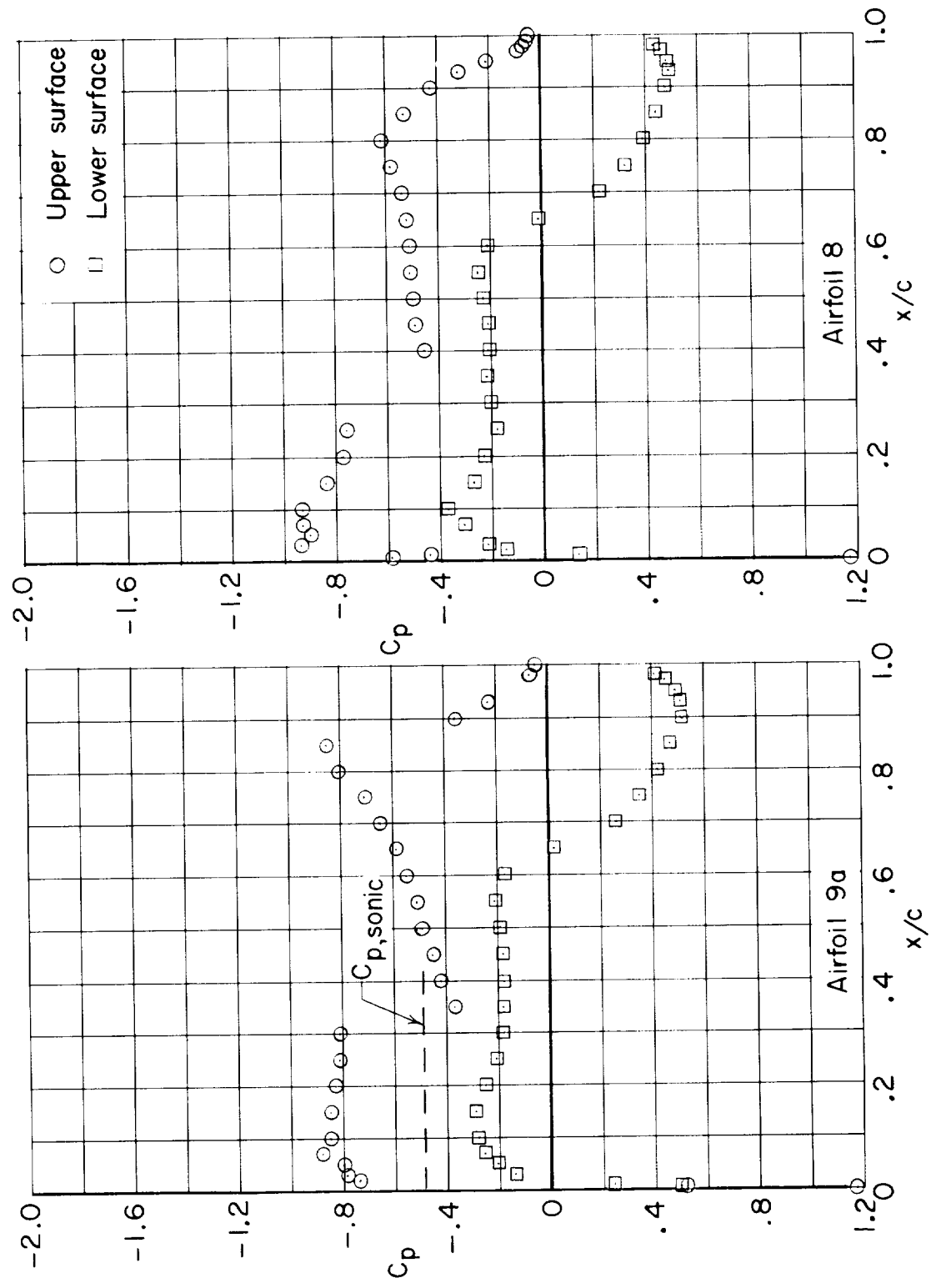

(j) M = 0.78; $\alpha = 0.5^{\circ}$.

Figure 12.- Continued.

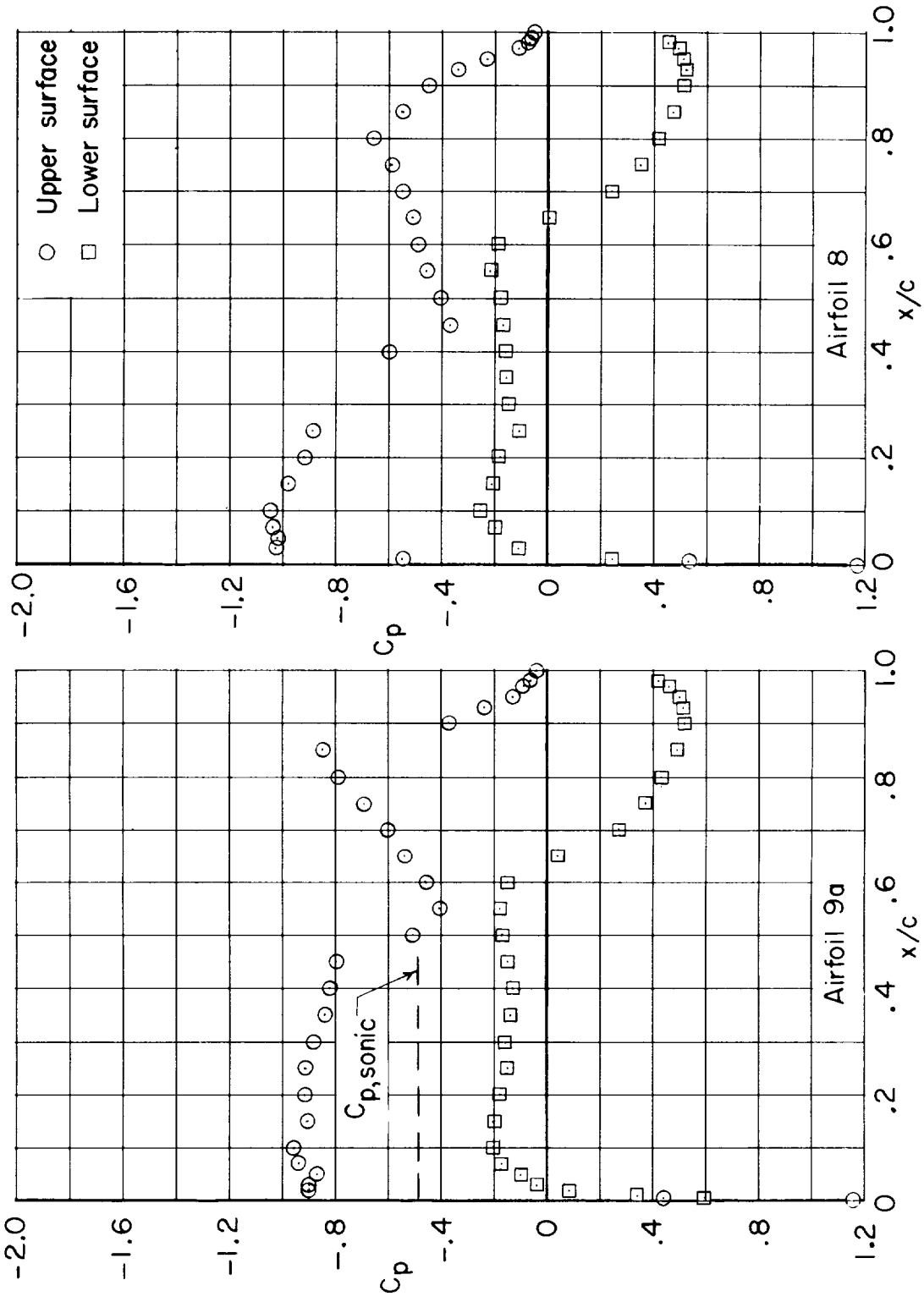

(k) M = 0.78; $\alpha = 1^{\circ}$.

Figure 12.- Continued.

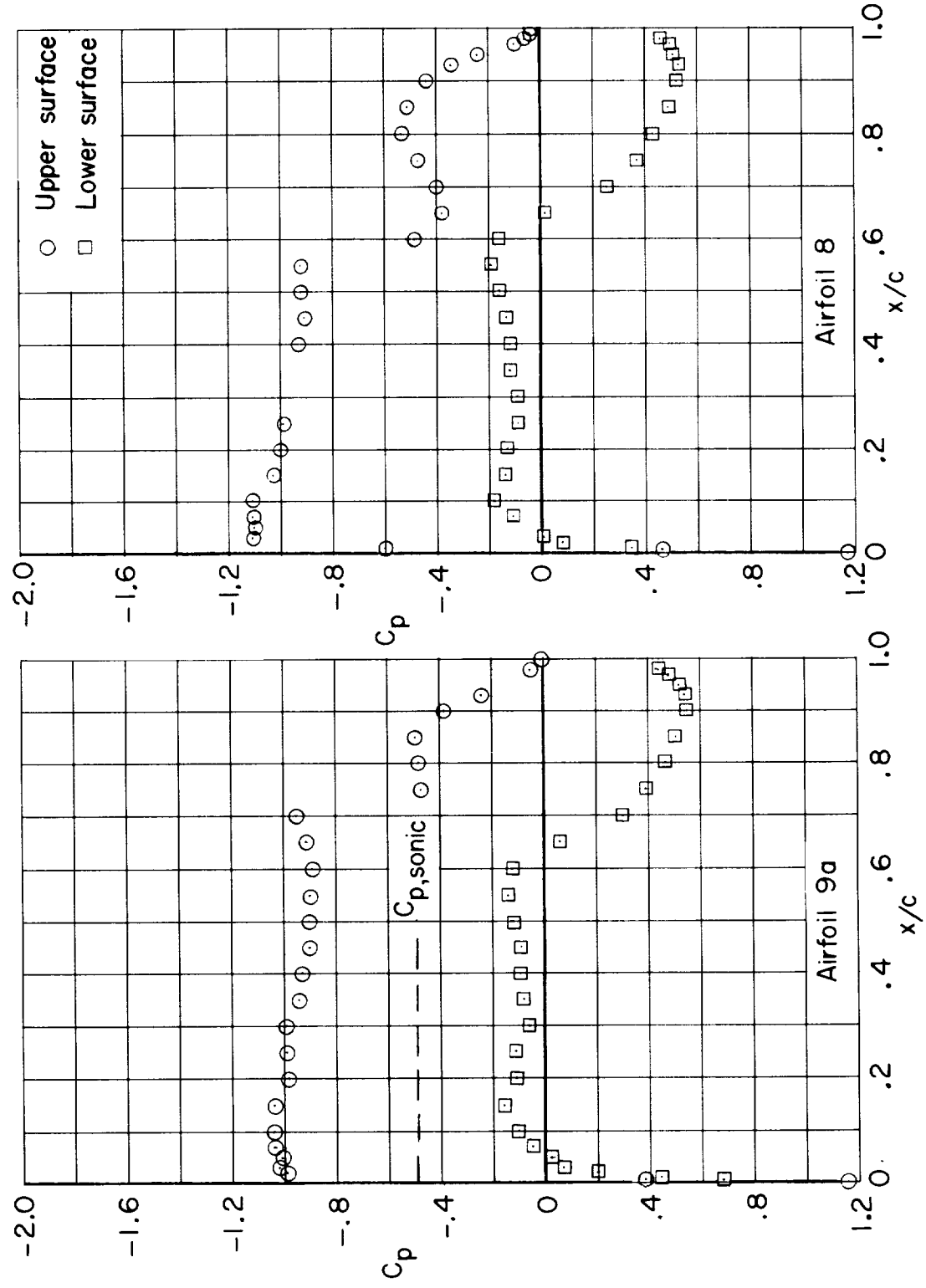

(l) $M = 0.78$; $\alpha = 1.5^{\circ}$.

Figure 12.- Continued.

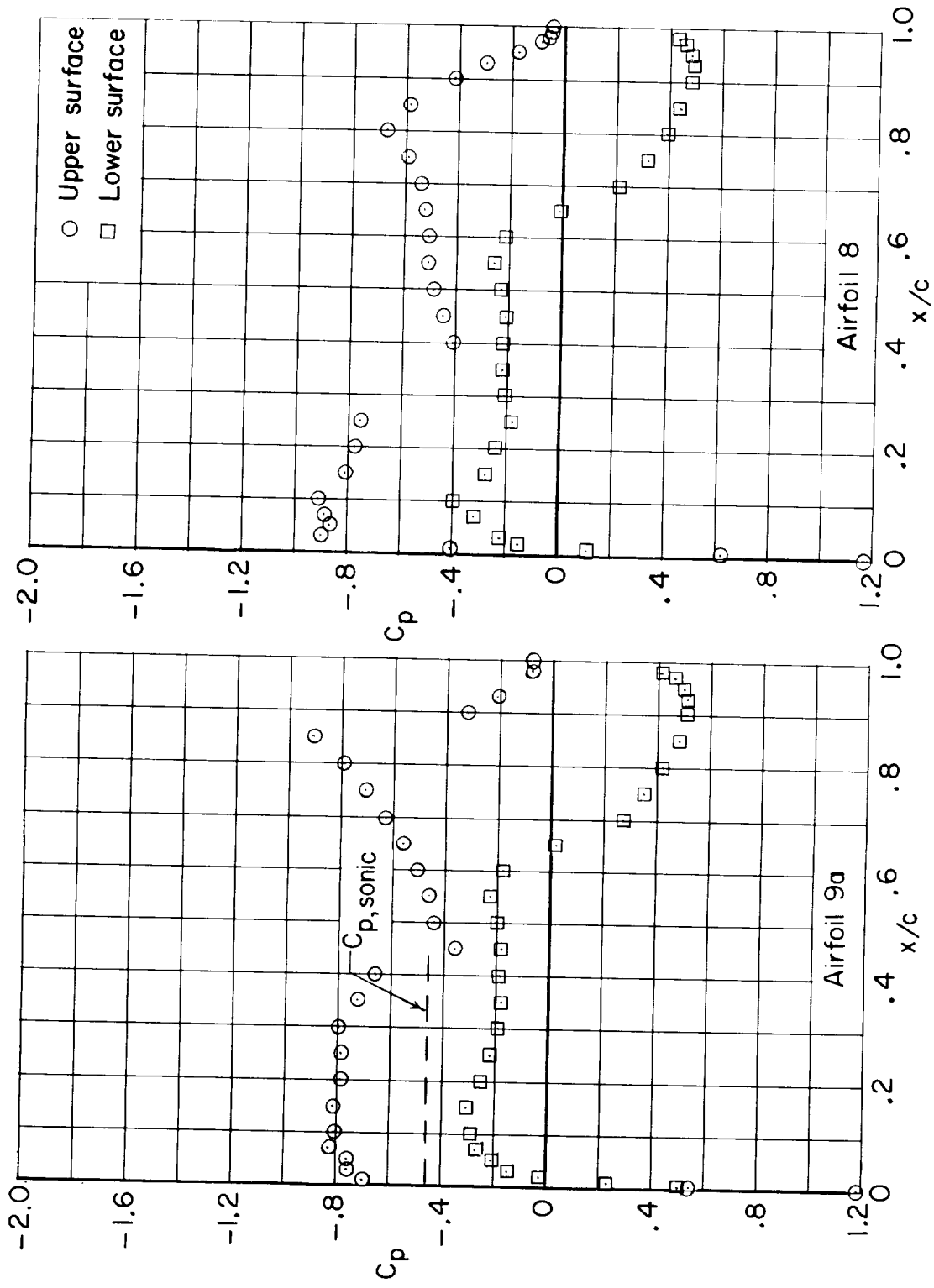

(m) $M = 0.79$; $\alpha = 0.5^{\circ}$.

Figure 12.- Continued.

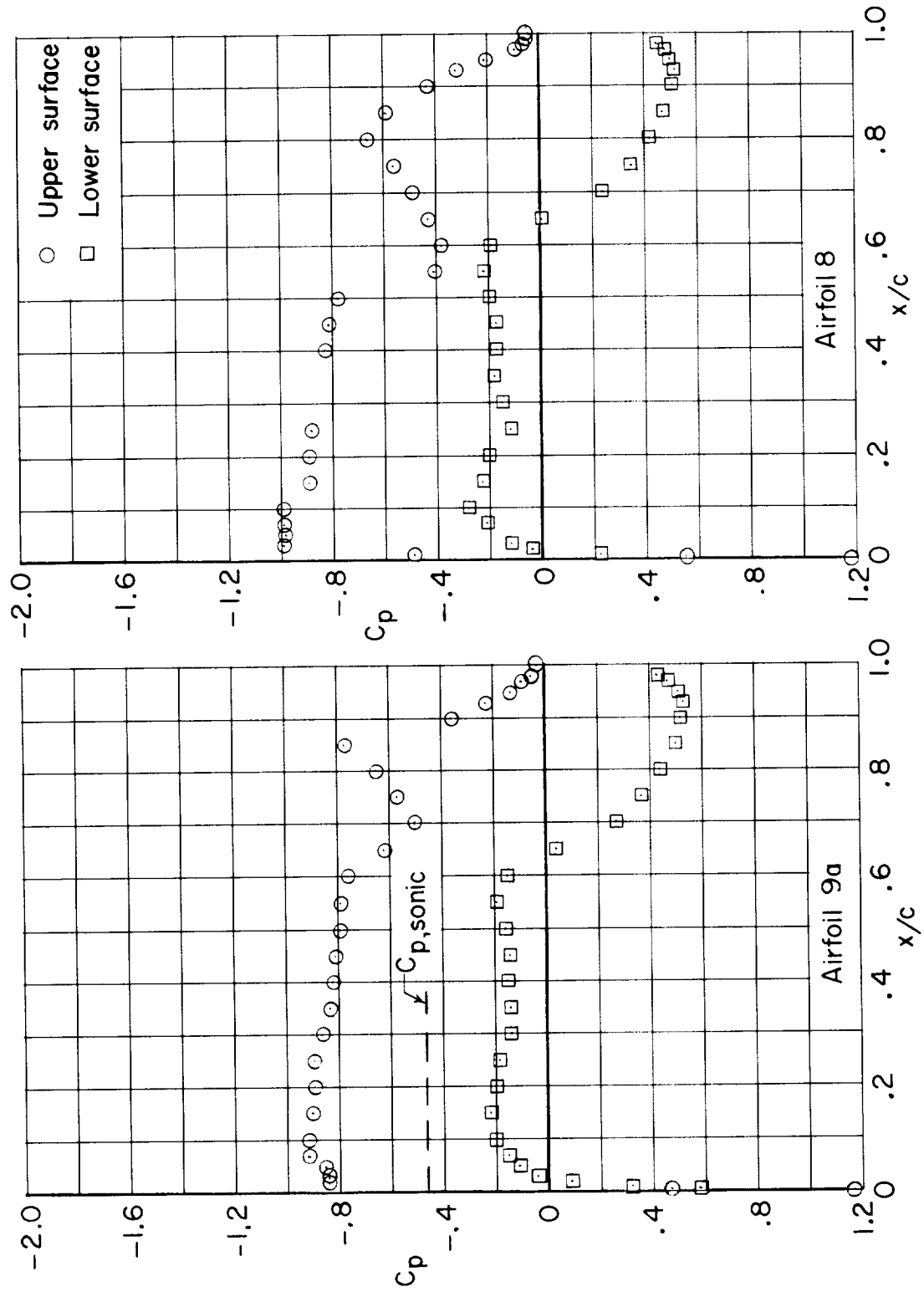

(n) $M = 0.79$; $\alpha = 1^\circ$.

Figure 12.- Continued.

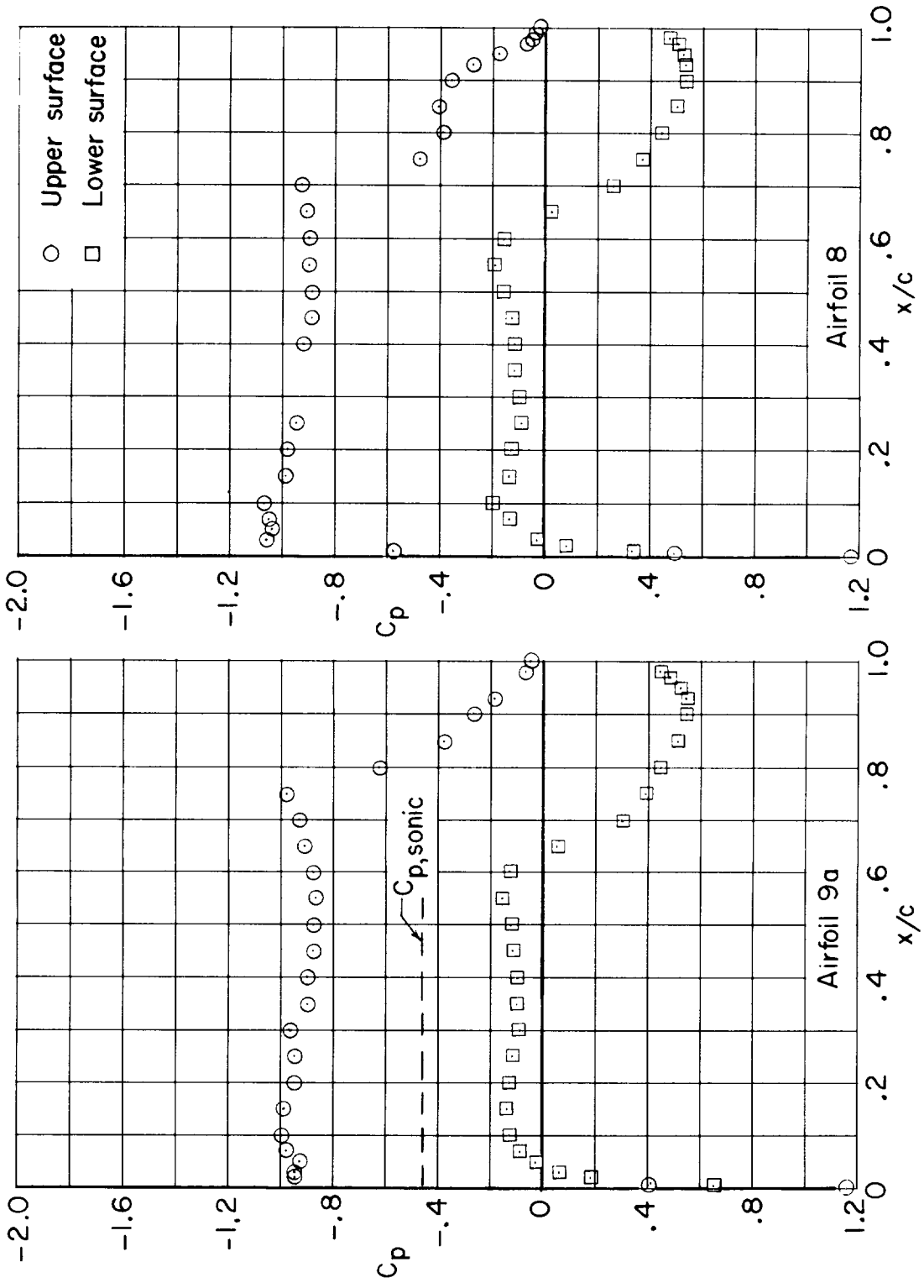

(o) M = 0.79; $\alpha = 1.5^{o}$.

Figure 12.- Continued.

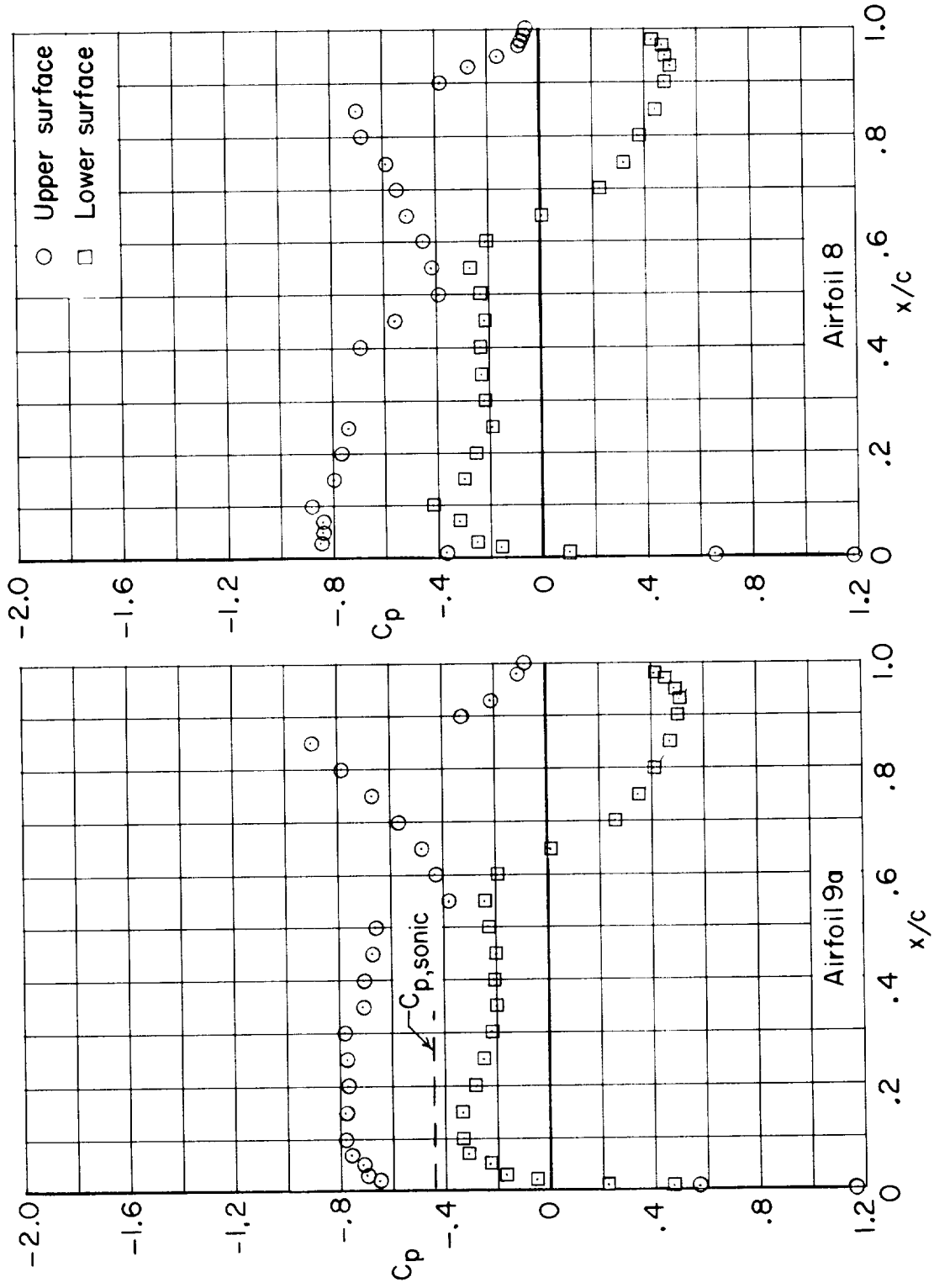

(p) $M = 0.80$; $\alpha = 0.5^{\circ}$.

Figure 12.- Continued.

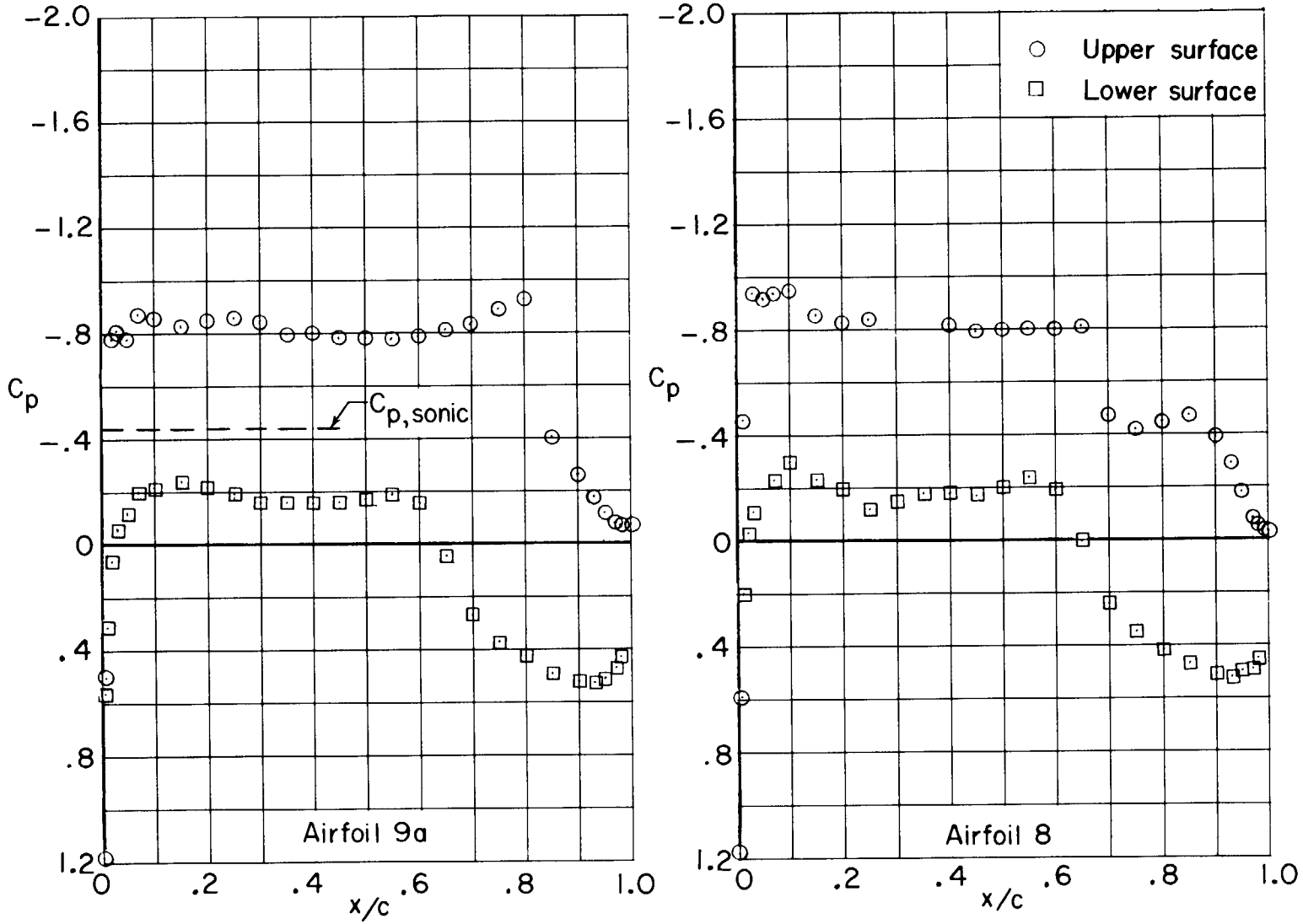

(q) M = 0.80; $\alpha = 1^{o}$.

Figure 12.- Continued.

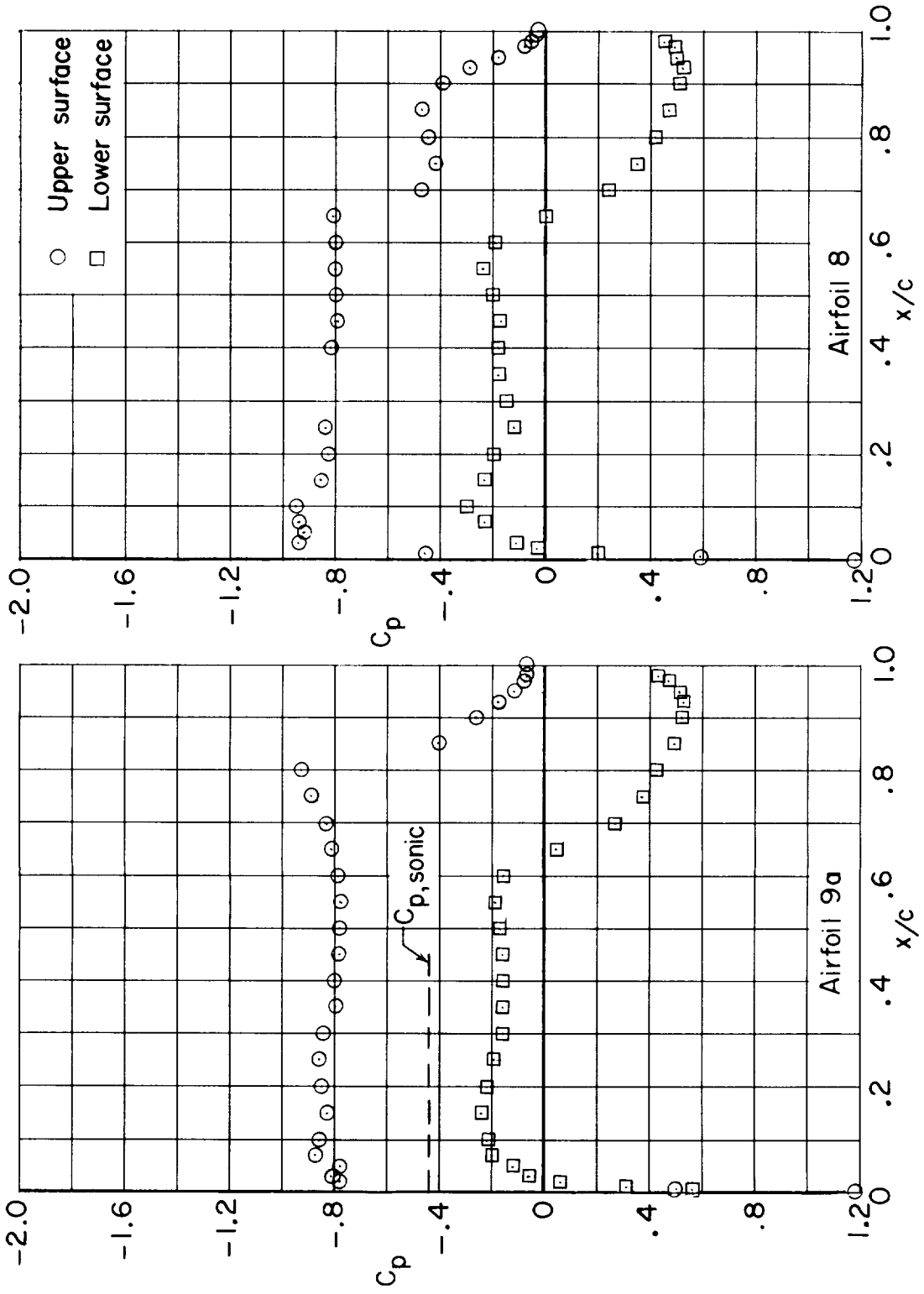

(q) $M = 0.80$; $\alpha = 1^\circ$.

Figure 12.- Continued.

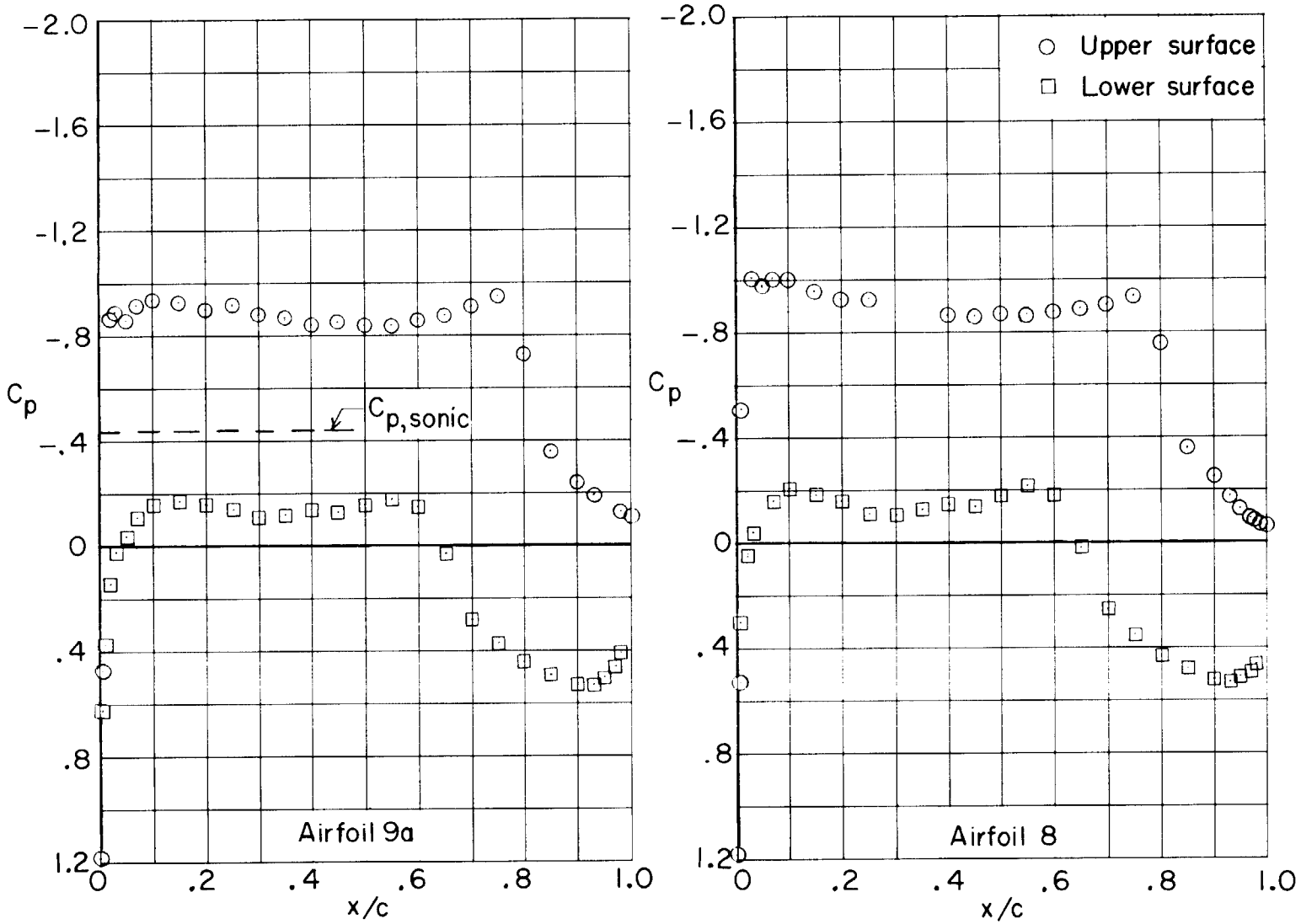

(r) M = 0.80; $\alpha = 1.5^{o}$.

Figure 12.- Continued.

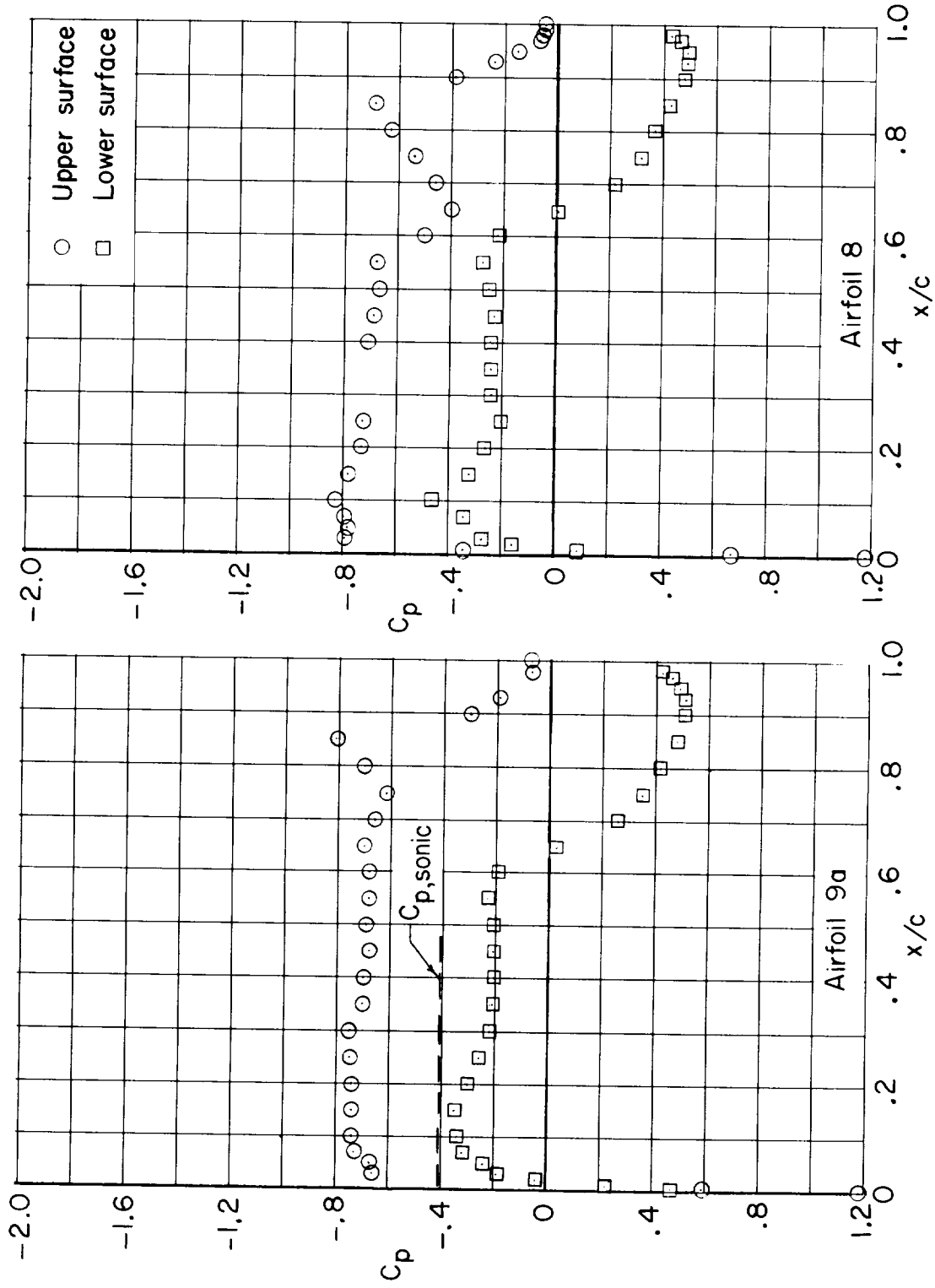

(s) M = 0.81; $\alpha = 0.5^{\circ}$.

Figure 12.- Continued.

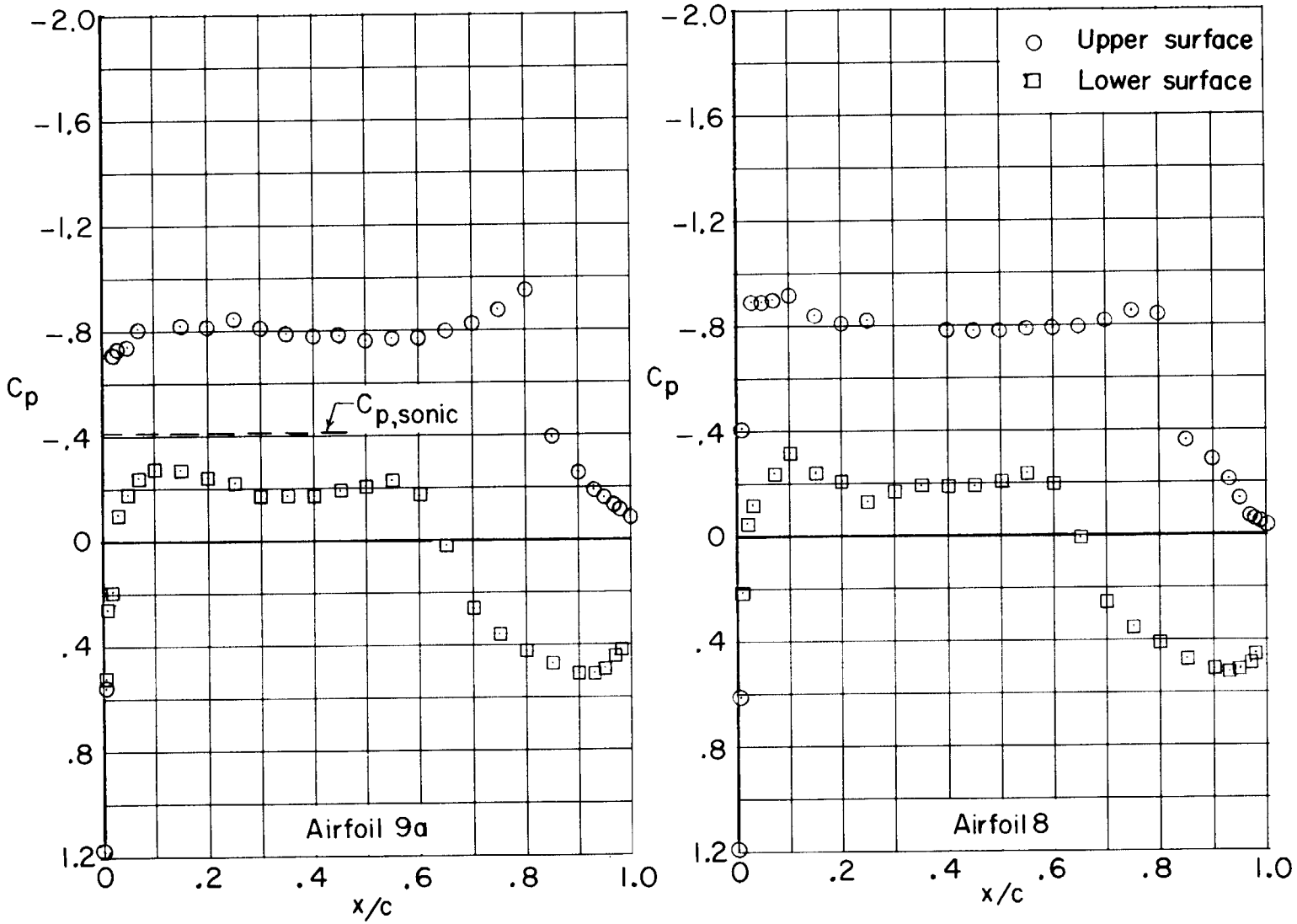

(t) M = 0.81; $\alpha = 1^{o}$.

Figure 12.- Continued.

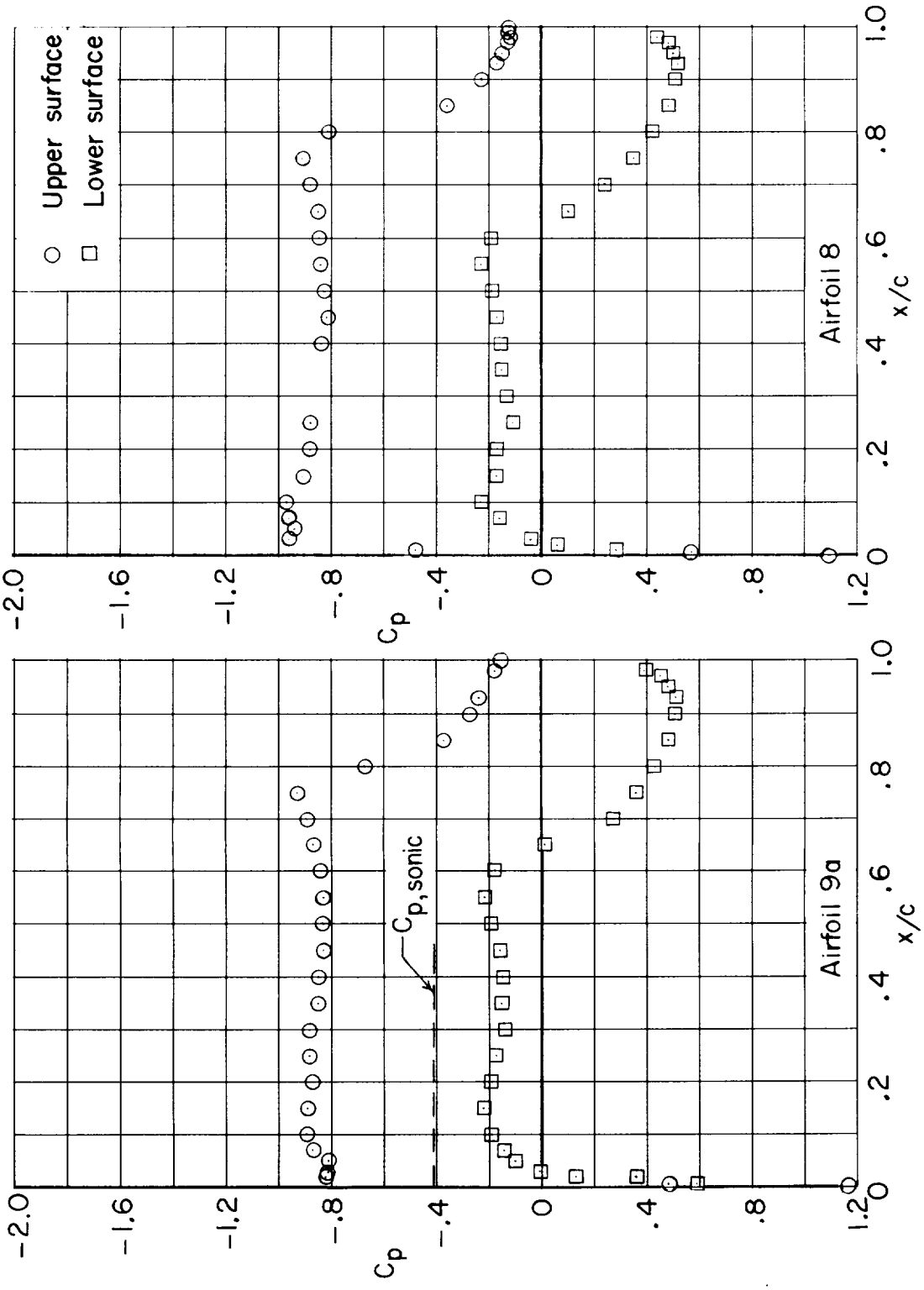

(u) M = 0.81; $\alpha = 1.5^{\circ}$.

Figure 12.- Concluded.

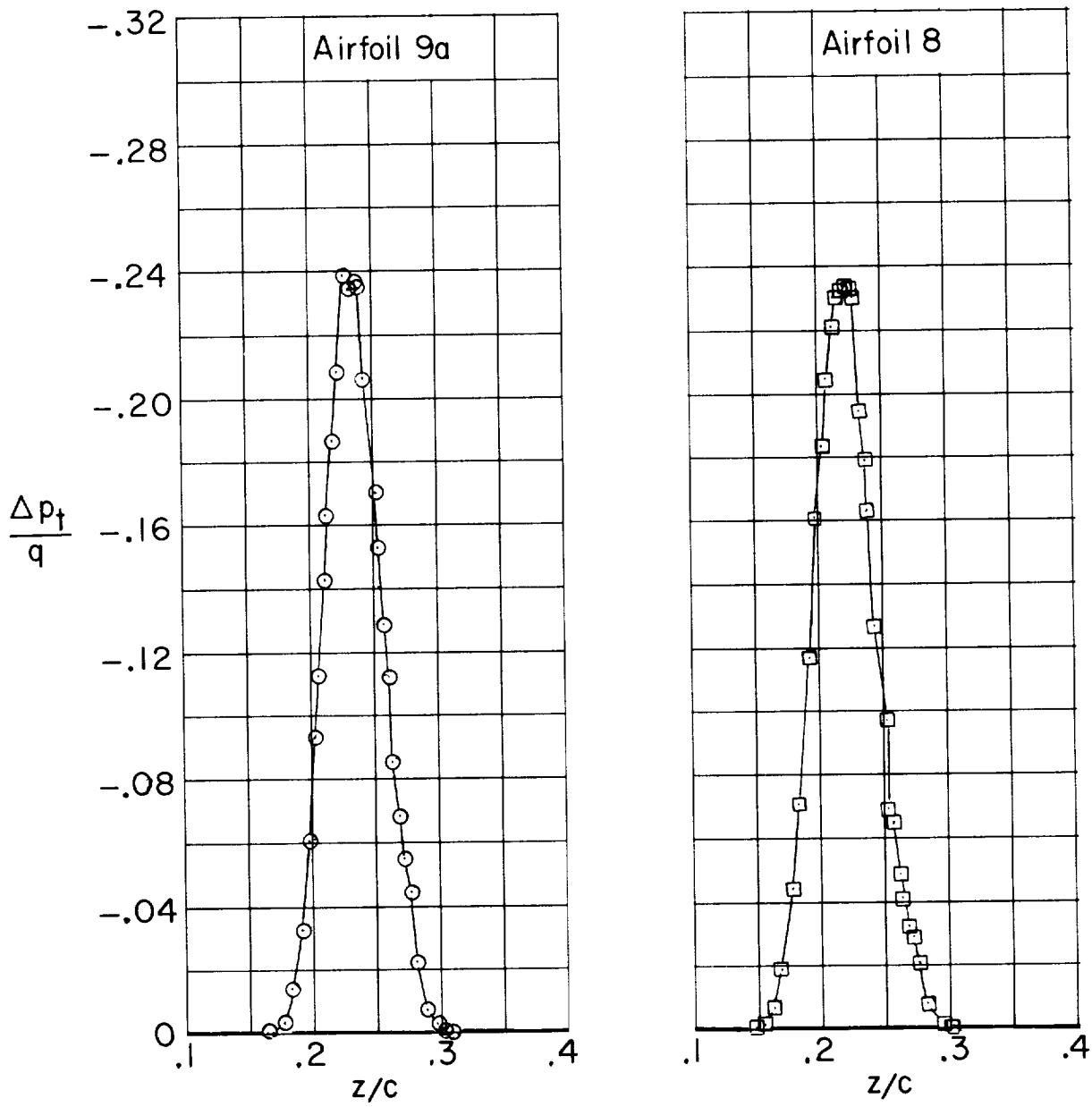

(a) M = 0.60; $\alpha = 1.5^{\circ}$.

Figure 13.- Representative wake profiles.

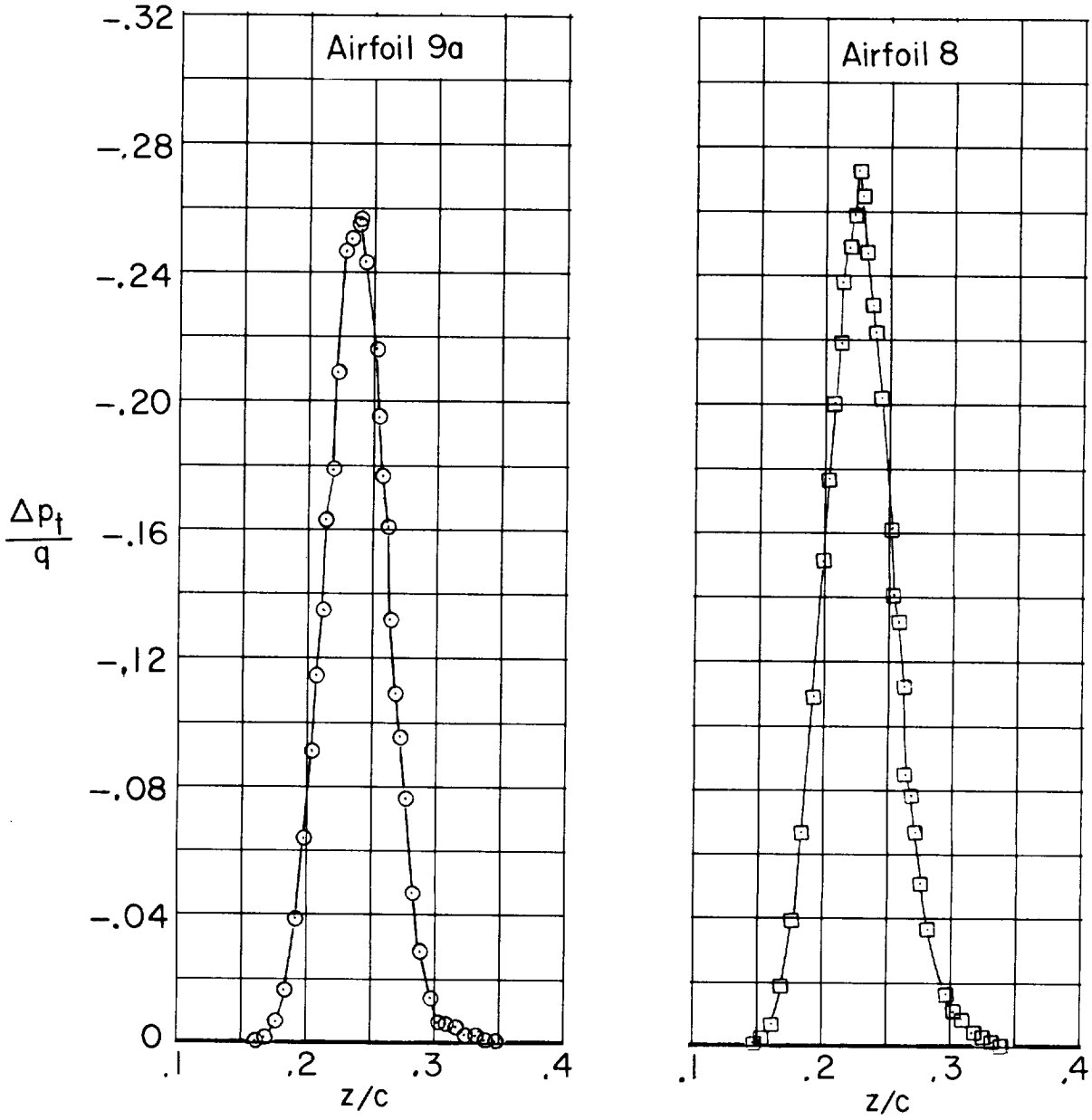

(b) M = 0.70; $\alpha = 1.5^{\circ}$.

Figure 13.- Continued.

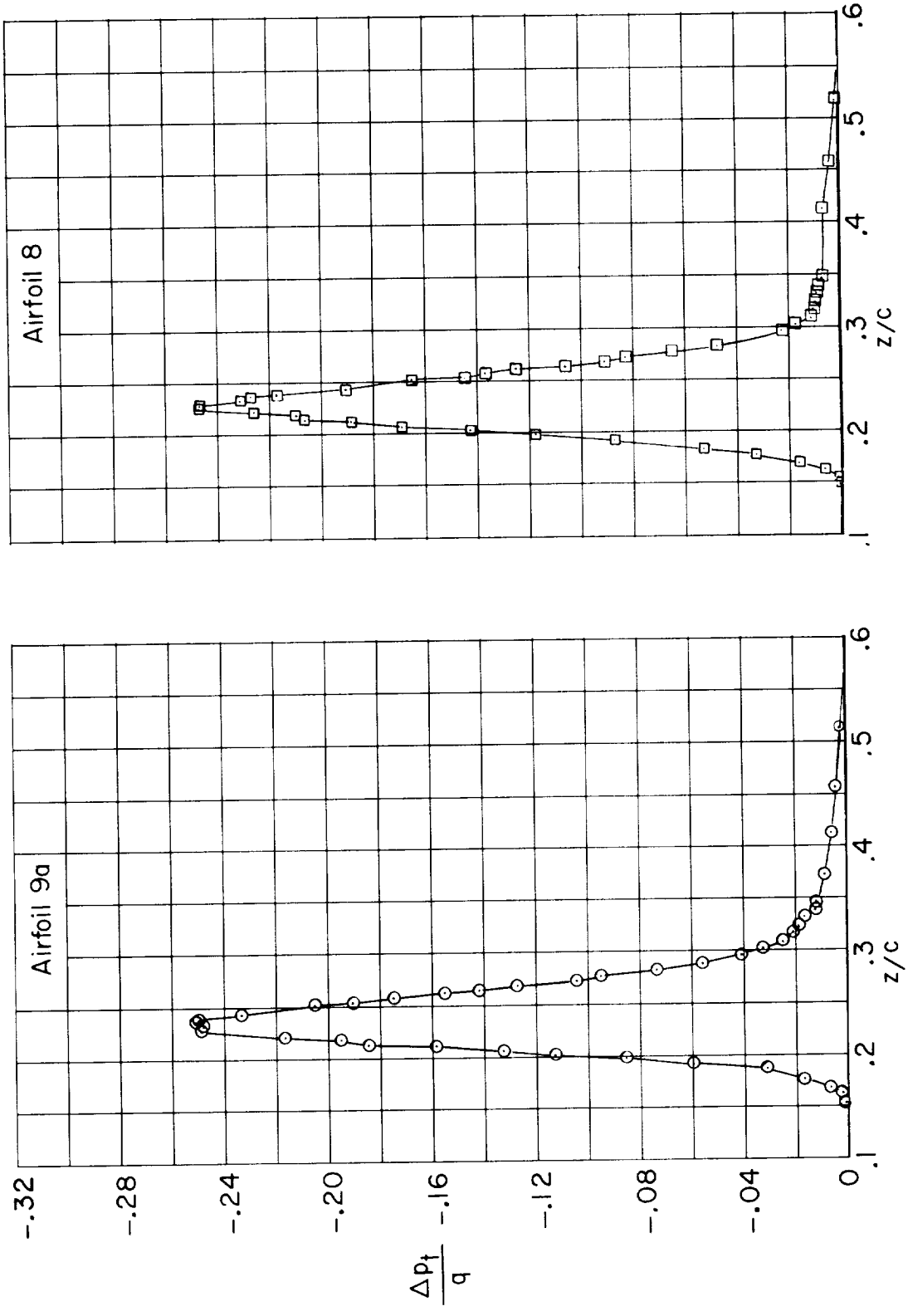

(c) M = 0.78; $\alpha = 1.0^{\circ}$.

Figure 13.- Continued.

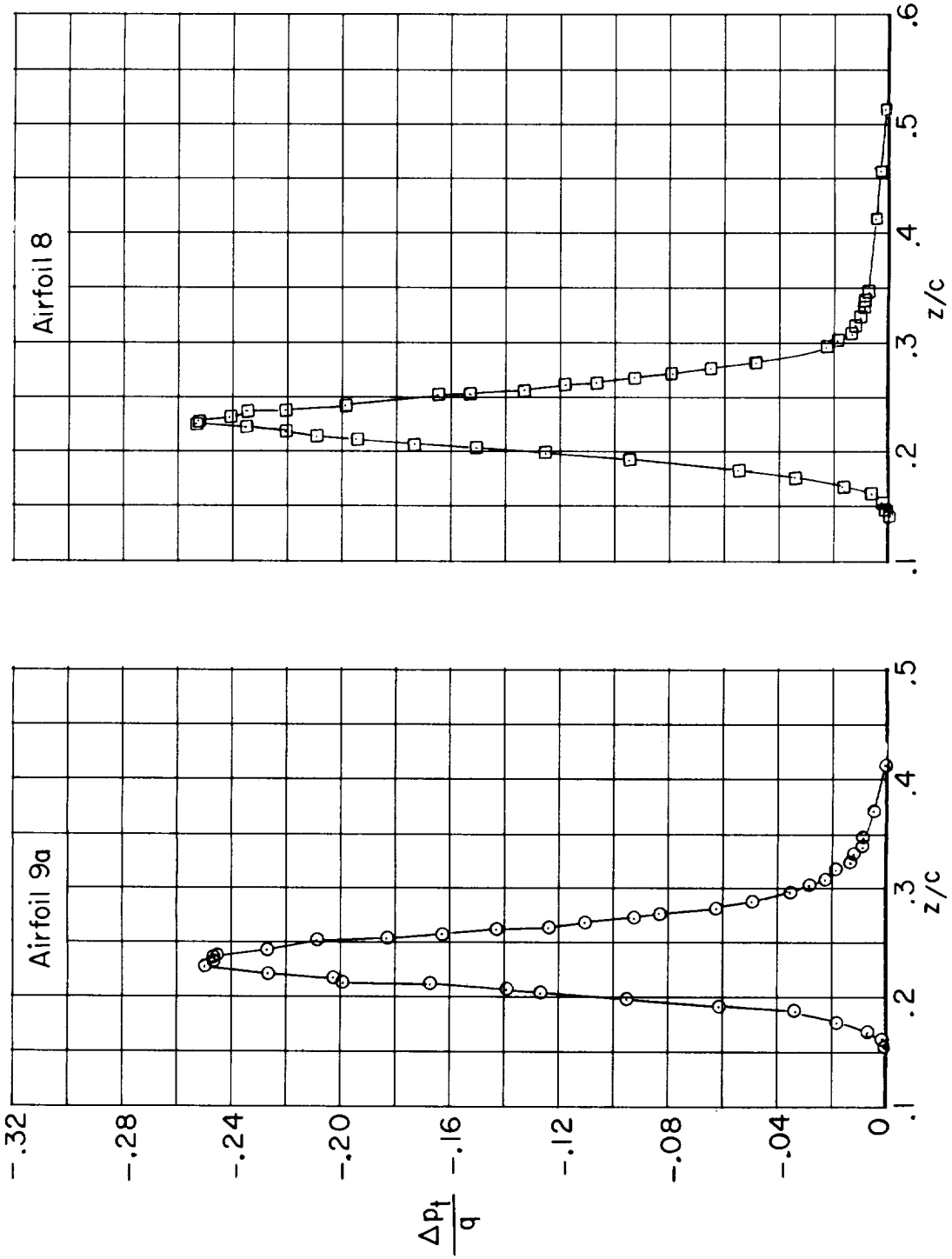

(d) M = 0.79; $\alpha = 1.0^{\circ}$.

Figure 13.- Concluded.